AD-A047 839 PENNSYLVANIA STATE UNIV UNIVERSITY PARK APPLIED RESE--ETC F/G 20/1
ACOUSTIC DIFFRACTION BY AN IMPEDANCE COVERED HALF-PLANE.(U)
DEC 76 R P KENDIG N00017-73-C-1418
UNCLASSIFIED TM-76-312 NL

1 OF 2
AD A047839

12

ACOUSTIC DIFFRACTION BY AN IMPEDANCE COVERED HALF-PLANE

Robert P. Kendig

Technical Memorandum
File No. TM 76-312
December 15, 1976
Contract No. N00017-73-C-1418

Copy No. 12

The Pennsylvania State University
Institute for Science and Engineering
APPLIED RESEARCH LABORATORY
Post Office Box 30
State College, PA 16801

NAVY DEPARTMENT

NAVAL SEA SYSTEMS COMMAND

SECURITY CLASSIFICATION OF THIS PAGE (When Data Entered)

REPORT DOCUMENTATION PAGE	READ INSTRUCTIONS BEFORE COMPLETING FORM
1. REPORT NUMBER: (14) TM-76-312 ✓	2. GOVT ACCESSION NO. (9) 3. RECIPIENT'S CATALOG NUMBER: Doctoral thesis,
4. TITLE (and Subtitle): (6) ACOUSTIC DIFFRACTION BY AN IMPEDANCE COVERED HALF-PLANE	5. TYPE OF REPORT & PERIOD COVERED: Ph.D. Thesis, March 1977
	6. PERFORMING ORG. REPORT NUMBER: TM 76-312
7. AUTHOR(s): (10) Robert Paul Kendig	8. CONTRACT OR GRANT NUMBER(s): (15) N00017-73-c-1418 ✓
9. PERFORMING ORGANIZATION NAME AND ADDRESS: The Pennsylvania State University, Applied Research Laboratory, P. O. Box 30, State College, PA 16801 ✓	10. PROGRAM ELEMENT, PROJECT, TASK AREA & WORK UNIT NUMBERS
11. CONTROLLING OFFICE NAME AND ADDRESS: (11) 15 Naval Sea Systems Command, Department of the Navy, Washington, D. C. 20362	12. REPORT DATE: Dec [redacted] 76
	13. NUMBER OF PAGES: 146 pages & figures (12) 159 pp.
14. MONITORING AGENCY NAME & ADDRESS(if different from Controlling Office)	15. SECURITY CLASS. (of this report): Unclassified, Unlimited
	15a. DECLASSIFICATION/DOWNGRADING SCHEDULE

16. DISTRIBUTION STATEMENT (of this Report)

Approved for public release, distribution unlimited, per NSSC (Naval Sea Systems Command), 2/16/77

17. DISTRIBUTION STATEMENT (of the abstract entered in Block 20, if different from Report)

18. SUPPLEMENTARY NOTES

19. KEY WORDS (Continue on reverse side if necessary and identify by block number)

acoustics
diffraction
backscattering
impedance
waves
half-plane

20. ABSTRACT (Continue on reverse side if necessary and identify by block number)

Exact, closed form solutions for diffraction and backscattering by a half-plane whose surfaces exhibit arbitrary impedances were determined for the cases of a point source, a line source, and a plane wave. An integral method was devised that could account for the impedance boundary conditions. Since the solution is in a closed form, interpretation of the influece of the impedance covered half-plane on the diffraction field is greatly facilitated. Specifically, the effect of each surface on the acoustic field dominates in the half-space in which it faces. Though the effect of each surface extends into →

next page

DD FORM 1 JAN 73 1473 EDITION OF 1 NOV 65 IS OBSOLETE UNCLASSIFIED

SECURITY CLASSIFICATION OF THIS PAGE (When Data Entered)

391 007

20. ABSTRACT (Continued)

the opposite half-space behind the barrier, this influence is very small and diminishes even more as the observer moves further behind the barrier.

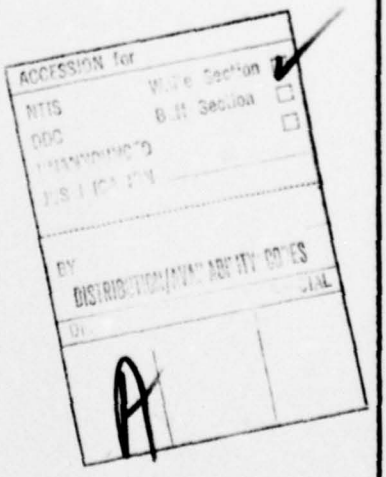

Acknowledgements

Without the guidance, patience, and breadth of knowledge of Dr. Sabik I. Hayek, the author's thesis advisor, the completion of this thesis would not have been possible. Discussions with Dr. Eugen Skudrzyk were helpful in gaining a clearer understanding of this problem.

The author also wishes to express his gratitude to Dr. William Thompson for his helpful suggestions, and to Drs. Vernon Neubert and Norman Davids for serving on his doctoral committee.

The support for this research originated from a contract with the U.S. Naval Sea Systems Command.

The author's wife, Bobbie, also deserves special recognition for inspiring and sustaining him through the many traumatic ordeals of graduate study.

TABLE OF CONTENTS

LIST OF TABLES

LIST OF FIGURES

List of Major Symbols

$P(r,\phi)$	scattered pressure
$p_d(r,\phi)$	diffracted pressure
k	acoustic wave number
$P(\cos\alpha)$	angular distribution of plane waves
α	variable of integration
γ	path of integration
$Z^{\pm}$	surface impedance of the half-plane
$\theta^{\pm}$	Brewster angle ($\sin\theta^{\pm} = \frac{\rho c}{Z^{\pm}}$)
ρ	density of acoustic medium
c	velocity of a propagating wave
(r_o,ϕ_o,z_o)	coordinates for the location of a point source
(r,ϕ,z)	location of the observer in cylindrical coordinates
(r_o,ϕ_o)	location of a line source
(r,ϕ)	location of an observer in polar coordinates
ϕ_o	angle of incidence
R	line source: $R = \sqrt{r^2+r_o^2-2rr_o\cos(\phi-\phi_o)}$
	point source: $R = \sqrt{r^2+r_o^2-2rr_o\cos(\phi-\phi_o)+(z-z_o)^2}$
S	line source: $S = \sqrt{r^2+r_o^2-2rr_o\cos(\phi+\phi_o)}$
	point source: $S = r^2+r_o^2-2rr_o\cos(\phi+\phi_o)+(z-z_o)^2$
R_1	line source: $R = r+r_o$
	point source: $R_1 = \sqrt{(r+r_o)^2+(z-z_o)^2}$
$\Psi_{1,2}(\alpha);\Phi_{1,2}(\alpha)$	special function that accounts for the arbitrary impedance cover

List of Major Symbols (continued)

C_r	coefficient of reflection; $\left(C_r = \dfrac{\sin\theta^{\pm} - \sin\phi_o}{\sin\theta^{\pm} + \sin\phi_o}\right)$
$C(a);S(a)$	Fresnel Integral $C(a) = \dfrac{\sqrt{2}}{\pi}\int_o^a \cos\tau^2 d\tau$ $S(a) = \dfrac{\sqrt{2}}{\pi}\int_o^a \sin\tau^2 d\tau$
$H_o^{(2)}$	Hankel Function of the second kind of degree zero

CHAPTER I

INTRODUCTION

1.1 Background

Whenever the propagation of a sound wave is obstructed by some obstacle, part of the sound wave is deflected or disturbed. This disturbance or interference gives rise to the phenomenon called diffraction.

The problem of diffraction, where the interfering obstacle is a semi-infinite half-plane, is a classical problem in the area of wave propagation. Recently, because of environmental concerns, there has been interest in using barriers and enclosures as a means of isolating noise from adjacent areas. Understanding the phenomenon of diffraction is important, since the sound waves will diffract around the barrier. Although, the geometry of the half-plane plays a dominant role in creating the diffracted pressure, the nature of the surface impedance also influences the behavior of the diffracted pressure. By adjusting the surface impedance of the half-plane, the diffracted pressure could be modified in some desirable fashion.

1.2 Review of Previous Investigations

Studies of diffraction have been extensively carried out in the fields of acoustics and optics. Many related publications may be easily found in the literature. This review is concerned specifically with those papers that are related to the diffraction of a wave by a half-plane and, in particular, an impedance covered half-plane.

Because of the geometry of the half-plane, the usual techniques for solving boundary value problems do not apply. Consequently, in order to solve the problem for sharp geometries like the half-plane, other methods have had to be formulated. It was Sommerfeld [1,2] who successfully used an integral expression to represent the scattered pressure. With the pressure expressed in an integral form and a concept of sources and image sources, he matched the conditions on the surfaces of the half-plane. In Sommerfeld's classical work, he was able to solve the problem only for the rather ideal boundary conditions of a perfectly soft (pressure release) or a perfectly hard (rigid) surface. Any impedance between those extremes could not be accommodated by his more or less heuristic formulation of the problem. Sommerfeld's solution accounts for the geometry of the diffracting obstacle but is limited in the sense that it does not account for arbitrary surface conditions.

After Sommerfeld, several researchers found a number of ways to solve the problem of diffraction by a half-plane based on the so-called Weiner-Hopf Technique. The Weiner-Hopf method is essentially an extension of Fourier-Laplace transforms which results in a complex variable equation that is analytic within a certain region. The fundamental step in the Weiner-Hopf method is to determine two functions, each of which satisfy a complex variable equation in different halves of the complex plane but together satisfy the equation in a proper overlapping region. The problem can be reduced to the task of splitting a complex function into two factors in such a way that each factor contains specific singularities. A variation

of the Weiner-Hopf method is a dual integral technique employed by Jones [3] and Clemmow [4]. In this method, two integral equations are found that are valid in separate half-planes of the complex plane. It is necessary to find a function that will satisfy each integral equation in its respective half-space. Jones and Clemmow applied the dual integral method to the specific problem of diffraction by a half-plane and found a solution exactly equivalent to Sommerfeld's solution. Again, they only considered ideal boundary conditions.

The Weiner-Hopf technique was successfully employed by Senior [5]. He attempts a problem in which a semi-infinite metallic sheet has some finite conductivity. The solution that he finds is exact but the function resulting from the Weiner-Hopf analysis is in integral form and cannot be easily computed.

Following Senior, Williams [6] extended the Weiner-Hopf technique to a more general problem of the diffraction by a wedge. He reduced the problem to the solution of an ordinary difference equation. This difference equation was then solved by means of a double Gamma function defined by Barnes [7]. If the wedge angle was of the form $p\,\pi/q$, where p and q are prime, and p is odd, a closed form solution could then be found. By choosing proper values of p and q, a wedge that is very close to a half-plane could be approximated. Rawlins [8] used the Weiner-Hopf technique to solve the diffraction by a half-plane with one side soft and the other side rigid. According to Rawlins, a "perfectly absorbing" surface can be modeled by adding the hard and soft surface solutions together and dividing by two.

From this he concludes that the absorbing surface will attenuate the diffracted pressure if it is on the illuminated surface.

The case of a half-plane with an arbitrary surface impedance has not been solved by the Weiner-Hopf technique. However, the Russian physicist, Malyuzhinets [9,10,11] has approached the problem by yet another method. Malyuzhinets used a Fourier Transform approach to find a single spectral function for the whole range of integration. The function is found to be a product of four integral functions that comprise the special functions derived by Malyuzhinets to account for the arbitrary surface impedance. Malyuzhinets demonstrates that each spectral function is a solution of a difference equation. Malyuzhinets and his colleagues have also applied their technique to a more general class of problem where the diffracting obstacle is an impedance covered wedge.

In most cases, the diffraction problem was solved considering an incident plane wave. Redfearn [12] considers various kinds of sources. Specifically, for a point source Redfearn discussed the practical uses of a half plane as a noise barrier. Finally, Clemmow [4] discusses the diffraction of a line source by a half-plane, where he derived the solution in terms of the Fresnel Integrals. A good summary of the work accomplished in the area of diffraction by edges and wedges is given by Pierce [13].

CHAPTER II

MATHEMATICAL FORMULATION FOR THE DIFFRACTION OF ACOUSTIC WAVES BY AN IMPEDANCE COVERED HALF-PLANE

2.1 Statement of the Problem

In this study, the problem of diffraction, where the disturbing obstacle is a half-plane, is considered. The acoustic impedance of the upper and lower surfaces of the half-plane will have an effect on the diffraction of a sound wave. Conventionally, this problem is approached by considering only the ideal surface conditions of a perfectly rigid or a perfectly soft half-plane. In this study, however, the effect of more realistic surface conditions are considered. These surface conditions can account for an arbitrary local reactance and an arbitrary absorption on both surfaces of the half-plane. Specifically, this study aims to determine exactly how the surface impedances on the two sides of a half-plane will affect the diffraction of sound.

In addition to this, various kinds of acoustic sources can produce the sound waves incident upon the half-plane. Subsequently, this study also investigates the diffraction for a plane wave, a line source, and a point source.

Often when dealing with the diffraction of a sound wave, interest concentrates only on how the diffracted field appears when an observer is located many wave lengths from the diffracting obstacle. However, it is a goal of this study to also investigate the diffraction when the observer distance from the edge may not

necessarily be great, as well as when the observer distance does become large.

A special case of diffraction results when the source and observer are located at the same position. This is called backscattering. Results of backscattering for various surface and source conditions are also to be analyzed.

In short, the goals of this study are to develop analytical models and exact solutions that account for arbitrary realistic surface conditions, source and observer locations, for the acoustic diffraction and backscattering by a half-plane.

2.2 Assumptions

The problem that is modeled here is based upon the existence of a semi-infinite thin plane. Needless to say, one cannot realize such an edge physically.

Perhaps of more significance are the assumptions and restrictions that are made concerning the acoustical behavior of the semi-infinite plane surfaces. For several reasons, the surfaces are considered to have locally reacting impedances. This is chosen in the first place because it represents many real acoustic situations reasonably well. Secondly, it can be handled mathematically by a comparatively simple formulation.

What then is meant by a locally reacting surface? Suppose an acoustic wave impinges on a surface. Some of the energy of the acoustic wave could be reflected, some could be absorbed, and some could be used to set the surface itself into motion. If the surface

itself is set into motion, it is possible, depending on the material making up the surface, for that motion to propagate along the surface. For a locally reacting surface, this is not possible.

It may be possible for the surface to be set into motion by an incident acoustic wave in such a way that each point on the surface moves independently of all adjacent points. In other words, there is no coupling of the motion of the neighboring points of the surface, so consequently, no allowances are made for the propagation of a wave along or through the surface. It is important to recognize that this means there are no elastic waves propagating in the surface nor are there any waves transmitting through the surface. However, surface waves in the acoustic medium are accounted for in this analysis.

The motion of the surface at a given point is determined by the pressure of the acoustic wave at that point. It turns out that the pressure is proportional to the component of velocity normal to the surface. The motion of the acoustic fluid tangent to the surface will not cause any motion in the surface. This is the true provided the acoustic fluid is considered invisid or at least has negligible viscosity. Thus, the ratio of the acoustic pressure at the surface to the outward normal component of the velocity at the surface at a given point is called the acoustic impedance of the surface at that point. It is usually signified by $Z = \frac{p}{v_n}$. The half-plane is considered to have different impedances on its two surfaces which will be denoted by Z^+ and Z^-, respectively.

In general, the acoustic impedance of the surface may be complex. The imaginary part of the impedance corresponds to the reactive component of the surface impedance. This means that the surface can be locally idealized as consisting of a series of isolated masses and springs. The real part of the impedance physically represents the acoustic energy that is absorbed by the surface.

In brief, the assumptions imposed to facilitate the mathematical formulation are (i) a thin half-plane, and (ii) locally reacting impedances on the surfaces.

2.3 Integral Representation

In order to have an exact solution to a diffraction problem, it is necessary to satisfy three basic requirements. First, the solution must satisfy the wave equation. Second, the solution must account for the boundary conditions on the surfaces of the diffracting half-plane and be continuous throughout the physical space. Third, the solution must correspond to the given type of excitation, be it a plane wave, a line source, or a point source. If all these requirements are met, then the resulting solution must be unique to the problem as it is posed. In this regard, the analytical method used in this study exploits an integral representation that must satisfy these requirements.

Since the Fourier Integral transforms are useful in the formulation of the problem, they are introduced here. Define the Fourier Transform pair as

$$f(x) = \frac{1}{2\pi} \int_{-\infty}^{\infty} F(\gamma) e^{-i\gamma x} \, d\gamma \tag{2.1}$$

and

$$F(\gamma) = \int_{-\infty}^{\infty} f(x) e^{i\gamma x} \, dx \quad . \tag{2.2}$$

Consider now the wave equation for the pressure

$$\nabla^2 p = \frac{1}{c^2} \frac{\partial^2 p}{\partial t^2} \quad , \tag{2.3}$$

where c is the velocity of propagation of an acoustic wave in free space. Assuming the pressure to be periodic in time as $e^{i\omega t}$, then Equation (2.3) becomes

$$\nabla^2 p + k^2 p = 0 \quad , \tag{2.4}$$

where $k = \omega/c$.

Applying Fourier Transforms on Equation (2.4), one obtains

$$\frac{d^2 \bar{p}}{dy^2} + (k^2 - \gamma^2) \bar{p} = 0 \tag{2.5}$$

or

$$\frac{d^2 \bar{p}}{dy^2} + \beta^2 \bar{p} = 0 \quad , \tag{2.6}$$

where

$$\beta = k\sqrt{\left(1 - \frac{\gamma^2}{k^2}\right)} \quad .$$

The solution to the differential equation in Equation (2.6) is

$$\bar{p} = A(\gamma)e^{\pm i\beta y} \quad . \tag{2.7}$$

The (+) or (-) sign in the exponent corresponds to the two possible independent solutions of Equation (2.6). To choose the proper sign, consider the physical situation. The pressure p is meant to represent the diffraction from the edge. Consequently, the solution must reflect the behavior of outgoing waves from the edge rather than an incoming wave from infinity. The requirement for outgoing waves can be assured by using the plus sign (+) for $y<0$, and the minus sign (-) for $y>0$.

Taking the inverse transform of $\bar{p}$ gives the following integral representation,

$$p(x,y) = \int_{-\infty}^{\infty} \left[A(\gamma)e^{\pm i\beta y}\right] e^{-i\gamma x}\, d\gamma \tag{2.8}$$

Since the integral representation in Equation (2.8) satisfies the wave equation, p(x,y) is then chosen as a suitable representation for the scattered pressure. Letting $\lambda = \gamma/k$ then Equation (2.8) becomes

$$p(x,y) = \frac{k}{2\pi} \int_{-\infty}^{\infty} A(\lambda) e^{\pm iky\sqrt{1-\lambda^2}} \; e^{-ik\lambda x} \, d\lambda \qquad (2.9)$$

Another way to consider this integral representation is through a more heuristic explanation of the physical meaning. The exponent of the integrand can be regarded as waves propagating in all directions in the x,y plane. This part will satisfy the wave equation. The function $A(\lambda)$ of the integrand can be regarded as a spectrum function. This is to say that $A(\lambda)$ represents a weighting or distribution of waves that will propagate in any given direction. From this explanation, it is argued that, since the integral itself is made up of a superposition of waves that individually satisfy the wave equation, then, this superposition of waves in the form of the integral will also satisfy the wave equation. Subsequently, the integral in Equation (2.9) is often referred to as a spectrum of plane waves.

A final step at arriving at an appropriate integral representation is to express the integral of Equation (2.9) in polar coordinates. This is accomplished by adopting two transformations. First, let

$$x = r \cos\phi,$$

and

$$y = r \sin\phi \; . \qquad (2.10)$$

Next use the following change of variable for λ:

$$\lambda = \cos\alpha \quad . \tag{2.11}$$

Thus, the corresponding path of integration in the α-plane must be computed.

Making use of Equations (2.10) and (2.11), the integral expression may be expressed in polar coordinates as follows:

$$p(r,\phi) = k\int_{\gamma} A(\cos\alpha)\,\sin\alpha\;\; e^{-ikr(\cos\phi\,\cos\alpha \pm \sin\phi\,\sin\alpha)}d\alpha \quad , \tag{2.12}$$

with (+) for the upper half-plane when $y>0$, and (-) for the lower half-plane when $y<0$, and where γ is the path of integration. Letting $P(\cos\alpha) = k\,A(\cos\alpha)\,\sin\alpha$ and using the appropriate identity in the exponent, one arrives at the following integral representation:

$$p(r,\phi) = \int_{\gamma} P(\cos\alpha)\; e^{-ikr\,\cos(\phi\mp\alpha)}\; d\alpha \tag{2.13}$$

(-) upper half-plane
(+) lower half-plane

In this form, it is easier to recognize that Equation (2.13) represents an angular distribution of plane waves.

It is necessary to carefully investigate what occurs under the change of variables chosen in Equation (2.11). Starting with the equation for λ:

$$\lambda = \cos(\alpha_r + i\,\alpha_i)$$

and

$$\lambda_r + i\,\lambda_i = \cos\alpha_r \cosh\alpha_i - i \sinh\alpha_i \sin\alpha_r \quad , \tag{2.14}$$

where λ_r and α_r are the real parts of λ and α and λ_i and α_i are the imaginary parts of λ and α. Equating the real and imaginary parts, it follows that

$$\lambda_r = \cos\alpha_r \cosh\alpha_i \tag{2.15}$$

and

$$\lambda_i = - \sinh\alpha_i \sin\alpha_r \quad . \tag{2.16}$$

Due to the periodicity of $\cos\alpha_r$ and $\sin\alpha_r$, the entire complex λ-plane will map into a strip of width π in the α-plane, and then repeat itself in subsequent strips of width equal to π.

To understand this, consider λ_i negative, or the lower half of the complex λ-plane, then $- \sinh\alpha_i \sin\alpha_r$ must be negative. This is met

1) for $\alpha_i < 0$ and $\sin\alpha_r < 0$

   if $(2\eta-1)\pi \leq \alpha \leq 2\eta\pi$

and

2) for $\alpha_i > 0$ and $\sin\alpha_r > 0$

   if $2\eta\pi \leq \alpha_r \leq (2\eta+1)\pi$. (2.17)

If, on the other hand, λ_i is positive and thus represents the upper half of the complex λ-plane, then $-\sinh\alpha_i \sin\alpha_r$ must also be positive. Consequently, this condition is also satisfied:

1) for $\alpha_i < 0$ and $\sin\alpha_r > 0$

if $2\eta\pi \leq \alpha_r \leq (2\eta+1)\pi$

and

2) for $\alpha_i > 0$ and $\sin\alpha_r < 0$

if $(2\eta-1)\pi \leq \alpha_r \leq 2\eta\pi$. (2.18)

Using the conditions stated in Equations (2.17) and (2.18), Figure 2.1 shows the mapping of the entire complex λ-plane to a multiplicity of strips in the complex α-plane.

Because the λ-plane maps itself every π in the α-plane, it then follows that the path of integration from $-\infty$ to $+\infty$ in the λ-plane must likewise exhibit the same repetitive behavior. Considering the expression for the real part of λ in the Equation (2.15) to determine the path for λ from $-\infty$ to $+\infty$, certain values for α_r and α_i must be chosen. Starting at $-\infty$ and moving to $+\infty$ in the λ-plane the corresponding values for α_r and α_i are indicated in Table 2.1. From Table 2.1, it follows that the path of integration in the α-plane can be made by picking any combination of values of α_i and α_r.

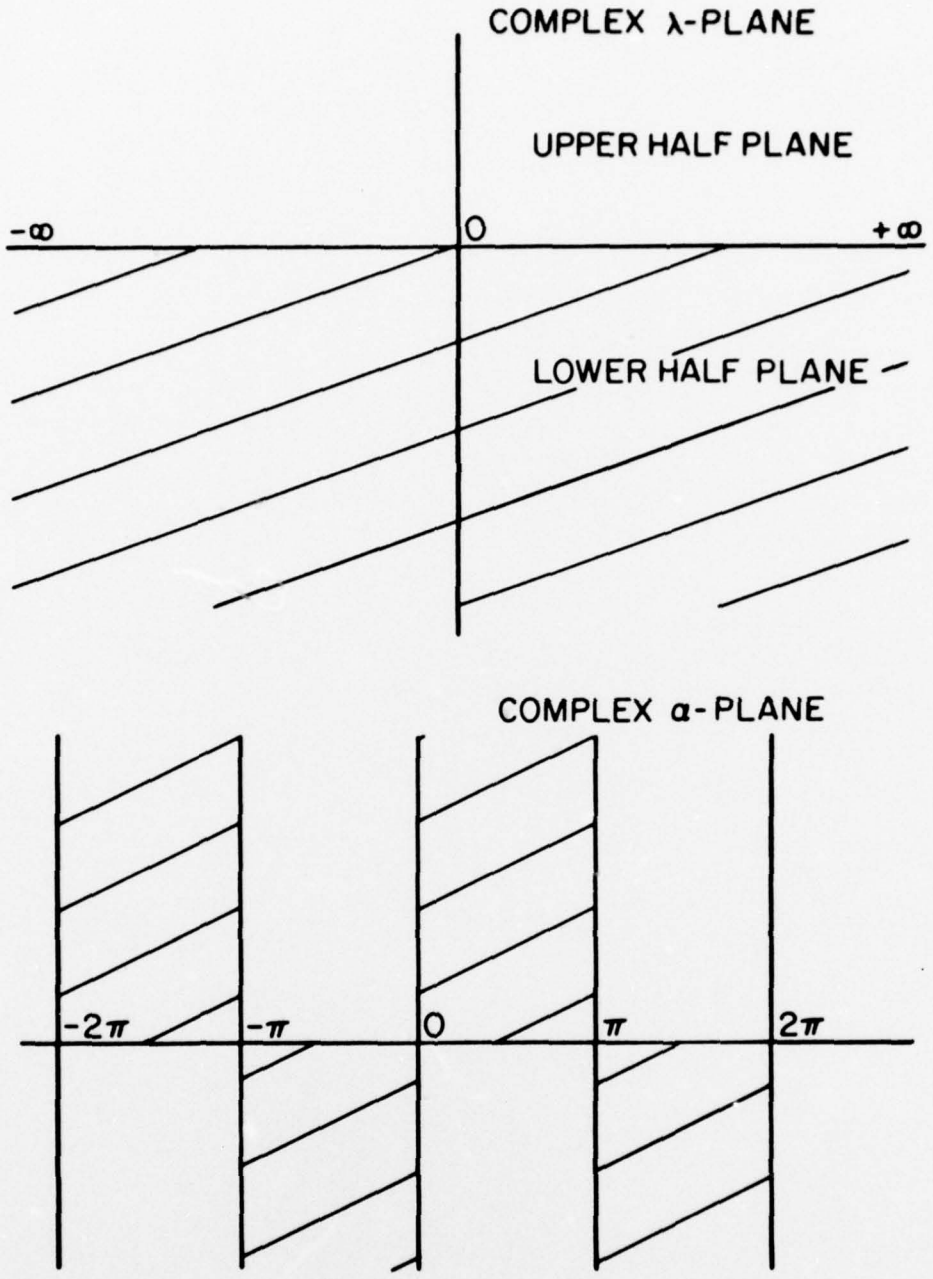

Figure 2.1. Mapping of the complex λ-plane to the complex α-plane. The shaded regions correspond to the lower half-plane of the λ-plane.

Table 2.1. The path of integration in the λ-plane and the Corresponding α-plane.

λ	$-\infty \rightarrow$	$-1 \rightarrow$	$0 \rightarrow$	$1 \rightarrow$	∞
α_i	$\pm\infty$	0	0	0	$\pm\infty$
α_r	$(n+1)\pi$	$(n+1)\pi$	$\frac{n+1}{2}\pi$	$n\pi$	$n\pi$

There is one last detail to consider before actually defining the γ-path. There is a negative sign introduced in the integral by the change of variable in Equation (2.11). To compensate for that minus sign, the path is simply followed in the opposite direction. Taking this fact into account, and the values of α_r and α_i from Table 2.1, the possible paths that may define the γ-path in the α-plane are shown in Figure 2.2. Any path that joins $\lambda = +\infty$ to $\lambda = -\infty$ is an acceptable γ-path for the integral representation of Equation (2.13). It is now evident that there is also a multiplicity of γ-paths.

Although all the γ-paths described in the previous section do indeed represent a path from $-\infty$ to $+\infty$, not all paths are suitable choices. The reason lies in the behavior of the exponent in the integrand of Equation (2.13). One requirement for this integral to exist is that it must converge. Since the integration is in the

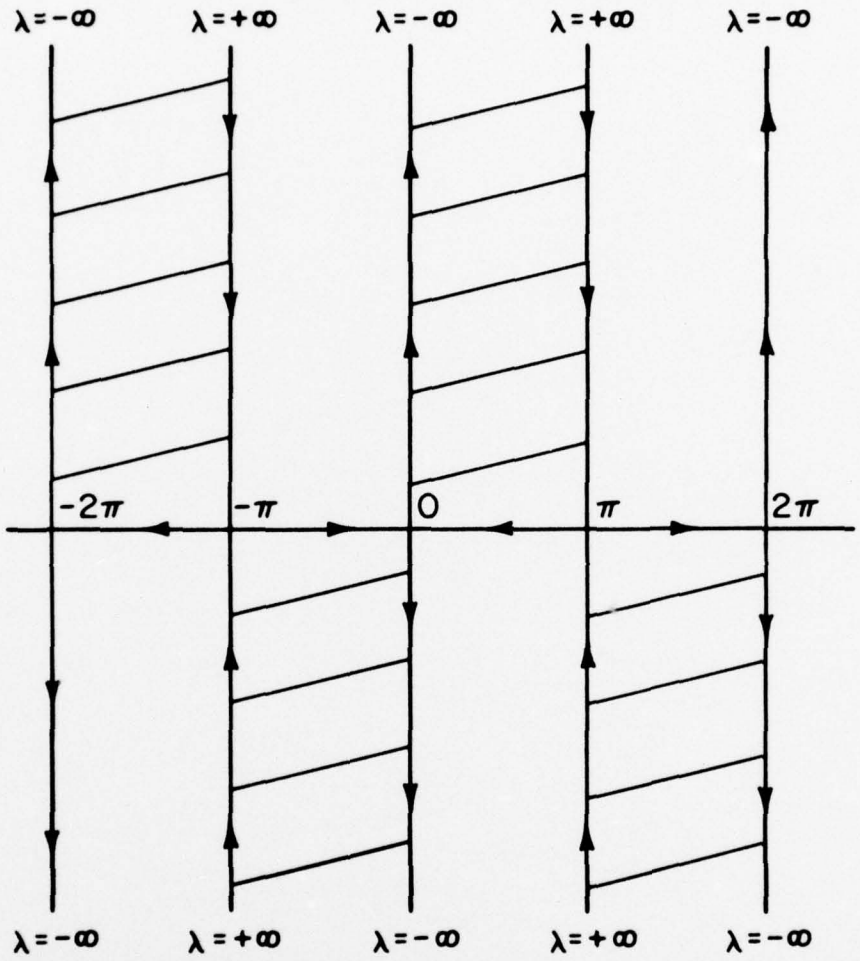

Figure 2.2. The γ-paths. Any path that connects the points $\lambda = -\infty$ to $\lambda = +\infty$ in the direction of the arrows is a possible γ-path.

complex α-plane, one must be careful to insure that the γ-path will lie in a region where the exponent will insure convergence of the integral. Thus one can find these regions in the α-plane by finding where the real part of the exponent is negative as follows:

$$\text{Re}\left[-ikr\left\{\cos(\phi-\alpha_r)\cosh\alpha_i \pm i\sinh\alpha_i \sin(\phi-\alpha_r)\right\}\right] < 0. \qquad (2.19)$$

Consider the case when $y > 0$, so one may choose the upper sign. Then the real part of the exponential becomes $kr\sinh\alpha_i\sin(\phi-\alpha_r)$. For $\alpha_i < 0$, then, $\sin(\phi-\alpha_r) > 0$ which implies

$$\phi + (2n-1)\pi \leq \alpha_r \leq \phi + 2n\pi \quad .$$

For $\alpha_i > 0$, then, $\sin(\phi-\alpha_r) < 0$, so that

$$\phi + 2n\pi \leq \alpha_r \leq \phi + (2n+1)\pi \quad .$$

For any arbitrary angle ϕ in the upper half-plane, the regions of convergence with a suitable γ-path are shown in Figure 2.3. The regions of convergence are of width π and also exhibit repetitive behavior.

The choice of the γ-path also will be sufficient to satisfy the Sommerfeld Radiation Condition. For the two-dimensional case of plane wave radiation, this condition is

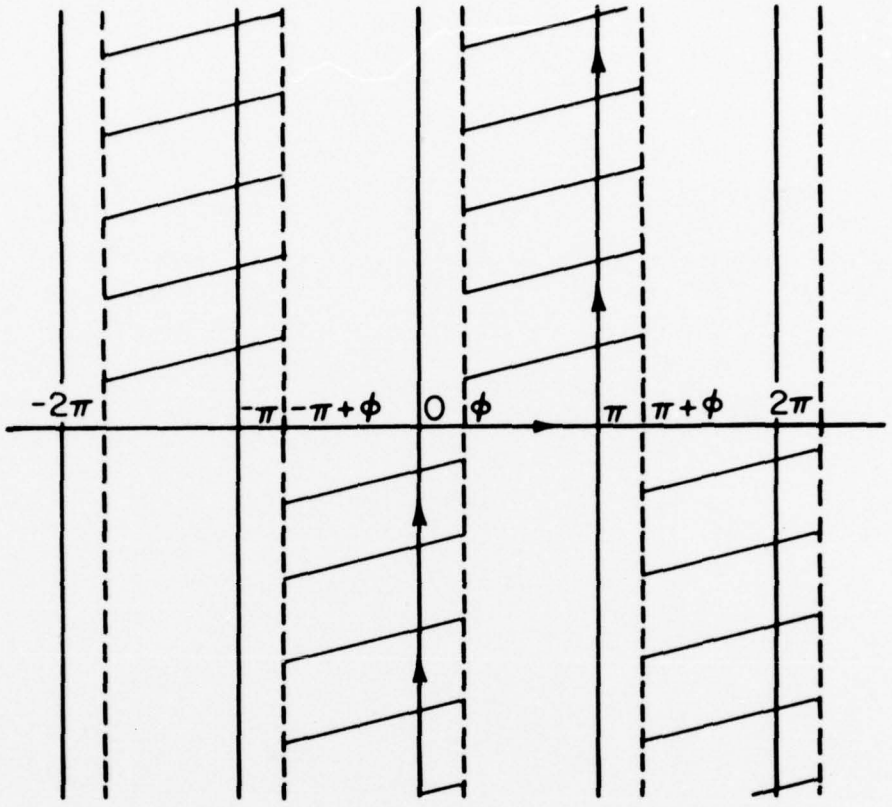

Figure 2.3. Regions of convergence with a suitable γ-path.

$$\lim_{r\to\infty} \left\{ \sqrt{r} \left[\frac{\partial p}{\partial r} + ikp \right] \right\} \to 0 \quad . \tag{2.20}$$

Substituting the expression for the scattered pressure into the Sommerfeld Radiation Condition yields

$$\lim_{r\to\infty} \left\{ \sqrt{r} \left[\int P(\cos\alpha)(1-\cos(\phi\mp\alpha))\ e^{-ikr\ \cos(\phi\mp\alpha)}\ d\alpha \right] \right\} \to 0 \quad . \tag{2.21}$$

Again, this limit can be satisfied if the γ-path lies in a region where the exponential decay allows convergence as r approaches infinity. Thus, the Sommerfeld Condition is satisfied by the proper choice of γ-path.

2.4 Formulation of the Integral Equations for an Incident Plane Wave

The preceding section shows that an integral representation for the scattered pressure does comply with one of the basic requirements for a solution. Specifically, it satisfies the homogeneous wave equation and the Sommerfeld Radiation condition through the choice of γ-path. In this section, the details of applying this representation to the diffraction of the half-plane with impedance boundary conditions will be worked out.

The diffracting obstacle is the half-plane defined by $x < o$, $y = o$ and $-\infty < z < +\infty$. The integral representation to be used is expressed in terms of polar coordinates so one measures angles from the positive x-axis. Thus, the upper surface of the half-plane is located at an angle $\phi = +\pi$, while the lower surface is located at

an angle $\phi = -\pi$. An incident plane wave can be represented as follows:

$$p_i = p_o e^{ikr\cos(\phi-\phi_o)} \quad . \tag{2.22}$$

The angle ϕ_o, also measured from the positive x-axis, will denote the angle of incidence. Finally, the upper and lower surfaces have impedances of Z^+ and Z^-, respectively. The geometry for the half-plane is depicted in Figure 2.4.

The surface impedance is the ratio of the total pressure at the surface to the outward normal component of the total velocity at the surface. The transverse component of velocity may be expressed in terms of the pressure p by

$$v_\phi = \frac{i}{k\rho c} \cdot \frac{1}{r} \frac{\partial p}{\partial \phi} \tag{2.23}$$

It follows that the transverse component of the velocity for the incident plane wave is given by

$$v_{i\phi} = \frac{i}{k\rho c r} \frac{\partial}{\partial \phi} \left[p_o e^{ikr\cos(\phi-\phi_o)} \right] ,$$

$$= \frac{p_o \sin(\phi-\phi_o)}{\rho c} \; e^{ikr\cos(\phi-\phi_o)} , \tag{2.24}$$

and also the velocity for the diffracted pressure is given by

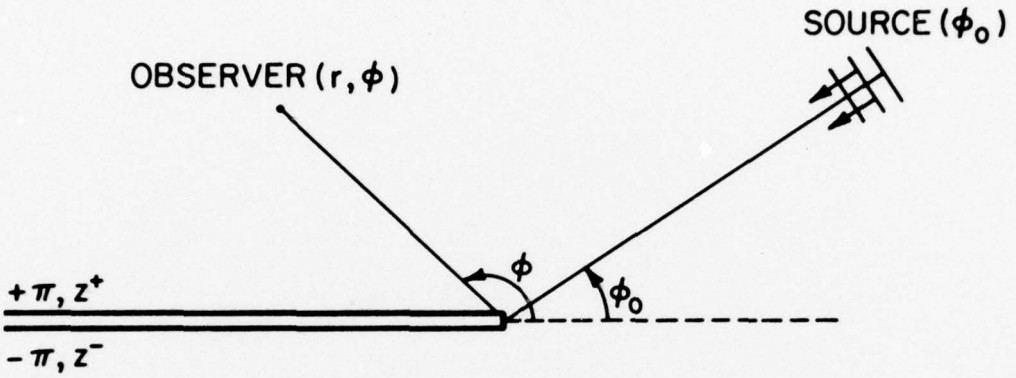

Figure 2.4. Geometry for the impedance covered half-plane.

$$v_\phi = \frac{i}{k\rho cr}\frac{\partial}{\partial\phi}\left[\int_\gamma P(\cos\alpha)\, e^{-ikrcos(\phi\mp\alpha)}\, d\alpha\right],$$

$$= \int_\gamma -\frac{\sin(\phi\mp\alpha)}{\rho c}\, P(\cos\alpha)\, e^{-ikrcos(\phi\mp\alpha)}\, d\alpha \quad . \tag{2.25}$$

The following boundary conditions at the upper and lower faces of the half-plane must be satisfied,

$$\frac{P_{tot}}{v_{tot}} = \frac{p_i+p}{(v_i+v)}\Bigg|_{\pm\pi} = z^{\pm} \tag{2.26}$$

or

$$p_i+p\Big|_{\pm\pi} = z^{\pm}(v_i+v)\Big|_{\pm\pi} \quad . \tag{2.27}$$

Using the expressions found in Equations (2.13), (2.22) (2.23) and (2.24) for the pressures and velocities, and from the boundary condition of Equation (2.27), one can determine specific relationships that satisfy the boundary conditions. The boundary condition for the upper surface at $\phi = \pi$ becomes:

$$\int_\gamma P(\cos\alpha)e^{ikrcos\alpha}d\alpha + p_o e^{-ikrcos\phi_o}$$

$$= -\frac{z^+}{\rho c}\int_\gamma \sin\alpha P(\cos\alpha)e^{ikrcos\alpha}d\alpha + \frac{p_o z^+ \sin\phi_o}{\rho c}\, e^{-ikrcos\phi_o} \quad . \tag{2.28}$$

A similar expression for the lower surface at $\phi = -\pi$ is

$$\int_{\gamma} P(\cos\alpha)e^{ikr\cos\alpha}d\alpha + p_o e^{-ikr\cos\phi_o}$$

$$= \frac{z^-}{\rho c}\int_{\gamma} \sin\alpha P(\cos\alpha)e^{ikr\cos\alpha}d\alpha - \frac{p_o z^-}{\rho c}\sin\phi_o e^{-ikr\cos\phi_o} \quad (2.29)$$

Let

$$\sin\theta^+ = \frac{\rho c}{z^+}$$

and

$$\sin\theta^- = \frac{\rho c}{z^-}\,, \quad (2.30)$$

where θ^+ and θ^- are known as Brewster angles. These angles have an important physical significance. There will be no reflection of a plane wave from an infinite plane if the angle of incidence of the plane wave is equal to the Brewster angle. In short, it is the angle of no reflection.

Using the relationships in Equation (2.30), Equations (2.28) and (2.29) may be rewritten as follows:

$$\int_{\gamma} P(\cos\alpha)(\sin\theta^+ + \sin\alpha)e^{ikr\cos\alpha}d\alpha = -p_o(\sin\theta^+ - \sin\theta_o)e^{-ikr\cos\phi_o} \quad (2.31)$$

and

$$\int_{\gamma} P(\cos\alpha)(\sin\theta^{-}-\sin\alpha)e^{ikr\cos\alpha}d\alpha = - p_o(\sin\theta^{-}+\sin\phi_o)e^{-ikr\cos\phi_o} \tag{2.32}$$

Equations (2.31) and (2.32) represent two integral equations that satisfy the impedance boundary conditions.

It is necessary that the integral representations for the pressure and the velocity be continuous in the physical space. There is a change in sign in the exponent of the integral representation as one crosses from the upper half-plane to the lower half-plane. To guarantee continuity, the pressure and velocity in the upper region, $y > 0$, and the pressure and velocity in the lower region, $y < 0$, must be equal where the two regions are joined; namely, at $\phi = 0^o$. The two regions are not joined together at π or $-\pi$ because the half-plane physically separates them. Checking the continuity of the pressure at $\phi = 0^o$, it follows from Equations (2.13) and (2.22) that

$$\int_{\gamma} P(\cos\alpha)e^{-ikr\cos\alpha}d\alpha + p_o e^{ikr\cos\phi_o}$$

$$= \int_{\gamma} P(\cos\alpha)e^{-ikr\cos\alpha}d\alpha + p_o e^{ikr\cos\phi_o} \quad . \tag{2.33}$$

This equation implies that the pressure is continuous. However, for the velocity at $\phi = 0$ one finds from Equations (2.24) and (2.25) that

$$\int_\gamma - \frac{P(\cos\alpha)\sin\alpha}{\rho c} e^{-ikr\cos\alpha} d\alpha + p_o e^{ikr\cos\phi_o}$$

$$= \int_\gamma \frac{P(\cos\alpha)\sin\alpha}{\rho c} e^{-ikr\cos\alpha} d\alpha + \frac{p_o \sin\phi_o}{\rho c} e^{ikr\cos\phi_o} , \qquad (2.34)$$

which, when simplified, becomes:

$$\int_\gamma P(\cos\alpha)\sin\alpha\ e^{-ikr\cos\alpha} d\alpha = \int_\gamma -P(\cos\alpha)\sin\alpha\ e^{-ikr\cos\alpha} d\alpha . \qquad (2.35)$$

The three integral Equations (2.31), (2.32) and (2.35) are a set of integral equations that satisfy all the requirements for a solution to this diffraction problem. Specifically, these equations satisfy the wave equation and the impedance boundary conditions for an incident plane wave. To solve the problem one must determine some function $P(\cos\alpha)$, still unkonwn, that will satisfy all of these integral equations.

2.5 The Solution of the Integral Equations for Plane Wave Incidence

Solving for the function $P(\cos\alpha)$ is undoubtedly the most onerous detail of this study. One attempts to construct the unknown function $P(\cos\alpha)$ by considering functions with properties that are sufficient to satisfy each of the integral equations.

Toward this end, one seeks to close some γ-path within a region of convergence and then evoke the Cauchy Integral Theorem to determine the nature of $P(\cos\alpha)$. If the Cauchy Integral Theorem is to apply, then certain restrictions are subsequently imposed upon the functional

behavior of $P(\cos\alpha)$. From these restrictions one deduces a functional form for $P(\cos\alpha)$. If this procedure can be accomplished, one has a solution to the diffraction problem.

To initiate this procedure, one must specify a γ-path and the regions of convergence through which the γ-path may be closed. Starting with the integral Equations (2.31) and (2.32) corresponding to the boundary conditions at $\phi = \pm\pi$, and recalling the earlier section defining the regions of convergence in Equations (2.21) and (2.22), it follows that these regions are

for $\alpha_i < 0$

$$2n\pi \leq \alpha_r \leq (2n+1)\pi ,$$

and for $\alpha_i > 0$

$$(2n-1)\pi \geq \alpha_r \leq 2n\pi .$$

Figure 2.5 shows representative γ-paths and how they may be closed. For example, one such path originates at $-i\infty$, travels to 0, then to π and terminates at $\pi-i\infty$. It is then closed at infinity along the line from $\pi-i\infty$ to $-i\infty$. In order to close the path in this manner, it will be convenient if the integral along the part of the path at infinity is zero. For this condition to be valid, certain restrictions on the behavior of the function $P(\cos\alpha)$ at infinity must be imposed. In particular, this condition maintains that the absolute value of $P(\cos\alpha)$ must be bounded at infinity. The condition on $P(\cos\alpha)$ is

$$\left| P(\cos\alpha) \right| \leq \frac{M}{(\cos\alpha)^{\delta}} \qquad \text{as } \alpha_i \to \infty \tag{2.36}$$

and for $\delta > 0$.

Now consider, for example, the integral Equation (2.31):

$$\int_{\gamma} P(\cos\alpha)(\sin\theta^{+}+\sin\alpha)e^{ikr\cos\alpha}d\alpha = p_o(\sin\theta^{+}-\sin\phi_o)e^{-ikr\cos\alpha}.$$

If the γ-path is closed in the manner described, one finds that the integral around a closed path equals the value of the right hand side of the equation which is $p_o(\sin\theta^{+}-\sin\phi_o)e^{-ikr\cos\phi_o}$. By virtue of the Cauchy Integral Formula, this means that there must be simple poles at $(2n-1)\pi\pm\phi_o$ and the residues are $\frac{p_o}{2\pi}(\sin\theta^{+}-\sin\phi_o)e^{-ikr\cos\phi_o}$ for some γ-path, see Figure 2.5. Likewise, the integral in Equation (2.32) also suggest the existence of poles, but with a residue of $\frac{p_o}{2\pi i}(\sin\theta^{-}+\sin\phi_o)e^{-ikr\cos\phi_o}$, for some γ-paths. There are two major features about the behavior of $P(\cos\alpha)$. They are:

1. $P(\cos\alpha)$ is bounded for $\alpha_i \to \infty$.
2. $P(\cos\alpha)(\sin\theta^{\pm}\pm\sin\alpha)$ has simple poles at $(2n-1)\pi\pm\phi_o$ and corresponding residues of $\frac{p_o}{2\pi i}(\sin\theta^{\pm}\ \sin\phi_o)e^{-ikr\cos\phi_o}$.

On the basis of this limited knowledge, the function $P(\cos\alpha)$ must be deduced.

It is difficult to proceed without giving some considerations to the physics of the problem. In particular, each of the poles at $(2n-1)\pi\pm\phi_o$ have distinct physical significance. As has been

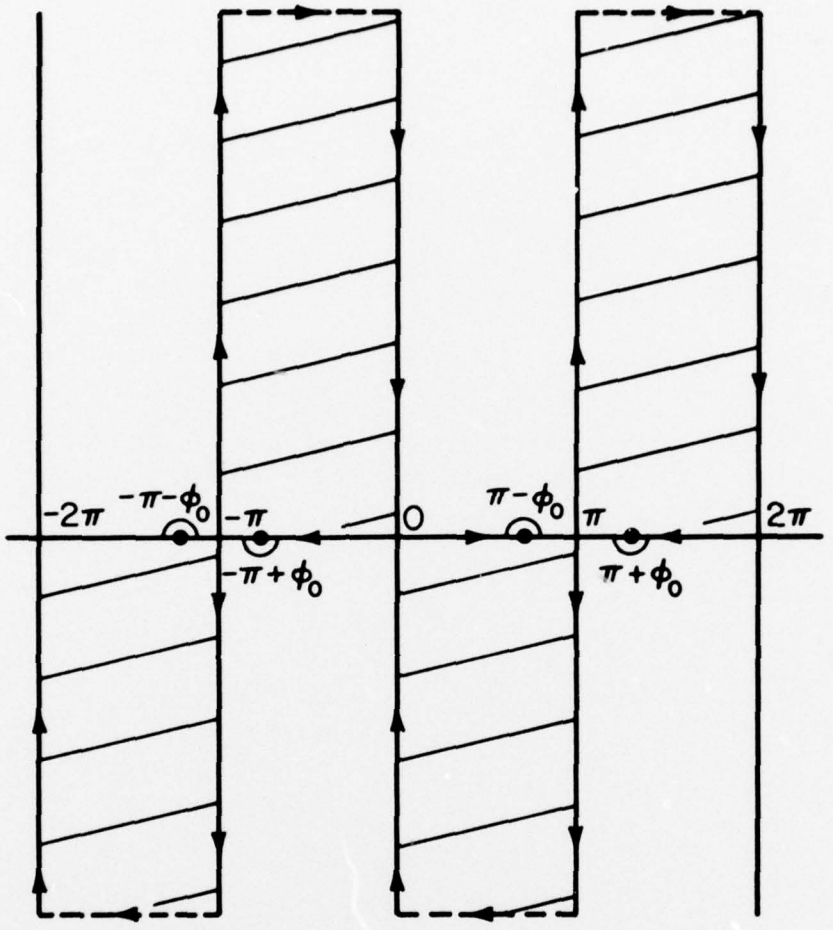

Figure 2.5. The γ-paths being closed at infinity in the shaded regions of convergence along the dotted lines.

previously discussed, there is a multiplicity behavior in the complex α-plane, so the poles $-\pi-\phi_o$, $-\pi+\phi_o$, $\pi-\phi_o$, and $\pi+\phi_o$ represent a family that will subsequently be repeated. These poles represent the following physical significance:

a. $-\pi-\phi_o$ represents the angle of the specular reflection from the lower surface.

b. $-\pi+\phi_o$ represents the angle of the geometric shadow boundary.

c. $\pi-\phi_o$ represents the angle of the specular reflection from the upper surface.

d. $\pi+\phi_o$ represents the angle of the geometric shadow boundary.

For example, when the pole of Equation (2.37a) representing the reflection from the lower surface is enclosed by a γ-path, Equation (2.32) must be satisfied. Likewise, when the pole in Equation (2.37c) representing the reflection from the upper surface is enclosed, it must satisfy the other integral Equation (2.31). To accommodate all these requirements, the solution is considered as a product of two parts. One part contains the necessary singularities while the other part contains an analytic function that adjusts the residues to the proper values.

Two functions that have the proper singularities are chosen as

$$\frac{1}{\sin\frac{\alpha+\pi}{2} - \sin\frac{\phi_o}{2}} \tag{2.38}$$

and

$$\frac{1}{\sin\frac{\alpha-\pi}{2} - \sin\frac{\phi_o}{2}} \quad . \tag{2.39}$$

If the first function in Equation (2.38) is enclosed by a γ-path that includes a simple pole at $\pi-\phi_o$, the reflection from the upper surface, one must modify the function to yield the appropriate residue. Such a function that will provide the proper residue is found by trial and error to have the form:

$$\frac{p_o \cos\phi_{o/2}}{2\pi i \cos\phi_{o/2}} \frac{(\sin\phi_o - \sin\theta^+)}{(\sin\theta^- + \sin\phi_o)} \frac{(\sin\theta^- + \sin\phi_o)}{(\sin\theta^+ + \sin\phi_o)} e^{-ikr\cos\phi_o}$$

$$= \frac{p_o}{2\pi i} \frac{(\sin\phi_o - \sin\theta^+)}{(\sin\phi_o + \sin\theta^+)} e^{-ikr\cos\phi_o} .$$

This happens to be exactly what is necessary to satisfy Equation (2.31).

Consider the function in Equation (2.39) and enclose the simple pole at $\phi = -\pi - \phi_o$ for the reflection from the lower surface. A suitable choice that will satisfy Equation (2.32) is

$$- \frac{p_o \cos\frac{\phi_o}{2}}{\left[4\pi i \sin\left(\frac{\alpha-\pi}{2}\right) - \sin\frac{\phi_o}{2}\right]}$$

$$\times \frac{(\sin\alpha + \sin\theta^-)\left(\sin\theta^+ + 2\cos\frac{\alpha}{2}\left[\cos\left(\frac{\alpha+\phi_o-\pi}{4}\right) - \sin\left(\frac{\alpha-\phi_o-\pi}{4}\right)\right]\right)}{\left(\sin\theta^+ + 2\cos\frac{\alpha}{2}\cos\frac{\phi_o}{2}\right)\left(\sin\theta^- + 2\cos\frac{\alpha}{2}\left[\cos\left(\frac{\alpha+\phi_o-\pi}{4}\right) - \sin\left(\frac{\alpha-\phi_o-\pi}{4}\right)\right]\right)} . \quad (2.41)$$

Again, the residue at $\phi = -\pi - \phi_o$ is given by

$$\frac{p_o \cos\frac{\phi_o}{2} (\sin\phi_o + \sin\theta^-)(\sin\phi_o - \sin\theta^+)}{4\pi i \frac{1}{2} \cos\frac{\phi_o}{2} (\sin\theta^+ - \sin\phi_o)(\sin\theta^- - \sin\phi_o)} e^{-ikr\cos\phi_o}$$

$$= \frac{p_o}{2\pi i} \frac{(\sin\phi_o + \sin\theta^-)}{(\sin\theta^- - \sin\phi_o)} e^{-ikr\cos\phi_o} ,$$

which is what is required by Equation (2.32). The sum of the two functions in Equations (2.40) and (2.41) then represents $P(\cos\alpha)$. Separately, the two functions represent the contribution to the diffracted field due to the influence of the upper and lower surfaces, respectively. In the parlance of Riemann sheets, they correspond to the solution in two separate sheets. The continuity Equation (2.35) implies that the solution $P(\cos\alpha)$ is continuous where they join or overlap; namely, at the shadow boundaries. As a result, if the integral is closed by a γ-path that encloses the geometric shadow boundary located at $-\pi+\phi_o$ and, again, if the integral is closed by a γ-path surrounding the shadow boundary located at $\pi+\phi_o$, these two must satisfy Equation (2.35).

If one checks this requirement for the assumed functions of Equations (2.40) and (2.41), one finds that the residues at the poles $-\pi+\phi_o$ and $\pi+\phi_o$ in Equation (2.35) are, respectively:

$$\frac{p_o \cos\phi_o}{2\pi i \cos\phi_o} \frac{(\sin\theta^+ + \sin\phi_o)(\sin\theta^- + \sin\phi_o)\sin\phi_o \; e^{-ikr\cos\phi_o}}{(\sin\theta^- + \sin\phi_o)(\sin\theta^+ + \sin\phi_o)}$$

$$= -\frac{p_o \sin\phi_o}{2\pi i} e^{-ikr\cos\phi_o}$$

and

$$+ \frac{p_o \cos\frac{\phi_o}{2}\,(\sin\theta^- - \sin\phi_o)(\sin\theta^+ - \sin\phi_o)\sin\phi_o\; e^{-ikr\cos\phi_o}}{2\pi i \cos\frac{\phi_o}{2}\,(\sin\theta^+ - \sin\phi_o)(\sin\theta^- - \sin\phi_o)}$$

$$= \frac{p_o \sin\phi_o}{2\pi i}\, e^{-ikr\cos\phi_o} .$$

From this result, Equation (2.35) is also satisfied. Therefore, the solution for $P(\cos\alpha)$ is given by

$$P(\cos\alpha) = -\frac{p_o \cos\frac{\phi_o}{2}}{4\pi i\left[\sin\left(\frac{\alpha+\pi}{2}\right) - \sin\frac{\phi_o}{2}\right]}$$

$$\left\{\frac{(\sin\alpha - \sin\theta^+)\left(\sin\theta^- 2\cos\frac{\alpha}{2}\left[\cos\left(\frac{\alpha+\phi_o+\pi}{4}\right)+\sin\left(\frac{\alpha-\phi_o+\pi}{4}\right)\right]\right)}{\left(\sin\theta^- + 2\cos\frac{\alpha}{2}\cos\frac{\phi_o}{2}\right)\left(\sin\theta^+ + 2\cos\frac{\alpha}{2}\left[\cos\left(\frac{\alpha+\phi_o+\pi}{4}\right)+\sin\left(\frac{\alpha-\phi_o+\pi}{4}\right)\right]\right)}\right\}$$

$$- \frac{p_o \cos\frac{\phi_o}{2}}{4\pi i\left[\sin\frac{\alpha-\pi}{2} - \sin\frac{\phi_o}{2}\right]}$$

$$\left\{\frac{(\sin\alpha + \sin\theta^-)\left(\sin\theta^+ + 2\cos\frac{\alpha}{2}\left[\cos\left(\frac{\alpha+\phi_o-\pi}{4}\right)-\sin\left(\frac{\alpha-\phi_o-\pi}{4}\right)\right]\right)}{\left(\sin\theta^+ + 2\cos\frac{\alpha}{2}\cos\frac{\phi_o}{2}\right)\left(\sin\theta^- + 2\cos\frac{\alpha}{2}\left[\cos\left(\frac{\alpha+\phi_o-\pi}{4}\right)-\sin\left(\frac{\alpha-\phi_o-\pi}{4}\right)\right]\right)}\right\}$$

$$= \frac{p_o \cos\frac{\phi_o}{2}}{4\pi i}\left\{\frac{\Psi_1(\alpha)}{\left[\sin\frac{\alpha+\pi}{2} - \sin\frac{\phi_o}{2}\right]} + \frac{\Psi_2(\alpha)}{\left[\sin\left(\frac{\alpha-\pi}{2}\right) - \sin\frac{\phi_o}{2}\right]}\right\} , \qquad (2.42)$$

where

$$\Psi_{1,2}(\alpha)$$

$$= \frac{(\sin\alpha \mp \sin\theta^{\pm})\left(\sin\theta^{\mp}+2\cos\frac{\alpha}{2}\left[\cos\left(\frac{\alpha+\phi_o \pm\pi}{4}\right) \pm\sin\left(\frac{\alpha-\phi_o \pm\pi}{4}\right)\right]\right)}{\left(\sin\theta^{\mp}+2\cos\frac{\alpha}{2}\cos\frac{\phi_o}{2}\right)\left(\sin\theta^{\pm}+2\cos\frac{\alpha}{2}\left[\cos\left(\frac{\alpha+\phi_o \pm\pi}{4}\right) \pm\sin\left(\frac{\alpha-\phi_o \pm\pi}{4}\right)\right]\right)} \quad (2.43)$$

All that remains to be done for the solution of the diffracted field is to evaluate the integral in Equation (2.13) using the solution shown in Equation (2.42) for the function P(cosα).

2.6 The Far-Field Solution by the Method of Steepest Descent

To find the far-field solution for the diffracted pressure when kr is large, one may use the method of steepest descent which is also known as the saddle point method. Essentially, the method is one of finding the saddle point and integrating on the path of steepest descent through the saddle point. Along this path, the major contribution to the integral will result near the saddle point. If the γ-path is closed along the steepest descent path, then the value of the integral on γ can be replaced by the steepest descent approximation at the saddle point plus any enclosed residues.

Consider the integral in Equation (2.13):

$$p(r,\phi) = \int_{\gamma} P(\cos\alpha)\, e^{-ikr\cos(\phi \mp \alpha)}\, d\alpha \ ,$$

for the case when $0<\phi<\pi$ so one may pick the upper sign. The saddle point is that point where the exponent has an extremum, i.e. when

$$\frac{\partial}{\partial\alpha}\,(-ikr\cos(\phi-\alpha)) = 0$$

or

$$-ikr\sin(\phi-\alpha) = 0$$

and the saddle points are located at

$$\alpha = \phi \pm 2n\pi \quad . \tag{2.44}$$

The corresponding steepest descent paths are determined by

$$\mathrm{Im}[-ikr\cos(\phi-\alpha)] = I_m[-ikr] \equiv \text{constant}$$

which is

$$-ikr\cos(\phi-\alpha_r)\cosh\alpha_i = -ikr$$

or

$$\cos(\phi-\alpha_r)\cosh\alpha_i = 1 \quad . \tag{2.45}$$

Write Equation (2.43) as

$$\cos(\phi-\alpha_r) = \frac{1}{\cosh\alpha_i} \quad ;$$

then, for $\alpha_i \to \pm\infty$,

$$\cos(\phi-\alpha_r) = 0$$

or

$$a_r = \phi \pm (2n-1)\frac{\pi}{2} \quad . \tag{2.46}$$

Equation (2.46) predicts the asymptotes of the paths as they tend to infinity.

Finding the slope of the path is also useful in locating this path. The slope is determined from the following:

$$\frac{d\alpha_i}{d\alpha_r} = -\frac{\sin(\phi-\alpha_r)\cosh^2\alpha_i}{\sinh\alpha_i}$$

$$= \pm \frac{\sqrt{1-\cos^2(\phi-\alpha_r)\cosh^2\alpha_i}}{\sqrt{\cosh^2\alpha_i - 1}}$$

$$= \pm \frac{\sqrt{\dfrac{\cosh^2\alpha_i - 1}{\cosh^2\alpha_i}}}{\sqrt{\cosh^2{}_i - 1}} \cdot \cosh^2\alpha_i$$

$$= \pm \cosh\alpha_i \quad . \tag{2.47}$$

From Equation (2.47), the slope at the saddle point, $\alpha_i = 0$, is 1 and the slope of the asymptotes are $\pm\infty$. As a result of Equations

(2.46) and (2.47), the steepest descent path is shown in Figure 2.6. For an observer angle $\pi-\phi_o<\phi<\pi$, the steepest descent path is chosen according to Equations (2.46) and (2.47) and the requirement that it also must lie in a shaded region of convergence. It should be noted that the pole at $\pi-\phi_o$ is contained within the closed path.

To determine the far-field solution, use the Residue Theorem to evaluate the integral over the γ-path.

Using the Residue Theorem yields

$$\int_\gamma P(\cos\alpha)\, e^{-ikr\cos\phi-\alpha}\, d\alpha + \int_{SDP} P(\cos\alpha)\, e^{-ikr\cos(\phi-\alpha)}\, d\alpha$$

$$- \pi i\, \mathrm{Res}(\pi-\phi_o) = -2\pi i\, \mathrm{Res}(\pi-\phi_o) \quad .$$

Then using the steepest descent approximation, Erdelyi [14], it follows that

$$\int_\gamma P(\cos\alpha)\, e^{-ikr\cos(\phi-\alpha)}\, d\alpha = - \pi i\, \mathrm{Res}(\pi-\phi_o)$$

$$-\int_{SDP} P(\cos\alpha)\, e^{-ikr\cos(\phi-\alpha)}\, d\alpha$$

$$= - \frac{p_o}{2}\left(\frac{\sin\phi_o-\sin\theta^+}{\sin\phi_o+\sin\theta^+}\right) e^{ikr\cos(\phi-\phi_o)}$$

$$+ \left[\frac{2\pi}{kr}\right]^{1/2} \frac{e^{-ikr}}{4\pi i}\, e^{i\pi/4}\, p_o \cos\phi_{o/2}$$

$$\times\left\{\frac{\Psi_1(\phi)}{\left[\sin\left(\frac{\phi+\pi}{2}\right) - \sin\frac{\phi_o}{2}\right]} + \frac{\Psi_2(\phi)}{\left[\sin\left(\frac{\phi-\pi}{2}\right) - \sin\frac{\phi_o}{2}\right]}\right\}$$

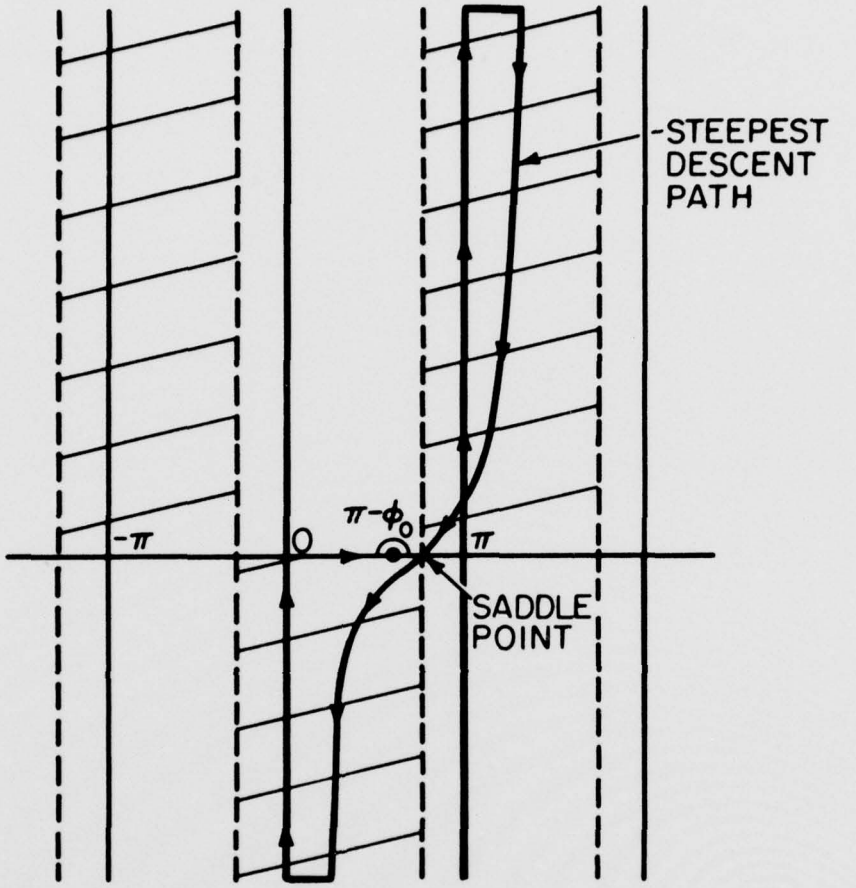

Figure 2.6. Steepest descent path for the far-field pre[illegible] with $\pi-\phi_o < \phi < \pi$.

for kr large

$$\int_{\gamma} P(\cos\alpha)\, e^{-ikr\cos(\phi-\alpha)}\, d\alpha = \frac{P_o}{2} C_r\, e^{-ikr\cos(\phi-\phi_o)} + \frac{e^{i\pi/4} e^{-ikr} p_o \cos\phi_o/2}{2\sqrt{2\pi kr}} \left\{ \frac{\Psi_1(\phi)}{\left[\sin\frac{\phi+\pi}{2} - \sin\frac{\phi_o}{2}\right]} + \frac{\Psi_2(\phi)}{\left[\sin\left(\frac{\phi-\pi}{2}\right) - \sin\frac{\phi_o}{2}\right]} \right\} , \tag{2.48}$$

where

$$C_r = \frac{\left(\sin\theta^{+} - \sin\phi_o\right)}{\left(\sin\phi_o + \sin\theta^{+}\right)}$$

is the reflection coefficient and $\Psi_{1,2}$ are defined in Equation (2.43). It is interesting to note that the residue of the pole that is surrounded by the closed path contributes the geometrical optic term, namely, the specular reflection, while the steepest descent path contributes the diffraction term. Consequently, the far-field diffraction, without the geometrical optic terms, can be expressed simply as

$$P_d(r,\phi) = \frac{e^{i\pi/4} e^{-ikr} p_o \cos\phi_o/2}{2\sqrt{2\pi kr}} \left\{ \frac{\Psi_1(\phi)}{\left[\sin\left(\frac{\phi+\pi}{2}\right) - \sin\frac{\phi_o}{2}\right]} \quad \frac{\Psi_2(\phi)}{\left[\sin\left(\frac{\phi-\pi}{2}\right) - \sin\frac{\phi_o}{2}\right]} \right\}. \tag{2.49}$$

Next, consider the case when the observer angle ϕ is $0<\phi<\pi-\phi_o$. The path is closed along the steepest descent path but the pole at $\pi-\phi_o$ is surrounded in a different manner as indicated in Figure 2.7. This causes a change in sign of the geometric term in Equation (2.49) and the solution in this region becomes

$$P(r,\phi) = \int_\gamma P(\cos\alpha)\, e^{-ikr\cos(\phi-\alpha)}\, d\alpha$$

$$= -\frac{P_o}{2} C_r\, e^{+ikr\cos(\phi-\phi_o)} + P_d(r,\phi) \quad . \tag{2.50}$$

This jump in the specular term physically represents the sudden transition across the reflection shadow boundary at $\pi-\phi_o$. In short, one finds that there are three distinct regions to the solution; these regions are listed in Table 2.2 and the corresponding physical regions are shown in Figure 2.8.

Table 2.2. The three regions for the far-field solution.

Region I $\pi - \phi_o < \phi < \pi$	$P_{diffraction} + P_{reflection} + P_{inc}$
Region II $-\pi + \phi_o < \phi < \pi - \phi_o$	$P_{diffraction} + P_{inc}$
Region III $-\pi < \phi < -\pi + \phi$	$P_{diffraction}$

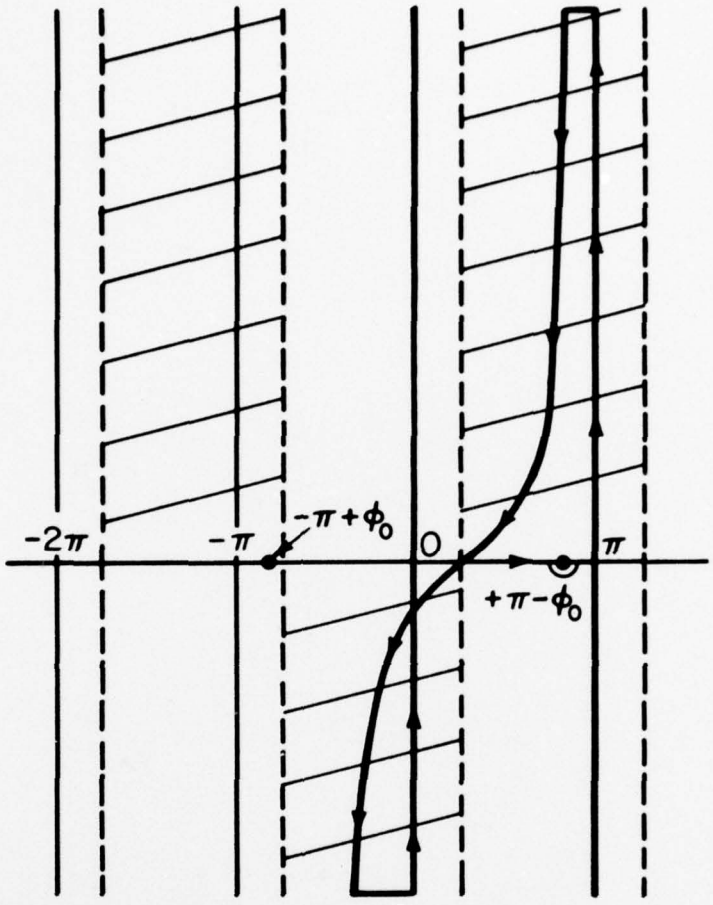

Figure 2.7. Steepest descent path for the far-field with $0 < \phi < \pi-\phi_o$.

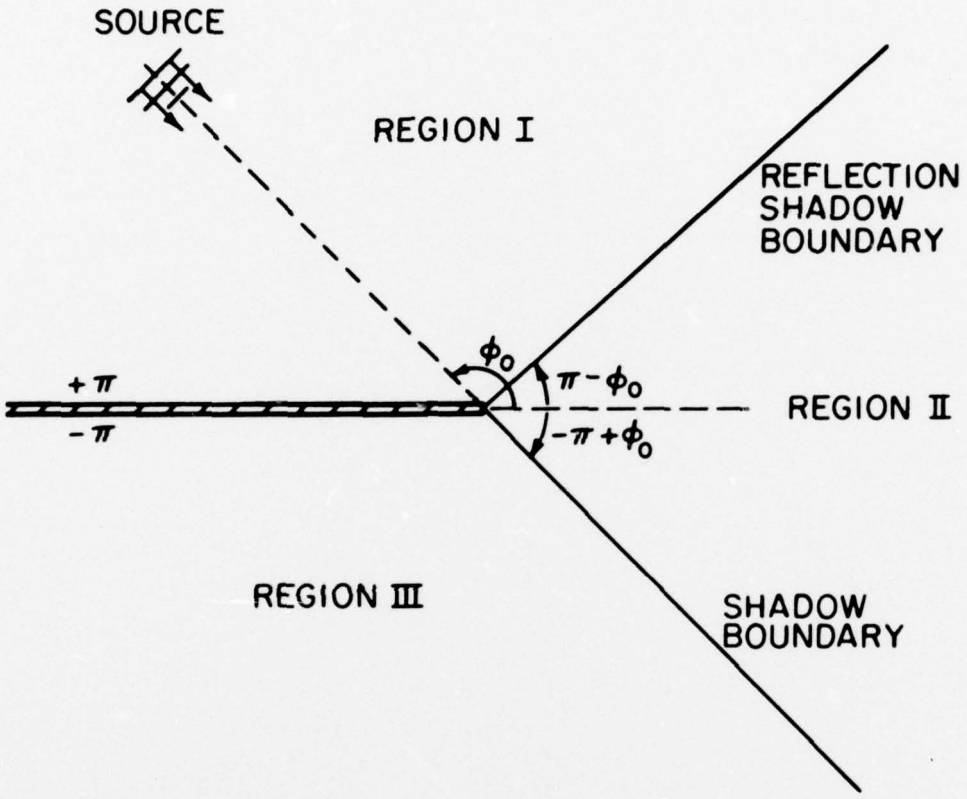

Figure 2.8. The three regions for the far-field pressure solution.

The far-field solution is helpful in searching for the nulls in the diffracted and backscattered field. If the solution is considered in the form shown in Equation (2.49), an expression for the zeroes of the diffracted and backscattered pressures may be found.

For the case of diffraction an expression that locates the nulls may be determined if both surfaces have the same real impedance. This expression is given by

$$\sin\phi/2 = \frac{1}{2}\frac{\sin\theta}{\sin\phi_{o/2}} \quad , \tag{2.51}$$

where $\theta=\theta^{+}=\theta^{-}=\rho c/z$.

It may be determined from Equation (2.51), that when the impedance is real there can be at most one null in the diffraction function. An expression may also be found for the nulls of the backscattered pressure. In this case there can be at most two nulls in the solution, if the impedance is real. When the impedances are the same on both surfaces, the expression for the location of the nulls is given by

$$\sin\phi = \sqrt{\frac{1}{2}\sin\theta} \quad . \tag{2.52}$$

2.7 The Near-Field Solution for the Diffraction of a Plane Wave

In the far-field approximation, one notices a jump at the geometrical shadow boundaries. In reality the transition across the shadow boundaries is continuous. This contridiction occurs because the steepest descent approximation is not valid if the saddle point is in the vicinity of a pole. As a result, an exact solution is

needed to evaluate the solution there and in the near-field of the edge.

To achieve an exact solution, consider $P(\cos\alpha)$ in the form

$$P(\cos\alpha) = \frac{\Phi_1(\alpha)}{\cos\left(\frac{\alpha+\phi_o}{2}\right)} + \frac{\Phi_2(\alpha)}{\cos\left(\frac{\alpha-\phi_o}{2}\right)} \quad , \tag{2.53}$$

where the functions $\Phi_{1,2}(\alpha)$ are defined as:

$$\Phi_{i,2}(\alpha) = \frac{P_o}{4\pi i}\left\{\frac{A(\theta^{\pm},\alpha)}{B(\theta^{\pm},\alpha)} + \frac{A(\theta^{\mp},\alpha)}{B(\theta^{\mp},\alpha)} \pm \left[\frac{A(\theta^{\mp},\alpha)}{B(\theta^{\mp},\alpha)} + \frac{A(\theta^{\pm},\alpha)}{B(\theta^{\pm},\alpha)}\right]\cos\left(\frac{\alpha\pm\theta_o}{2}\right) + \frac{C(\theta^{+},\theta^{-},\alpha)}{B(\theta^{+},\alpha)\cdot B(\theta^{-},\alpha)}\right\}, \tag{2.54}$$

where

$$A(\theta^{\pm},\alpha) = (\sin\theta^{\pm} \mp \sin\alpha)\left(\sin\theta^{\mp} + 2\cos\alpha/2\left[\cos\left(\frac{\alpha+\phi_o\pm\pi}{4}\right) \pm \sin\left(\frac{\alpha-\phi_o\pm\pi}{4}\right)\right]\right), \tag{2.55}$$

$$\beta(\theta^{\pm},\alpha) = (\sin\theta^{\pm} + 2\cos\alpha/2\,\cos\phi_o/2)\left(\sin\theta^{\mp} + 2\cos\alpha/2\left[\cos\left(\frac{\alpha+\phi_o\pm\pi}{4}\right) \pm \sin\left(\frac{\alpha-\phi_o\pm\pi}{4}\right)\right]\right), \tag{2.56}$$

and

$$C(\theta^{+},\theta^{-},\alpha) = (\sin\theta - \sin\theta)\sin\frac{\phi_o}{2}\cdot(D\cdot\sin\theta^{+}\cdot\sin\theta^{-} + [\sin\theta^{+}+\sin\theta^{-}] \cdot E + 2\cos\alpha/2\,\cos\phi_{o/2}\cdot E),$$

with

$$D = \left(\cos\left(\frac{\alpha+\phi_o+\pi}{4}\right) + \cos\left(\frac{\alpha+\phi_o-\pi}{4}\right) + \sin\left(\frac{\alpha-\phi_o+\pi}{4}\right) - \sin\left(\frac{\alpha-\phi_o-\pi}{4}\right) - \cos\phi_{o/2}\right),$$

and

$$E = 2\cdot\cos\alpha/2\cdot\left[\cos\left(\frac{\alpha+\phi_o+\pi}{4}\right) + \sin\left(\frac{\alpha-\phi_o+\pi}{4}\right)\right]\cdot\left[\cos\left(\frac{\alpha+\phi_o-\pi}{4}\right) - \sin\left(\frac{\alpha-\phi_o-\pi}{4}\right)\right].$$

(2.57)

A special case exists when one surface is rigid; i.e., θ^+ or θ^- equals zero. In this event then, Φ_1 and Φ_2 can be simplified into the form

$$\Phi_{1,2}(\alpha) = \frac{P_o}{4\pi i}$$

$$\left[\pm (\sin\theta^+ \sin\alpha)(\sin\theta^+ + 2\cos\alpha/2\cdot\cos\phi_{o/2}\cdot\sin\left(\frac{\alpha\pm\pi\pm\phi_o}{4}\right)\right.$$

$$- \left(\sin\theta^+ + 4\cdot\cos\alpha/2\cdot\cos\alpha/4\cdot\cos\left(\frac{\phi_o-\pi}{4}\right)\right)\cdot\left(\sin\theta^+ + 4\cos\alpha/2\ \cos\alpha/4\cdot\cos\left(\frac{\phi_o+\pi}{4}\right)\right.$$

$$\left.\left.\cos\left(\frac{\alpha\pm\pi\pm\phi_o}{4}\right)\right]\right.$$

$$\times \frac{1.0}{\left[\sin\theta^+ + 4\cos\alpha/2\cdot\cos\alpha/4\cdot\cos\left(\frac{\phi_o+\pi}{4}\right)\right]\left[\sin\theta^+ + 2\cos\alpha/2\cdot\cos\phi_{o/2}\right]},$$

(2.58)

when $\theta^- = 0^\circ$

and

$$\Phi_{2,1}(\alpha) = \frac{P_o}{4\pi i}$$

$$\left[(\sin\theta^- \mp \sin\alpha)\ \sin\theta^- + 2\cos\alpha/2 \cdot \cos\phi_{o/2} \cdot \cos\left(\frac{\alpha \pm \pi \mp \phi_o}{4}\right) \right.$$

$$\mp \left(\sin\theta^- + 4 \cdot \cos\alpha/2 \cdot \cos\alpha/4 \cdot \cos\left(\phi_{o/4} - \pi/4\right) \right)$$

$$\left. \left(\sin\theta^- + 4 \cdot \cos\alpha/2 \cdot \cos\alpha/4 \cdot \cos\left(\frac{\phi_o + \pi}{4}\right) \sin\left(\frac{\alpha \pm \pi \mp \phi_o}{4}\right) \right) \right]$$

$$\times \frac{1.0}{\left[\sin\theta^- + 4 \cdot \cos\alpha/2 \cdot \cos\alpha/4 \cdot \cos\left(\frac{\phi_o + \pi}{4}\right) \right] \left[\sin\theta^- + 2 \cdot \cos\alpha/2 \cdot \cos\phi_{o/2} \right]} \tag{2.59}$$

when $\theta^+ = 0^o$.

The singularities of P(cos) are contained in the terms that appear in the denominator of Equation (2.53) while the functions $\Phi_{i,2}(\alpha)$ are smooth and well behaved.

One seeks to find the near-field solution by closing the γ-path along the steepest descent path and then evaluating the integral along the entire length of this path rather than just at the saddle point. To achieve this, consider the integral along the steepest descent path as

$$\int_{SDP} P(\cos\alpha)\, e^{-ikr\cos(\phi-\alpha)}\, d\alpha$$

$$= \int_{SDP} \left[\frac{\Phi_1(\alpha)}{\cos\left(\frac{\alpha+\phi_o}{2}\right)} + \frac{\Phi_2(\alpha)}{\cos\left(\frac{\alpha-\phi_o}{2}\right)} \right] e^{-ikr\cos(\phi-\alpha)}\, d\alpha \quad . \qquad (2.60)$$

It may be argued that since $\Phi_1(\alpha)$ and $\Phi_2(\alpha)$ are smooth and slowly varying functions near the saddle point, then they may be removed from under the integral in Equation (2.56) and evaluated at the saddle point $\alpha=\phi$. This results in the following integral along the steepest descent path:

$$\int_{SDP} P(\cos\alpha)\, e^{-ikr\cos(\phi-\alpha)}\, d\alpha$$

$$= \Phi_1(\phi) \int_{SDP} \frac{e^{-ikr\cos(\phi-\alpha)}\, d\alpha}{\cos\left(\frac{\alpha+\phi_o}{2}\right)} + \Phi_2(\alpha) \int_{SDP} \frac{e^{-ikr\cos(\phi-\alpha)}\, d\alpha}{\cos\left(\frac{\alpha-\phi_o}{2}\right)} \quad . \qquad (2.61)$$

For the moment, consider only the first integral with a change of variable $\alpha=\phi-\alpha$. This change of variable will affect the γ-path, the regions of convergence, and the steepest descent path merely by a lateral shift of the angle ϕ. In particular, the equation for the steepest descent path becomes

$$\cos\alpha_r = \frac{1}{\cosh\alpha_i} \quad . \qquad (2.62)$$

This change of variable transforms the first term in Equation (2.61) to

$$\Phi_1(\phi)\int_{SDP} \frac{e^{-ikr\cos\alpha}}{\cos\left(\frac{\alpha-\phi_o-\phi}{2}\right)}\, d\alpha$$

$$= \Phi_1(\phi)\int_{SDP} \frac{1}{2}\left[\frac{1}{\cos\left(\frac{\alpha-\phi-\phi_o}{2}\right)} + \frac{1}{\cos\left(\frac{\alpha+\phi+\phi_o}{2}\right)}\right] e^{-ikr\cos\alpha}\, d\alpha \ . \tag{2.63}$$

Using the steepest descent path from Equation (2.62) and rearranging the integrand, Equation (2.63) becomes

$$\Phi_1(\phi)\int_{SDP} \frac{e^{-ikr\cos\alpha}}{\cos\left(\frac{\alpha-\phi-\phi_o}{2}\right)}\, d\alpha$$

$$= \Phi_1(\phi)\cdot 2\cdot\cos\left(\frac{\phi+\phi_o}{2}\right)\int_{SDP} \frac{\cos\alpha/2\ e^{-ikr-kr\sinh\alpha_i\sin\alpha_r}}{[\cos\alpha + \cos(\phi+\phi_o)]}\, d\alpha \ . \tag{2.64}$$

It also follows from Equation (2.62) that

$$\sin\alpha_r = \tanh\alpha_i \ . \tag{2.65}$$

Substituting from Equation (2.65) into the integral in Equation (2.64) it follows that

$$\Phi_1(\phi)\int_{SDP} \frac{e^{ikr\cos\alpha}\,d\alpha}{\cos\left(\frac{\alpha-\phi-\phi_o}{2}\right)}$$

$$= \Phi_1(\phi)\cdot 2\cdot\cos\left(\frac{\phi+\phi_o}{2}\right)\int_{SDP} \frac{\cos\alpha/2\cdot e^{-ikr}\, e^{-kr\sinh\alpha_i\tanh\alpha_i}}{[\cos\alpha + \cos(\phi+\phi_o)]}\,d\alpha \tag{2.66}$$

Since the exponent in the left side of Equation (2.66) decreases monotonically away from its maximum value of 1 at $\alpha_i = 0$ to $-\infty$, it is convenient to change the variable from α to τ,

where

$$\sinh\alpha_o\tanh\alpha_i = \tau^2 \tag{2.67}$$

such that, as τ runs from $-\infty$ to ∞, it traverses the steepest descent path. Thus the steepest descent integral may then be made into an integral whose limits extend from $-\infty$ to $+\infty$.

The change of variable that is needed is then

$$\tau = \sqrt{2}\; e^{-i\pi/4}\sin\alpha/2 \tag{2.68}$$

with

$$d\tau = \frac{\sqrt{2}}{2}\; e^{-i\pi/4}\cos\alpha/2\; d\alpha\ . \tag{2.69}$$

Substituting Equations (2.68) and (2.69) into Equation (2.67) it follows that

$$\Phi_1(\phi)\int_{SDP}\frac{e^{-ikr\cos\alpha}d\alpha}{\cos\left(\frac{\alpha-\phi-\phi_o}{2}\right)}$$

$$=\Phi_1(\phi)\ 2\ \cos\left(\frac{\phi+\phi_o}{2}\right)\int_{-\infty}^{\infty}\frac{\cos\alpha/2\ e^{-ikr}e^{-kr\tau^2}d\tau}{[\cos\alpha+\cos(\phi+\phi_o)]\cos\alpha/2\ e^{-i\pi/4}\frac{\sqrt{2}}{2}}\ ,$$

$$=-e^{-ikr}e^{i\pi/4}\Phi_1(\phi)\ \frac{2}{\sqrt{2}}\ \cos\left(\frac{\phi+\phi_o}{2}\right)\int_{-\infty}^{\infty}\frac{e^{-kr\tau^2}d\tau}{[2\cos^2\frac{\phi+\phi_o}{2}-2\sin^2\alpha/2]}\ ,$$

$$=\Phi_1(\phi)e^{-ikr}e^{-i\pi/4}2\cdot\sqrt{2}\ \cos\frac{\phi+\phi_o}{2}\int_{-\infty}^{\infty}\frac{e^{-kr\tau^2}d\tau}{\left[\tau^2+i\cdot2\cdot\cos^2\left(\frac{\phi+\phi_o}{2}\right)\right]}\ ,$$

$$=\Phi_1(\phi)e^{-ikr}e^{-i\pi/4}2\cdot b\int_{-\infty}^{\infty}\frac{1}{[\tau^2+ib^2]}\ e^{-kr\tau^2}d\tau\ , \qquad (2.70)$$

where

$$b=\sqrt{2}\ \cos\left(\frac{\phi+\phi_o}{2}\right)\ . \qquad (2.71)$$

The integral in Equation (2.70) can be expressed in terms of the complex Fresnel Integral. Consider the integral

$$I=b\int_{-\infty}^{\infty}\frac{e^{-\nu\tau^2}}{\tau^2+ib^2}\ d\tau \qquad (2.72)$$

with $\nu = kr$. From Equation (2-72), it follows that

$$\frac{d}{d\nu}\left(Ie^{-ib^2\nu}\right) = -b\int_{-\infty}^{\infty} e^{-(\tau^2+ib^2)\nu}\, d\tau \quad ,$$

$$= \frac{-be^{-ib^2\nu}}{\sqrt{\nu}}\int_{-\infty}^{\infty} e^{-\tau'^2}\, d\tau \quad ,$$

with

$$\tau' = \sqrt{\nu}\ \tau$$

$$= \frac{be^{-ib^2\nu}\sqrt{\pi}}{\sqrt{\nu}} \quad . \tag{2.73}$$

From Equation (2.73) the integral in Equation (2.72) may be written as

$$I = \sqrt{\pi}\ be^{ib^2\nu}\int_{\nu}^{\infty} \frac{e^{-ib^2\nu}}{\sqrt{\nu}}\, d\nu \ . \tag{2.74}$$

Letting $\nu = \tau^2/b^2$ and considering b positive, then Equation (2.74) becomes

$$I = 2\sqrt{\pi}\ e^{ib^2\nu}\int_{b\sqrt{\nu}}^{\infty} e^{-i\tau^2}\, d\tau \ ,$$

$$= 2\pi\ F\left(\cos\left(\frac{\phi+\phi_o}{2}\right)\sqrt{2kr}\right), \tag{2.75}$$

where F(a) is the complex Fresnel Integral defined by

$$F(a) = e^{ia^2}\int_a^\infty e^{-i\tau^2}\, d\tau \quad . \tag{2.76}$$

Some useful properties of F(a) are quoted from Clemmow [4]. For

$$F(a) = e^{ia^2}\int_a^\infty e^{-i\tau^2}\, d\tau$$

and

$$F_o(a) = e^{ia^2}\int_o^{(a)} e^{-i\tau^2}\, d\tau \ , \tag{2.77}$$

the following identities are found to be useful:

$$F(a) + F_o(a) = \frac{1}{2}\sqrt{\pi}\ e^{-i\pi/4}\ e^{ia^2} \tag{2.78}$$

and

$$F(a) + F(-a) = \sqrt{\pi}\ e^{-i\pi/4}\ e^{ia^2} \quad . \tag{2.79}$$

Since the integral in Equation (2.72) is an odd function of b, the corresponding result when b is negative becomes

$$I = -2\sqrt{\pi}\ F(-b\sqrt{kr}\ ) \ , \tag{2.80}$$

so consequently,

$$I = \pm 2\sqrt{\pi}\ F(\pm b\sqrt{kr}\ ) \quad . \tag{2.81}$$

Substituting the expression in Equation (2.81) into Equation (2.66) and finding a similar result for the second term of the integral in Equation (2.61), it follows that an exact expression for the integration along the steepest descent path is

$$\int_{SDP} P(\cos\alpha)e^{-ikr\cos(\phi-\alpha)}d\alpha = \mp 4\Phi_1(\phi)\sqrt{\pi}\, e^{-ikr}e^{-i\pi/4}F\left[\pm\sqrt{2kr}\,\cos\frac{\phi+\phi_o}{2}\right]$$

$$\mp 4\Phi_2(\phi)\sqrt{\pi}\, e^{-ikr}e^{-i\pi/4}F\left[\pm\sqrt{2kr}\,\cos\frac{\phi-\phi_o}{2}\right] . \qquad (2.82)$$

Again, consider the first term of this expression. Using the identity found in Equation (2.78), it follows that

$$\mp 4\cdot\Phi_1(\phi)\sqrt{\pi}\, e^{-ikr}e^{-i\pi/4}F\left[\pm\sqrt{2kr}\,\cos\left(\frac{\phi+\phi_o}{2}\right)\right]$$

$$= \mp 4\cdot\Phi_1(\phi)\sqrt{\pi}\, e^{-ikr}e^{-i\pi/4}\left\{\frac{\sqrt{\pi}}{2}\, e^{-i\pi/4}e^{i2kr\cos^2\left(\frac{\phi+\phi_o}{2}\right)}\right.$$

$$\left. -e^{i2kr\cos^2\left(\frac{\phi+\phi_o}{2}\right)}\, F_o\left(\pm\sqrt{2kr}\,\cos\left(\frac{\phi+\phi_o}{2}\right)\right)\right\},$$

$$= \mp 4\cdot\Phi_1(\phi)\sqrt{\pi}\, e^{-ikr}e^{-i\pi/4}\left\{\frac{\sqrt{\pi}}{2}\, e^{-i\pi/4}e^{ikr}e^{ikr\cos(\phi+\phi_o)}\right.$$

$$-e^{ikr}e^{ikr\cos(\phi+\phi_o)}\,\frac{\sqrt{\pi}}{2}\,\left[C(\pm\sqrt{2kr}\,\cos(\phi+\phi_o)\right.$$

$$\left.\left. -iS(\pm\sqrt{2kr}\,\cos(\phi+\phi_o))\right]\right\} . \qquad (2.83)$$

where

$$C(a) = \sqrt{\frac{2}{\pi}} \int_o^a \cos\tau^2 d\tau \tag{2.84}$$

and

$$s(a) = \sqrt{\frac{2}{\pi}} \int_o^a \sin\tau^2 d\tau \ . \tag{2.85}$$

Equation (2.83) is finally written in the form

$$4 \cdot \Phi_1(\phi) e^{-ikr} e^{-i\pi/4} F\left[\pm\sqrt{2kr}\ \cos\left(\frac{\phi+\phi_o}{2}\right)\right]$$

$$= \pm 2\pi i \Phi_1(\phi) e^{ikr\cos(\phi+\phi_o)}$$

$$\left\{1.0 - \sqrt{2}\ e^{i\pi/4}\ C\left(\pm\sqrt{2kr}\ \cos\left(\frac{\phi+\phi_o}{2}\right)\right) - iS\left(\pm\sqrt{2kr}\ \cos\left(\frac{\phi+\phi_o}{2}\right)\right)\right\} \tag{2.86}$$

A similar expression found for the second term of the integral in Equation (2.82) is

$$\Phi_2(\phi) \int_{SDP} \frac{e^{-ikr\cos(\phi-\alpha)} d\alpha}{\cos\left(\frac{\alpha-\phi_o}{2}\right)} = \pm 2\pi i \Phi_2(\phi) e^{ikr\cos(\phi-\phi_o)}$$

$$\times \left\{1.0 - \sqrt{2}\ e^{i\pi/4}\left[C\left(\pm\sqrt{2kr}\ \cos\left(\frac{\phi-\phi_o}{2}\right)\right) - iS\left(\pm\sqrt{2kr}\ \cos\left(\frac{\phi-\phi_o}{2}\right)\right)\right]\right\} \ .$$

The near-field solution for the diffraction may now be written as

$$p_d(r,\phi) = \pm 2\pi i \Phi_1(\phi) e^{ikr\cos(\phi+\phi_o)}$$

$$\left\{1.0 - \sqrt{2}\, e^{i\pi/4}\left[C\left(\pm\sqrt{2kr}\,\cos\left(\frac{\phi+\phi_o}{2}\right)\right) - iS\,\pm\sqrt{2kr}\,\cos\left(\frac{\phi+\phi_o}{2}\right)\right]\right\}$$

$$\pm 2\pi i \Phi_2(\phi) e^{ikr\cos(\phi-\phi_o)}$$

$$\left\{1.0 - \sqrt{2}\, e^{i\pi/4}\left[C\left(\pm\sqrt{2kr}\,\cos\left(\frac{\phi+\phi_o}{2}\right)\right) - iS\left(\pm\sqrt{2kr}\,\cos\left(\frac{\phi-\phi_o}{2}\right)\right)\right]\right\} \tag{2.88}$$

2.8 Diffraction of Line Source Radiation

Up to this point, the type of excitation has been a plane wave. In this section, a line source disturbance will be considered. The incident radiation from a line source is given by

$$p_i = \sqrt{\frac{\pi}{2}}\, e^{-i\pi/4} p_o H_o^{(2)}(kR) \sim p_o \frac{e^{-ikR}}{\sqrt{kR}} \quad , \tag{2.89}$$

for $kR \gg 1$ and where R is the distance from the location of the source at r_o, ϕ_o.

It is helpful to express the line source in the same integral form of the preceding sections. Starting with a line source located at x_o, y_o and into the z direction the line source must satisfy the following wave equation:

$$\frac{\partial^2 p_i}{\partial x^2} + \frac{\partial^2 p_i}{\partial y^2} + k^2 p_i = 4\pi p_o \delta(x-x_o)\delta(y-y_o) \quad . \tag{2.90}$$

Applying Fourier Transforms on x and y, it follows that

$$\bar{\bar{p}}_i = \frac{4\pi}{k^2-\gamma^2-\eta^2} \quad ,$$

where

$$p_i = \frac{p_o}{\pi}\int_{-\infty}^{\infty}\int_{-\infty}^{\infty} \frac{e^{-i\eta(x-x_o)}e^{-i\gamma(y-y_o)}}{k^2-\gamma^2-\eta^2}\, d\gamma d\eta \quad . \tag{2.91}$$

Let $\nu = \frac{\eta}{k}$ and $\beta = k\sqrt{1-\nu^2}$,

then

$$p_i = \frac{1}{\pi} p_o \int_{-\infty}^{\infty} e^{-ik\nu(x-x_o)}\left[\int_{-\infty}^{\infty} \frac{e^{-i\gamma(y-y_o)}}{(\beta^2-\gamma^2)}\, d\gamma\right] d\nu \quad . \tag{2.92}$$

The inner integral in Equation (2.92) may be evaluated using the residue theorem, closing the path of integration from $-\infty$ to ∞ in the lower half-plane and enclosing the singularity at $+\beta$. This yields

$$p_i = -\int_{-\infty}^{\infty} p_o \frac{e^{-i\nu k(x-x_o)}e^{-i\beta(y-y_o)}}{i\beta}\, k d\nu \quad . \tag{2.93}$$

Next, let $x=r\cos\phi$, $x_o=r_o\cos\phi_o$, $y=r\sin\phi$, $y_o=r_o\cos\phi_o$, and $\nu=\cos\alpha$ which changes the integral in Equation (2.93) into polar coordinates and gives the following result:

$$p_i = \int_\gamma p_o e^{+ikr_o\cos(\phi_o-\alpha)} e^{-ikr\cos(\phi-\alpha)}\, d\alpha \quad . \tag{2.94}$$

It can be shown that the integral in Equation (2.93) is equal to $\pi i H_o^{(2)}(kr)$. With this knowledge and the help of Equation (2.89), the line source has an integral representation

$$p_i = \frac{p_o e^{-i\pi/4}}{\sqrt{2\pi}} \int e^{+ikr_o\cos(\phi_o-\alpha)} e^{-ikr\cos(\phi\ \alpha)}\, d\alpha \tag{2.95}$$

It is worth noting that the representation for a line source is a convolution and is obtained by multiplying the plane wave by $e^{-ikr\cos(\phi-\alpha)}$ and integrating with respect to α.

If such a procedure is also applied to the plane wave solution for the diffraction, a line source solution will result. This can be shown by considering the integral equations analogous to Equations (2.31) and (2.32) for the boundary conditions for a line source. They become, respectively,

$$\int_\gamma \int_\gamma P(\cos\alpha,\cos\beta)(\sin\theta^+ + \sin\alpha)e^{ikrcos\alpha}\left[\frac{e^{-i\pi/4}}{\sqrt{2\pi}}\, e^{-ikr_o\cos(\phi_o-\beta)}d\beta\right]d\alpha$$

$$= -\frac{p_o e^{-i\pi/4}}{\sqrt{2\pi}}\int_\gamma e^{-ikr_o\cos(\phi_o-\beta)}(\sin\theta^+ - \sin\beta)e^{-ikrcos\beta}d\beta \qquad (2.96)$$

and

$$\int_\gamma \int_\gamma P(\cos\alpha,\cos\beta)(\sin\theta^- - \sin\alpha)e^{-ikrcos\alpha}\left[\frac{e^{-i\pi/4}}{\sqrt{2\pi}}\, e^{-ikr_o\cos(\phi_o-\beta)}d\beta\right]d\alpha$$

$$= -\frac{p_o e^{-i\pi/4}}{\sqrt{2\pi}}\int_\gamma e^{-ikr_o\cos(\phi_o-\beta)}(\sin\theta^- - \sin\beta)e^{ikrcos\beta}d\beta \quad . \qquad (2.97)$$

Closing the path in the region of convergence and using the residue theorem, it is evident that the same functions found in Equation (2.42) satisfy these integral equations. As a result, the solution for the line source can be written as

$$P(r,\phi) = \frac{e^{-i\pi/4}}{\sqrt{2\pi}}\int_\gamma \int_\gamma \left[\frac{\Phi_1(\alpha)}{\cos\left(\frac{\alpha+\beta}{2}\right)} + \frac{\Phi_2(\alpha)}{\cos\frac{\alpha-\beta}{2}}\right]e^{-ikr_o\cos(\phi_o-\beta)}$$

$$e^{-ikrcos(\phi-\alpha)}d\rho d\alpha \quad , \qquad (2.98)$$

where $\Phi_1(\alpha)$ and $\Phi_2(\alpha)$ are given by Equations (2.53) through (2.57).

Evaluation of the integral in Equation (2.98) is much the same as the procedure for the exact solution derived in Section 2.7. Since the functions $\Phi_1(\alpha)$ and $\Phi_2(\alpha)$ are smooth functions, they are evaluated at the saddle point, $\alpha=\phi$, and removed from under the

integral sign. The resulting integral is

$$p(r,\phi) = \Phi_1(\phi)\frac{e^{-i\pi/4}}{\sqrt{2\pi}}\int_\gamma\int_\gamma \frac{e^{-ikr_o\cos(\phi_o-\beta)}e^{-ikr\cos(\phi-\alpha)}}{\cos\left(\frac{\alpha+\beta}{2}\right)}\,d\alpha d\beta$$

$$+ \Phi_2(\phi)\frac{e^{-i\pi/4}}{\sqrt{\pi}}\int_\gamma\int_\gamma \frac{e^{-ikr_o\cos(\phi_o-\beta)}e^{-ikr\cos(\phi-\alpha)}}{\cos\left(\frac{\alpha-\beta}{2}\right)}\,d\alpha d\beta \ . \quad (2.99)$$

Using the change of variable $\phi_o-\beta=\beta'$ and $\phi-\alpha=\alpha'$, the first term of the expression in Equation (2.99) now becomes

$$I_1 = \frac{\Phi_1(\phi)e^{-i\pi/4}}{\sqrt{2\pi}}\int_\gamma\int_\gamma \frac{1}{\cos\left(\frac{\phi+\phi_o-\alpha-\beta}{2}\right)}e^{-ikr_o\cos\beta}e^{-ikr\cos\alpha}\,d\alpha d\beta \ . \quad (2.100)$$

Multiplying the numerator and denominator by $\cos\left(\frac{\phi+\phi_o-\alpha+\beta}{2}\right)$, then,

$$I_1 = \Phi_1\frac{(\phi)e^{-i\ /4}}{\sqrt{2\pi}}\int_\gamma\int_\gamma \frac{\cos\left(\frac{\phi+\phi_o-\alpha+\beta}{2}\right)e^{-ikr_o\cos\beta}e^{-ikr\cos\alpha}}{\cos\left(\frac{\phi+\phi_o-\alpha-\beta}{2}\right)\cos\left(\frac{\phi+\phi_o-\alpha+\beta}{2}\right)}\,d\beta d\alpha \ ,$$

$$= \frac{\Phi_1(\phi)e^{-i\pi/4}}{2\sqrt{2\pi}}\int_\gamma\int_\gamma \frac{\cos\left(\frac{\phi+\phi_o-\alpha+\beta}{2}\right)e^{-ikr_o\cos\beta}e^{-ikr\cos\alpha}\,d\beta d\alpha}{\left[\cos\left(\frac{\phi+\phi_o-\alpha}{2}\right)-\sin\beta/2\right]\left[\cos\left(\frac{\phi+\phi_o-\alpha}{2}\right)+\sin\beta/2\right]} \ ,$$

$$= \frac{\Phi_1(\phi)e^{-i\pi/4}}{2\sqrt{2\pi}} \int_\gamma \int_\gamma \left\{ \frac{1}{\left[\cos\left(\frac{\phi+\phi_o-\alpha}{2}\right)-\sin\beta/2\right]} + \frac{1}{\left[\cos\left(\frac{\phi+\phi_o-\alpha}{2}\right)+\sin\beta/2\right]} \right\}$$

$$e^{-ikr_o\cos\beta} e^{-ikr\cos\alpha} d\alpha d\beta \quad . \tag{2.101}$$

In the first term of the integrand in Equation (2.101), change α to $-\alpha$, then

$$I_1 = \frac{4\ \Phi_1(\phi)e^{-i\ /4}}{\sqrt{2}} \int_\gamma \int_\gamma \frac{\cos\left(\frac{\phi+\phi_o}{2}\right)\cos\alpha/2\cos\beta/2\ e^{-ikr_o\cos\beta} e^{-ikr\cos\alpha} d\beta d\alpha}{\left[\cos\alpha+\cos\beta-2-4\sin\frac{\phi+\phi_o}{2}\sin\alpha/2\sin\beta/2+2\cos^2\frac{\phi+\phi_o}{2}\right]} \tag{2.102}$$

Now use the change of variable

$$\xi = \sqrt{2}\, e^{-i\pi/4}\sin\alpha/2 \text{ and } \eta = \sqrt{2}\, e^{-i\pi/4}\sin\beta/2 \tag{2.103}$$

which results in

$$I_1 = \frac{4\Phi_1(\phi)e^{-i\pi/4}}{\sqrt{2\pi}} \cos\frac{\phi+\phi_o}{2}\ e^{-ik(r+r_o)}$$

$$\int_{-\infty}^{\infty}\int_{-\infty}^{\infty} \frac{e^{-ikr_o\xi^2} e^{-ikr\eta^2} d\xi d\eta}{\left[\xi^2+\eta^2+2\sin\left(\frac{\phi+\phi_o}{2}\right)\eta\xi+2i\cos^2\left(\frac{\phi+\phi_o}{2}\right)\right]}. \tag{2.104}$$

Using another change of variable to ρ and γ, where

$$\xi = \sqrt{\frac{R_1}{r_o}}\,\rho\cos\gamma \quad \text{and} \quad \eta = \sqrt{\frac{R_1}{r}}\,\rho\sin\gamma \tag{2.105}$$

with

$$R_1 = (r+r_o), \tag{2.106}$$

it then follows that,

$$I_1 = -\frac{4e^{-i\pi/4}}{\sqrt{2\pi}}\,\Phi_1(\phi)e^{-ikR_1}\cos\left(\frac{\phi+\phi_o}{2}\right)\int_o^\infty \rho K(\rho)e^{-kR_1\rho^2}d\rho \quad , \tag{2.107}$$

where

$$K(\rho) = \frac{d\gamma}{\left\{\rho^2\left[\sqrt{\frac{r}{r_o}}\cos^2\gamma+\sqrt{\frac{r_o}{r}}\sin^2\gamma+2\sin\left(\frac{\phi+\phi_o}{2}\right)\sin\gamma\cos\gamma\right]+2i\sqrt{\frac{rr_o}{R_1}}\cos^2\left(\frac{\phi+\phi_o}{2}\right)\right\}} \tag{2.108}$$

The quantity $K(\rho)$ was evaluated according to Clemmow [4], such that

$$K(\rho) = \frac{2\pi\left|\sec\left(\frac{\phi+\phi_o}{2}\right)\right|}{\sqrt{\rho^4+2i\rho^2-\frac{4rr_o}{R_1^2}\cos^2\left(\frac{\phi+\phi_o}{2}\right)}} \quad . \tag{2.109}$$

Substituting Equation (2.109) into Equation (2.107) yields

$$I_1 = \pm\Phi_1(\phi)\sqrt{2\pi}\cdot 4\cdot e^{-i\pi/4}e^{-ikR_1}\int_0^{\infty}\frac{\rho e^{-kR_1\rho^2}}{\sqrt{\left[\rho^2+i\left(\frac{R_1-S}{R_1}\right)\right]\cdot\left[\rho^2+i\left(\frac{R_1+S}{R_1}\right)\right]}}\,, \quad (2.110)$$

with $S = \sqrt{r^2+r_o^2-2rr_o\cos\left(\frac{\phi+\phi_o}{2}\right)}$ and $\pm$ for $\cos\left(\frac{\phi+\phi_o}{2}\right) \gtrless 0$.

Set $i\lambda^2 = -ik(R_1-S) + kR_1\rho^2$, then the integral I_1 can be put into the form

$$I_1 = \pm\Phi_1(\phi)\cdot 4\cdot\sqrt{2\pi}\, e^{-i\pi/4}e^{-ikS}\int^{\infty}\frac{e^{-i\lambda^2}}{\sqrt{\lambda^2+2kS}}\,d\lambda\,. \quad (2.111)$$

When $k(r+r_o)>1$, an approximation for Equation (2.111) can be made by replacing the non-exponential part of the integrand by the value of λ at the lower limit and removing it from under the integral sign, such that

$$I_1 = \pm\frac{4\cdot\Phi_1(\phi)\sqrt{2\pi}\, e^{-i\pi/4}e^{-ikR_1}}{\sqrt{k(R_1+S)}}\int^{\infty} e^{-i\lambda^2}d\lambda\,,$$

$$= \pm\frac{4\Phi_1(\phi)\sqrt{2\pi}\, e^{-i\pi/4}e^{-ikR_1}}{\sqrt{k(R_1+S)}}\,F(\sqrt{k(R_1-S)}\,,$$

$$= \frac{4\pi i\Phi_1(\phi)e^{-ikS}}{\sqrt{2k(R_1+S)}}\left[1.0 - \sqrt{2}\, e^{-i\pi/4}\left\{C(\sqrt{k(R_1-S)}\,) - iS(\sqrt{k(R_1-S)}\,)\right\}\right]. \tag{2.112}$$

A similar expression can be determined for the second term I_2 in Equation (2.92). As a result, the solution for the line source when $k(r+r_o)>1$ can now be written:

$$\int_\gamma\int_\gamma P(\cos\alpha,\beta)e^{-ikr_o\cos(\phi_o-\beta)}e^{-ikr\cos(\phi-\alpha)}d\beta d\alpha$$

$$= \frac{4\pi i\Phi_1(\phi)e^{-ikS}}{\sqrt{2k(R_1+S)}}\left[1.0 - \sqrt{2}\, e^{-i/4}\left\{C(\sqrt{k(R_1-S)}\,) - iS(\sqrt{k(R_1-S)}\,)\right\}\right]$$

$$\frac{4\pi i\Phi_1(\phi)e^{-kR}}{\sqrt{2k(R_1+R)}}\left[1.0 - \sqrt{2}\, e^{i\pi/4}\left\{C(\sqrt{k(R_1-R)}\,) - iS(\sqrt{k(R_1-R)}\,)\right\}\right]$$

+ (Geometrical Optic Terms)

where

$$R = \sqrt{r^2+r_o^2-2rr_o\cos(\phi-\phi_o)}\ ,$$

$$S = \sqrt{r^2+r_o^2-2rr_o\cos(\phi+\phi_o)}\ ,$$

and

$$R_1 = r+r_o. \tag{2.113}$$

An asymptotic approximation for the line source solution may be made if the location of the line source and the observer are both very far from the half-plane, i.e., $kr \to \infty$ and $kr_o \to \infty$. Applying the method of steepest descent to the double integral in Equation (2.89), the far-field approximation becomes

$$p\ (r,\phi) = \frac{p_o e^{-i\ /4} e^{-ik(r+r_o)}}{\sqrt{2}\ \sqrt{2\pi kr}\ \sqrt{2\pi kr_o}} \quad \frac{\Phi_1(\phi)}{\cos\left(\frac{\phi+\phi_o}{2}\right)} + \frac{\Phi_2(\phi)}{\cos\left(\frac{\phi-\phi_o}{2}\right)} \quad , \qquad (2.114)$$

which may also be written as

$$p_d(r,\phi) = \frac{p_o e^{-i\ /4} e^{-ik(r+r_o)}}{\sqrt{2}\ \sqrt{2\pi kr}\ \sqrt{2\pi kr_o}} \left[\frac{\Psi_1(\phi)}{\left(\sin\left(\frac{\phi+\pi}{2}\right) - \sin\frac{o}{2}\right)} + \frac{\Psi_2(\phi)}{\left(\sin\left(\frac{\phi-\pi}{2}\right) - \sin\frac{o}{2}\right)} \right] . \qquad (2.115)$$

2.9 The Diffraction of Point Source Radiation

The diffraction caused by a point source excitation can be determined by considering the integral.

$$p(r,\phi,z) = \int_\gamma \frac{P(\cos\alpha) e^{-ik\sqrt{r^2+r_o^2+2rr_o\cos(\phi-\alpha)+(z-z_o)^2}}}{k\sqrt{r^2+r_o^2+2rr_o\cos(\phi-\alpha)+(z-z_o)^2}}\, d\alpha \ , \qquad (2.116)$$

where $P(\cos\alpha)$ is defined as in Equation (2.42). By analogy to the plane wave solution, this can be regarded as a spectrum of point sources. A point source located at r_o, ϕ_o, and z_o is expressed as

$$p_i(r, ,z) = \frac{p_o e^{-ik\sqrt{r^2+r_o^2-2rr_o\cos(\phi-\phi_o)+(z-z_o)^2}}}{k\sqrt{r^2+r_o^2-2rr_o\cos(\phi-\phi_o)+(z-z_o)^2}} \quad . \tag{2.117}$$

Applying the boundary condition on both surfaces yields integral equations analogous to Equations (2.31) and (2.32) which are expressed respectively as:

$$\int_\gamma P(\cos\alpha) \left\{ \sin\theta^+ + r_o \sin\alpha \left[1 - \frac{i}{kR}\right] \right\} \frac{e^{-ikR}}{kR} \, d\alpha$$

$$= -p_o \left\{ \sin\theta^+ - r_o \sin\phi_o \left[1 - \frac{i}{kR}\right] \right\} \frac{e^{-ikR^*}}{kR^*} \tag{2.118}$$

and

$$\int_\gamma P(\cos\alpha) \left\{ \sin\theta^- - r_o \sin\phi_o \left[1 - \frac{i}{kR}\right] \right\} \frac{e^{-ikR}}{kR} \, d\alpha$$

$$-p_o \left\{ \sin\theta^- + r_o \sin\phi_o \left[1 - \frac{i}{kR^*}\right] \right\} \frac{e^{-ikR^*}}{kR^*} \quad , \tag{2.119}$$

where

$$R = \sqrt{r^2+r_o^2-2rr_o\cos\alpha+(z-z_o)^2} \quad ,$$

and

$$R^* = \sqrt{r^2+r_o^2-2rr_o\cos\phi_o+(z-z_o)^2} \quad .$$

If the γ-path is closed in the region of convergence and the residue theorem is applied to the singularities enclosed, then the function $P(\cos\alpha)$ of Equation (2.42) will indeed satisfy Equations (2.118) and (2.119). This implies that the result in Equation (2.116) is the diffraction solution for a point source excitation.

Because the exponent in the integrand for the point source differs from plane wave integral, it is helpful to check the regions of convergence. Also, because of the square root term in the denominator, branch points must be accounted for.

Consider the function in the exponent

$$R(\alpha) = \sqrt{r^2+r_o^2+2rr_o\cos(\phi-\alpha)+(z-z_o)^2} \quad . \tag{2.120}$$

The branch points are located at values of α where $R(\alpha) = 0$, which implies

$$\begin{aligned} \frac{r^2+r_o^2+(z-z_o)^2}{2rr_o} &= \cos(\phi+\pi-\alpha) \\ &= \cos\alpha' \\ &= \cosh\alpha_i'\cos\alpha_r' \quad , \end{aligned} \tag{2.121}$$

where

$$\alpha' = \pi+\phi-\alpha \quad .$$

Since $(r-r_o)^2 = r^2+r_o^2-2rr_o \geq 0$, then $r^2+r_o^2 \geq 2rr_o$. It follows that

$$\left| \frac{r^2+r_o^2+(z-z_o)^2}{2rr_o} \right| \geq 1. \qquad (2.122)$$

As a result of Equations (2.122) and (2.121), the branch points are in the complex plane and located at

$$\alpha_r' = 2n\pi$$

and

$$\alpha_i' = \pm \cosh^{-1} \left(\frac{r^2+r_o^2+(z-z_o)^2}{2rr_o} \right) = \pm b$$

or

$$\alpha_r = (2n-1)\pi+\phi$$

and

$$\alpha_i = \pm b \quad . \qquad (2.123)$$

The branch cuts originate at $\alpha = (2n-1)\pi+\phi\pm ib$ and extend along straight lines to infinity at $\alpha = (2n-1)\pi+\phi\pm i\infty$. The function $R(\alpha)$ can be written in the form

$$R(\alpha) = |R|^{1/2} e^{i\psi} = |R|^{1/2} (\cos\psi+i\sin\psi) \ , \qquad (2.124)$$

where

$$\tan\psi = -\frac{2rr_o\sinh\alpha_i\sin(\phi-\alpha_r)}{r^2+r_o^2+2rr_o\cosh\alpha_i\cos(\phi-\alpha_r)} \quad . \tag{2.125}$$

To guarantee convergence, the condition $\sin\psi < 0$ is required. This is necessary so that the exponent will reflect a decaying behavior and, thus, allow convergence of the integral in Equation (2.116).

The Table 2.3 helps to locate the regions of convergence by listing the values of α such that $R(\alpha)$ is real. These values will determine the boundary between the regions of convergence and the regions of divergence. Consequently, from Equations (2.124), (2.125), and Table 2.3, the branch points and regions of convergence can now be illustrated in Figure 2.9.

Table 2.3. The values of α_r and α_i that describe the curve in the α-plane as $R(\alpha)$ traverses the real axis.

α_r	α_i	$R(\alpha)$
$(2n-1)\,\pi + \phi$	$\pm\,\infty$	$\pm\,\infty$
$(2n-1)\,\pi + \phi$	$\pm\,b$	0
$(2n-1)\,\pi + \phi$	0	$\pm\sqrt{(r+r_o)^2 + (Z-Z_o)^2}$
$(2n+1)\,\pi + \phi$	0	$\pm\sqrt{(r+r_o)^2 + (Z-Z_o)^2}$
$(2n+1)\,\pi + \phi$	$\pm\,b$	0
$(2n+1)\,\pi + \phi$	$\pm\,\infty$	$\pm\,\infty$

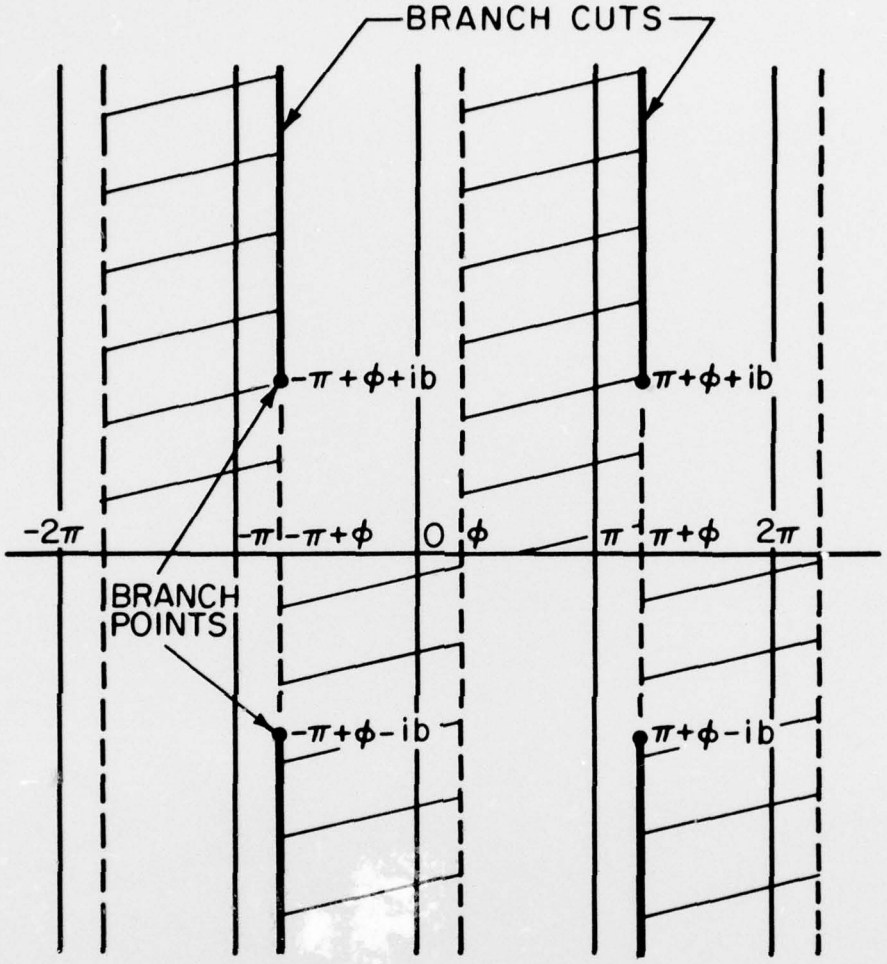

Figure 2.9. Branch points, branch cuts and the shaded regions of convergence for a point source.

Evaulation of the integral in Equation (2.116) proceeds in a manner similar to that for the plane wave and the line source. Using the function $P(\cos\alpha)$ in the form of Equation (2.53), the smooth part of the function is evaluated at the saddle point and removed from under the integral sign so that

$$p(r,\phi,z) = \Phi_1(\phi)\int_\gamma \frac{e^{-ikR(\alpha)}}{\cos\left(\frac{\alpha+\phi_o}{2}\right)kR(\alpha)}\,d\alpha$$

$$+\Phi_2(\phi)\int_\gamma \frac{e^{-ikR(\alpha)}}{\cos\left(\frac{\alpha-\phi_o}{2}\right)kR(\alpha)}\,d\alpha\ . \qquad (2.126)$$

Consider the first term and cose the γ-path along the line $i\infty+\phi$ to $-i\infty+\phi$. This results in the following integral for the first term:

$$I_1 = \Phi_1(\phi)\int_{-\infty}^{\infty} \frac{e^{-k\sqrt{r^2+r_o^2+2rr_o\cosh\alpha_i+(z-z_o)^2}}\,id\alpha_i}{\cos\left(\frac{i\alpha_i+\phi+\phi_o}{2}\right)\ k\sqrt{r^2+r_o^2\cosh\alpha_i+(z-z_o)^2}}$$

$$= \Phi_1(\phi)\int_{-\infty}^{\infty}\frac{1}{2}\left\{\frac{1}{\cos\left[\frac{\phi+\phi_o+i\alpha_i}{2}\right]}+\frac{1}{\cos\left[\frac{\phi+\phi_o-i\alpha_i}{2}\right]}\right\}$$

$$\frac{e^{-ik\sqrt{r^2+r_o^2+2rr_o+(z-z_o)^2-4rr_o\sinh^2\alpha_{i/2}}}\,id\alpha_i}{k\sqrt{r^2+r_o^2+2rr_o+(z-z_o)^2-4rr_o\sinh^2\alpha_{i/2}}}$$

$$= \Phi_1(\phi) \int_{-\infty}^{\infty} \frac{2\cos\frac{\phi+\phi_o}{2}\ \cosh\alpha_{i/2}}{[\cos(\phi+\phi_o)+\cosh\alpha_i]}$$

$$\frac{e^{-ik\sqrt{[(r+r_o)^2+(z-z_o)^2]}\ \sqrt{1-\frac{4rr_o\sinh^2\alpha_{i/2}}{(r+r_o)^2+(z-z_o)^2}}}}{k\sqrt{[(r+r_o)^2+(z-z_o)^2]}\left[1-\frac{4rr_o\sinh^2\alpha_{i/2}}{(r+r_o)^2+(z-z_o)^2}\right]}\ id\alpha_i \quad . \qquad (2.127)$$

Using the change of variable $\tau = \frac{2\sqrt{rr_o}}{R_1} e^{-i\pi/4}\sinh\alpha_{i/2}$, where $R_1 = \sqrt{(r+r_o)^2+(z-z_o)^2}$, and applying the identities $\cos(\phi+\phi_o)$ $= 2\cos^2\left(\frac{\phi+\phi_o}{2}\right) - 1$ and $\cosh\alpha_i = 1-2\sinh^2(\alpha_i/2)$, the integral in Equation (2.127) becomes

$$I_1 = \frac{\Phi_1(\phi)e^{-i\pi/4}}{kR}\left[\frac{2\sqrt{krr_o}}{R_1}\cos\left(\frac{\phi+\phi_o}{2}\right)\right]$$

$$\int_{-\infty}^{\infty} \frac{e^{-ikR_1\sqrt{1-i\tau^2}}\ d\tau}{\left[\tau^2+i\left\{\frac{4rr_o}{R_1^2}\cos^2\frac{\phi+\phi_o}{2}\right\}\right]}\ \sqrt{1-i\tau^2} \qquad (2.128)$$

Expand the exponent term, $kR_1\sqrt{1-\tau^2}$, in a Taylor series. If $kR_1 > 1$, retain only the first two terms of the expansion, evaluate the slowly varying function $(1-i\tau^2)^{1/2}$ in the denominator at the saddle point

$\tau = 0$, and remove it from under the integral sign. As a result, for $kR_1 > 1$, the integral becomes

$$I_1 = -\frac{i\Phi_1(\phi)}{kR_1}\, e^{+i\pi/4}\left[\frac{2\sqrt{krr_o}}{R_1}\cos\left(\frac{\phi+\phi_o}{2}\right)\right]$$

$$\int_{-\infty}^{\infty} \frac{e^{-ikR_1\left(1-\frac{i\tau^2}{2}\right)}}{\left\{\tau^2+i\left[\frac{4rr_o}{R_1^2}\cos^2\left(\frac{\phi+\phi_o}{2}\right)\right]\right\}}\, d\tau,$$

$$= -\frac{i\Phi_1(\phi)e^{i\pi/4}e^{-ikR_1}}{kR_1}\left[\frac{2\sqrt{krr_o}}{R_1}\cos\left(\frac{\phi+\phi_o}{2}\right)\right]$$

$$\int_{-\infty}^{\infty} \frac{e^{-\frac{kR_1\tau^2}{2}}\, d\tau}{\left\{\tau^2+i\left[\frac{4rr_o}{R_1^2}\cos^2\left(\frac{\phi+\phi_o}{2}\right)\right]\right\}}, \qquad (2.129)$$

which is in the form

$$I_1 = -\frac{i\Phi_1(\phi)e^{i\pi/4}e^{-ikR_1}\cdot b\cdot}{kR_1}\int_{-\infty}^{\infty} \frac{e^{-\frac{kR_1\tau^2}{2}}}{(\tau^2+ib^2)}\, d\tau \qquad (2.130)$$

where $b = \frac{2\sqrt{krr_o}}{R_1}\cos\left(\frac{\phi+\phi_o}{2}\right)$.

The integral in this form is identical to that of Equation (2.68) which now yields

$$I_1 = \frac{2\sqrt{\pi}\, i\Phi_1(\phi) e^{i\pi/4} e^{-ikR_1}}{kR_1} F\left[\pm\sqrt{\frac{2krr_o}{R_1}} \cos\left(\frac{\phi+\phi_o}{2}\right)\right], \qquad (2.131)$$

$$= \frac{\pi i\Phi_1(\phi) e^{-ikR_1} e^{\frac{ikrr_o}{R_1^2}[\cos(\phi+\phi_o)+1]}}{kR_1}$$

$$\times \left[1.0 - \sqrt{2}\, e^{i\pi/4} \left\{C\left(\sqrt{\frac{2krr_o}{R_1}} \cos\left(\frac{\phi+\phi_o}{2}\right)\right) - iS\left(\sqrt{\frac{2krr_o}{R_1}} \cos\left(\frac{\phi+\phi_o}{2}\right)\right)\right\}\right]$$

There is a similar expression for the second term; thus, the exact solution becomes

$$p_\alpha(r,\phi,z) = \frac{\pi i\Phi_1(\phi) e^{-ikR_1} e^{\frac{ikrr_o}{R_1}[1+\cos(\phi+\phi_o)]}}{kR_1}$$

$$\times \left[1.0 - \sqrt{2}\, e^{i\,/4} \left\{C\left(\sqrt{\frac{2krr_o}{R_1}} \cos\left(\frac{\phi+\phi_o}{2}\right)\right) - iS\sqrt{\frac{2krr_o}{R_1}} \cos\left(\frac{\phi+\phi_o}{2}\right)\right)\right\}\right]$$

(2.132)

$$\pm \frac{\pi i \Phi_2(\phi) e^{-ikR_1} e^{\frac{ikrr_o}{R_1}[1+\cos(\phi-\phi_o)]}}{kR_1}$$

$$\times \left[1.0 - \sqrt{2}\, e^{i\pi/4} \left\{ C\left(\sqrt{\frac{2krr_o}{R_1}} \cos\left(\frac{\phi-\phi_o}{2} \right) \right) - iS\left(\sqrt{\frac{2krr_o}{R_1}} \cos\left(\frac{\phi-\phi_o}{2} \right) \right) \right\} \right] .$$

The asymptotic approximation for the point source may also be made when $kR_1 \to \infty$, $kr \to \infty$, kr. In this event, Equation (2.116) may be simplified to

$$p(r,\phi,z) = \int_\gamma \frac{P(\cos\alpha) e^{-ikr_1} e^{\frac{ik2rr_o}{R_1} \sin^2\left(\frac{\phi-\alpha}{2}\right)}}{k\sqrt{r^2+r_o{}^2+2rr_o\cos(\phi-\alpha)+(z-z_o)^2}}\, d\alpha \quad . \tag{2.133}$$

Again, the steepest descent point is $\alpha = \phi$. The far-field approximation may then be written as

$$p(r, ,z) = \frac{\sqrt{2\pi}\, P(\cos\phi) e^{i\pi/4} e^{-ikR_1}}{\sqrt{kR_1}\,\sqrt{kr}\,\sqrt{kr_o}} \quad , \tag{2.134}$$

where $P(\cos\phi)$ can be found in Equation (2.42).

CHAPTER III

NUMERICAL RESULTS

3.1 Introduction

Numerical results for various source type and location, and impedance cover conditions are presented in this chapter. The parameters are varied to explore the dependence of the diffracted pressure and the backscattered pressure on the impedance cover. Calculations are also made for a variety of source and observer locations. Special attention is given to the far-field approximation. All graphs are polar plots of the angular distribution of the diffracted or backscattered pressure measured in decibels relative to the amplitude of the incident pressure.

3.2 Impedance Considerations

In the solution for the diffracted pressure for all three source cases, the parameter that determines the impedance condition is the variable θ^+ or θ^-. From Equation (2.30), one recalls that $\sin(\theta)=\rho c/z$. The various impedances that are considered in this study and their corresponding values of θ are listed in Table 3.1.

Table 3.1. Impedance Conditions and their corresponding Brewster Angles θ.

	Z	$\rho c/Z$	θ Brewster Angle
Pressure Release	0	∞	$i\infty$
Matched	ρc	1.000	90^o
	$1.16\rho c$	.866	60^o
	$2.00\rho c$	.500	30^o
Rigid	∞	0	0^o

Computations were performed using the impedances listed in Table 3.1 for specific reasons. The cases when $\theta = 5i$ or $\theta = 0^{o}$ are for the classical cases of pressure release (soft) and rigid boundary conditions respectively. The case of $\theta = 90^{o}$ is particularly interesting since this case represents a totally absorbing surface. The other cases are computed to complete a range of examples. For each of the different source cases, the far-field pressure has the same angular dependence as given by Equation (2.42). This angular dependence is calculated to indicate only the pattern of the far-field pressure. It is possible to have at most one zero occurring in the far-field diffracted pressure and, at most, two nulls occurring in the far-field backscattered pressure. The influence of the impedance on the location of nulls is also demonstrated by these computations.

3.3 Source Observer Considerations

The location of the observer is varied in an attempt to determine the effect of the radial parameter and the angle of incidence on the behavior of the diffracted or backscattered pressure. The dimensionless variables kr, kr_{o}, and $k(z-z_{o})$ are considered for a wide range of values to demonstrate the transition from the near-field to the far-field. Comparisons are also made between the three types of source conditions when the radial variables are considered.

In the case of diffraction, the angle of incidence was chosen to be $\phi_{o} = 120^{o}$ as a representative case. For backscatter, the angle of incidence and the observer angle are equal. In other words $\phi = \phi_{o}$ in Equation (2.42) for the backscatter pressure.

3.4 Diffraction and Backscattering of a Plane Wave by an Impedance Covered Half-Plane

All of the graphs for the diffracted and backscattered pressure are in polar form and are measured in decibels relative to the amplitude of the incident pressure. In the exact solution for the plane wave, the factor $\sqrt{kr}$ appears in the argument of the Fresnel Integrals as shown by Equation (2.86). Consequently, the magnitude of the pressure will diminish at a rate proportional to $1/\sqrt{kr}$. Because of this, it is desirable to normalize the pressure by the same factor in order to facilitate the comparison of successive diffraction plots. As a result, what is really being shown in the plots is $(r,\phi)\cdot\sqrt{kr}$. In effect, one is observing only the angular dependence of the diffracted or backscattered pressure. Throughout this chapter the term "illuminated" is borrowed from the field of optics and corresponds to the expression "insonified" in acoustics.

There are fourteen figures that deal with the diffraction of a plane wave by a half-plane. In all of these plots, the angle of incidence is set at $\phi_o = 120^o$

The influence of the impedance of the illuminated surface is considered in the first eight figures. These figures are plotted for the following parameters:

1. Figures 3.1 and 3.2 have an impedance on the illuminated surface, $\theta^+ = 30^o$, and $\theta^- = 0$ (rigid) on the unilluminated surface. In Figure 3.1, kr is 20 and 50 and in Figure 3.2, kr is 100 and infinity.

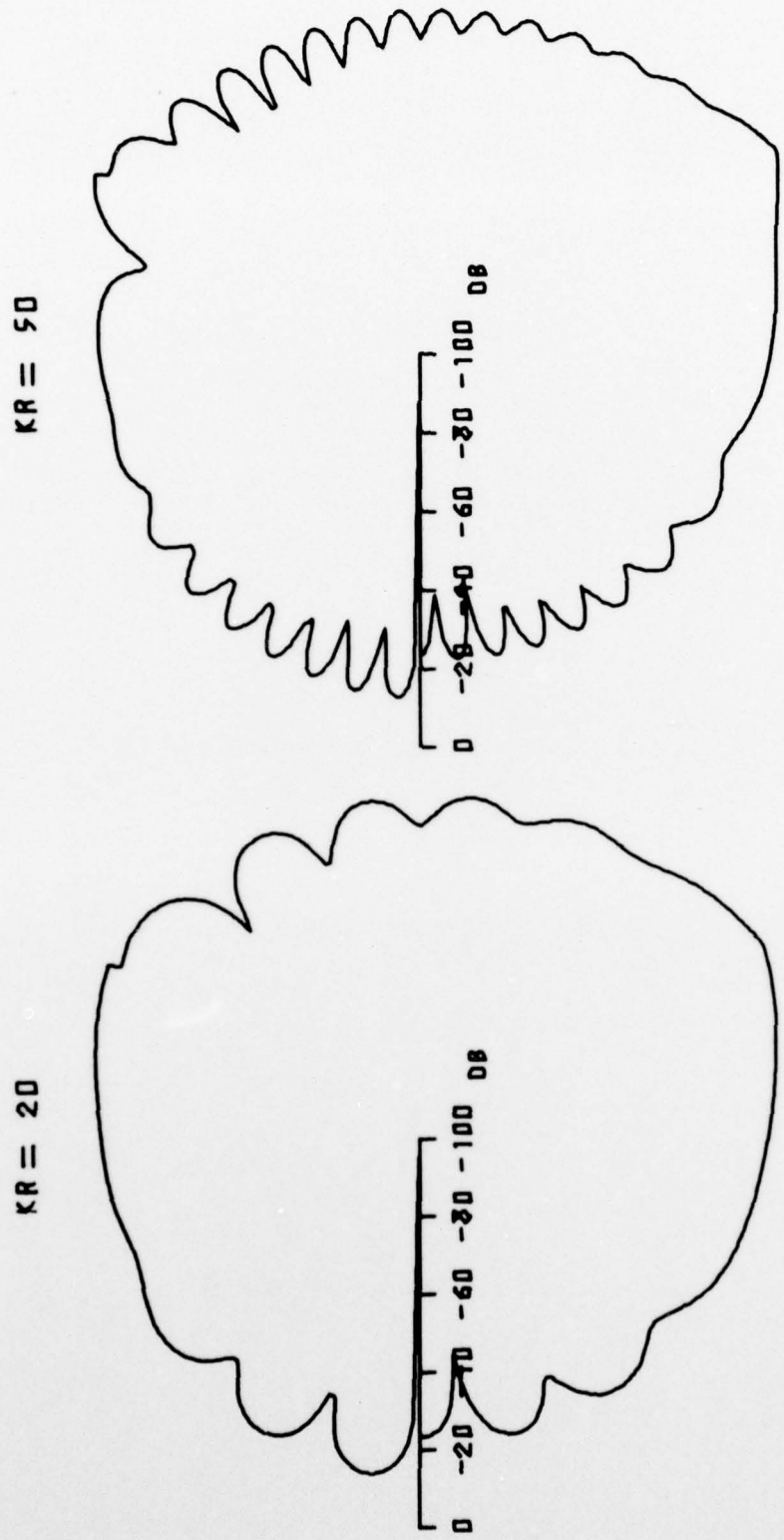

Figure 3.1. Diffraction of a plane wave with $\theta^+ = 30^\circ$, $\theta^- = 0^\circ$, and $\phi_o = 120^\circ$.

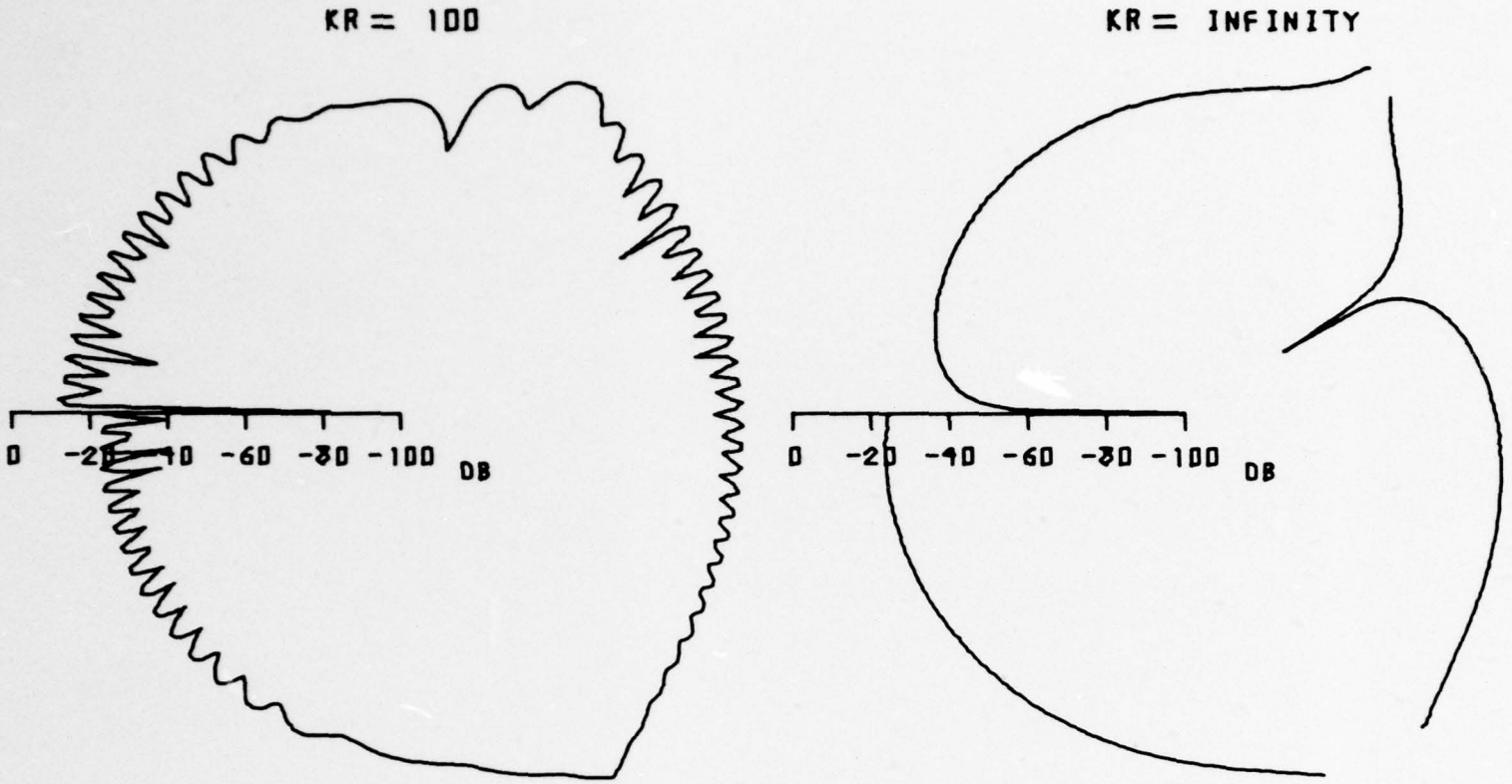

Figure 3.2. Diffraction of a plane wave with $\theta^+ = 30^\circ$, $\theta^- = 0^\circ$, and $\phi_o = 120^\circ$.

2. Figures 3.3 and 3.4 have $\theta^+ = 60^o$ and $\theta^- = 0^o$ (rigid). The values for kr are 20 and 50 in Figure 3.3; and 100, and infinity in Figure 3.4.

3. The impedance conditions are $\theta^+ = 90^o$ (totally absorbing) and $\theta^- = 0^o$ (rigid) in Figures 3.5 and 3.6. In Figure 3.5, kr is 20 and 50 and in Figure 3.6, kr is 100 and infinity.

4. Figures 3.7 and 3.8 represent the situation of pressure release on the illuminated surface $\theta^+ = i5$ and rigid on the opposite surface $\theta^- = 0^o$. The values of kr are 20 and 50 in Figure 3.7, and 100 in infinity in Figure 3.8.

The next four plots demonstrate how the impedance on the unilluminated surface influences the diffracted pressure. The angle of incidence is $\phi_o = 120^o$.

Figures 3.9 and 3.10 represent the diffraction by a half-plane with pressure release impedance on the unilluminated surface, i.e., $\theta^+ = 5i$, while the illuminated surface has $\theta^- = 0^o$ (rigid). Again, kr = 20, 50 in Figure 3.9 and kr = 100 and infinity in Figure 3.10.

The impedance condition on the upper surface in Figures 3.11 and 3.12 is $\theta^+ = 90^o$ (totally absorbing) while $\theta^- = 0^o$ remains the same. In Figure 3.11, kr = 20 and 50, while in Figure 3.12, kr = 100 and infinity.

The influence of an imaginary component of impedance is considered in Figures 3.13 and 3.14 where $\theta^+ = 30 + i.1$ and $\theta^- = 0^o$. The angle of incidence is $\phi_o = 120^o$ and kr = 20 and 50 in Figure 3.13, while kr = 100 and infinity in Figure 3.14.

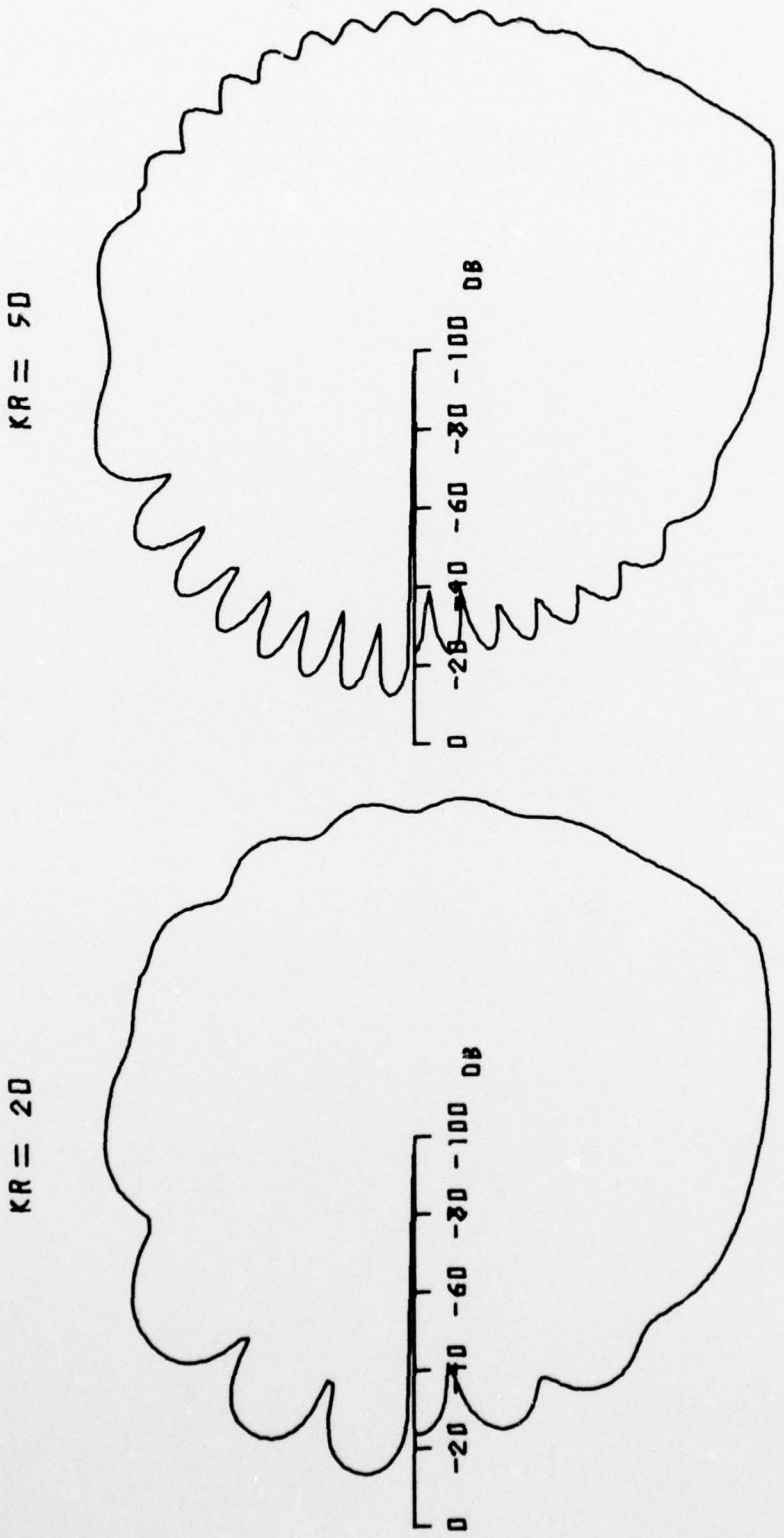

Figure 3.3. Diffraction of a plane wave with $\theta^+ = 60^o$, $\theta^- = 0^o$, and $\phi_o = 120^o$.

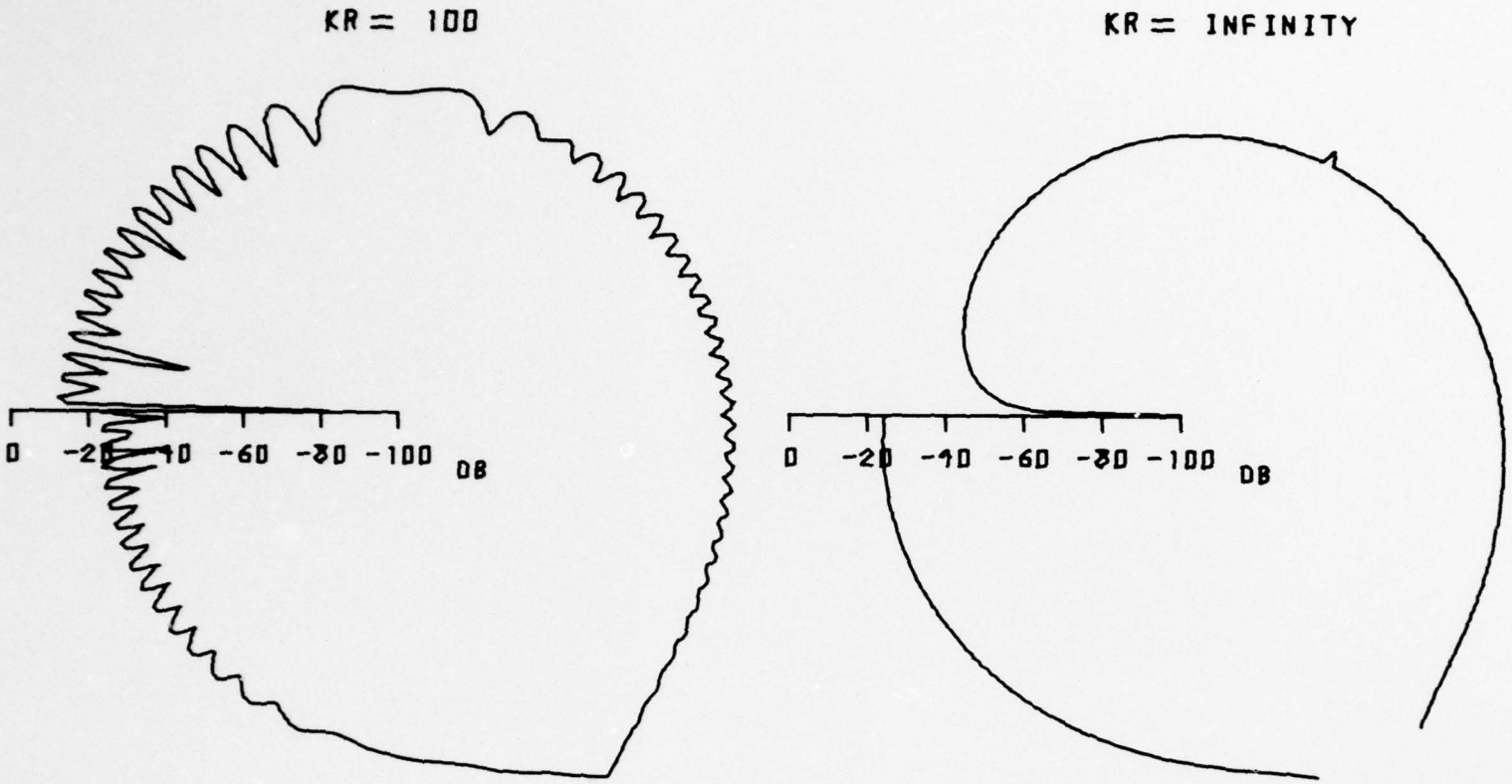

Figure 3.4. Diffraction of a plane wave with $\theta^+ = 60^o$, $\theta^- = 0^o$, $\phi_o = 120^o$.

AD-A047 839 PENNSYLVANIA STATE UNIV UNIVERSITY PARK APPLIED RESE--ETC F/G 20/1
ACOUSTIC DIFFRACTION BY AN IMPEDANCE COVERED HALF-PLANE.(U)
DEC 76 R P KENDIG N00017-73-C-1418
UNCLASSIFIED TM-76-312 NL

2 OF 2
AD
A047839

END
DATE
FILMED
1 -78
DDC

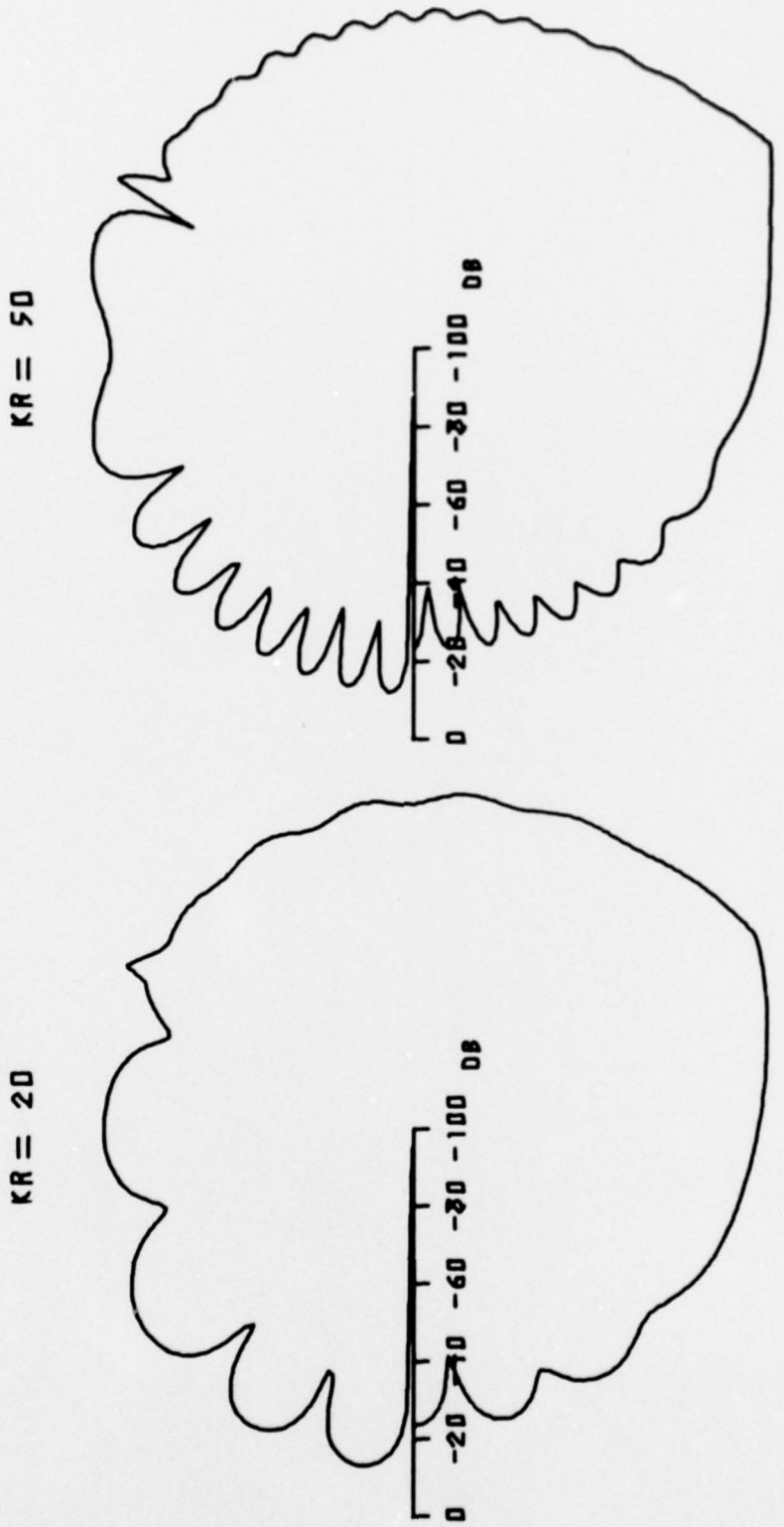

Figure 3.5. Diffraction of a plane wave with $\theta^+ = 90^\circ$, $\theta^- = 0^\circ$, and $\phi_o = 120^\circ$.

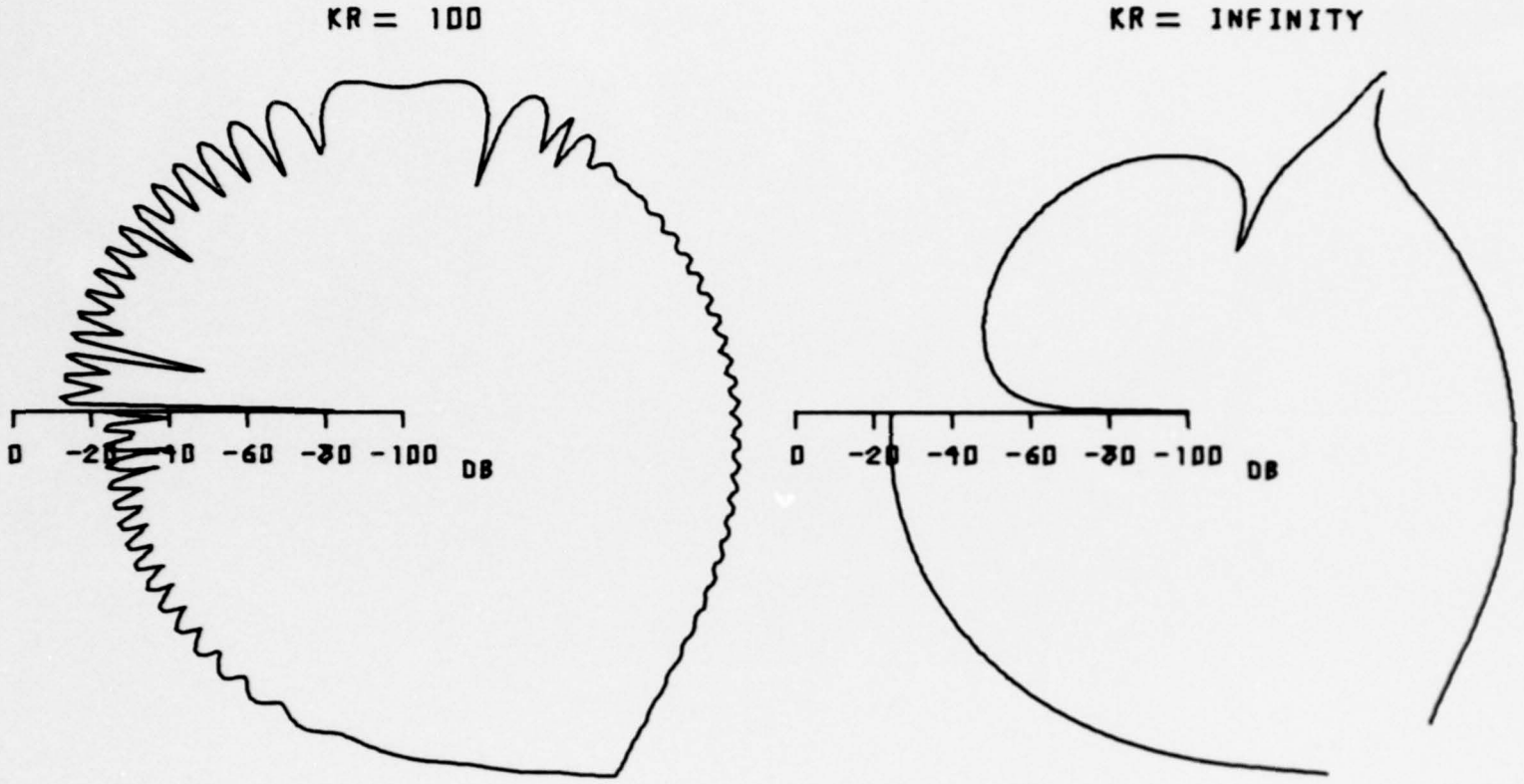

Figure 3.6. Diffraction of a plane wave with $\theta^+ = 90^\circ$, $\theta^- = 0^\circ$, and $\phi_o = 120^\circ$.

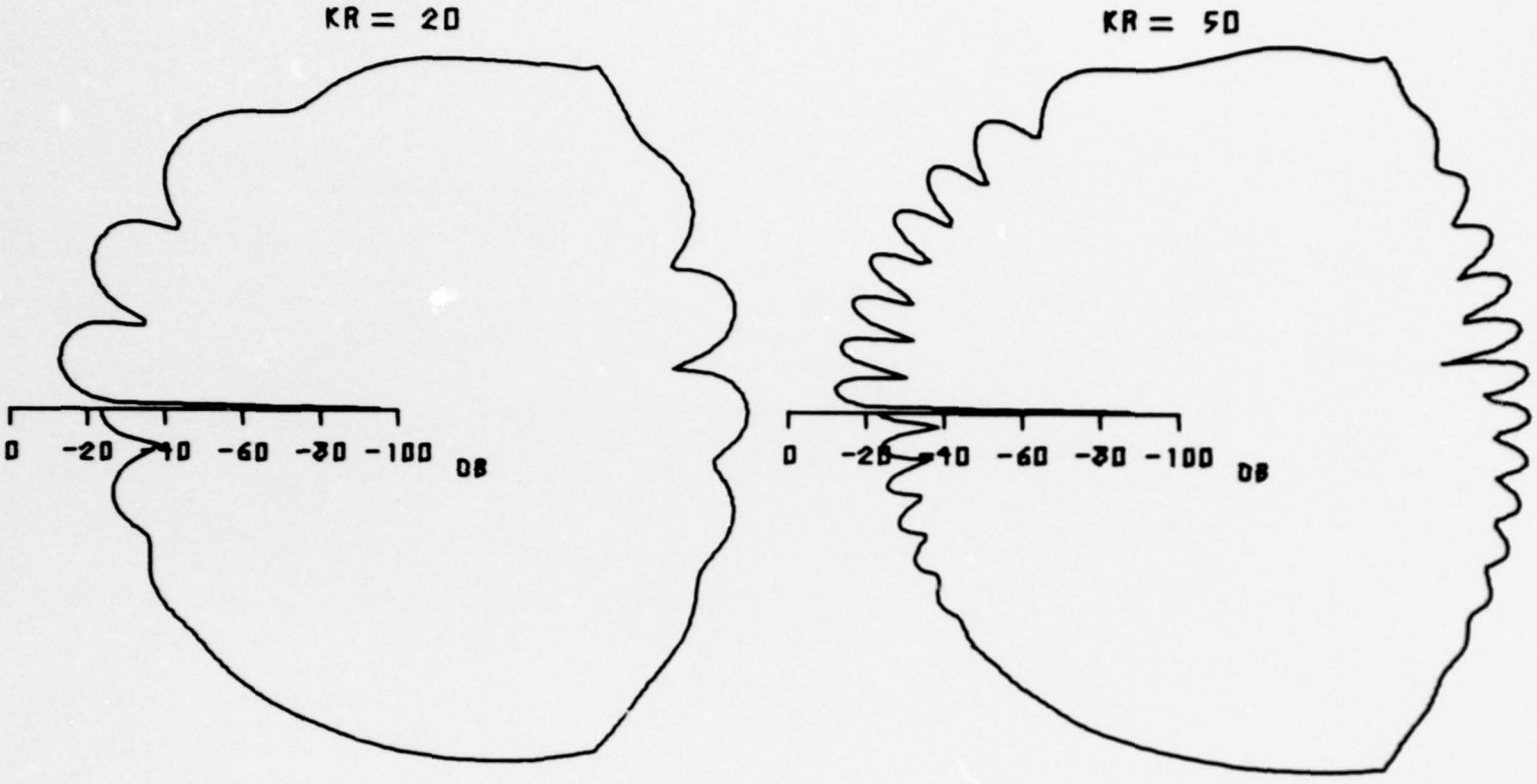

Figure 3.7. Diffraction of a plane wave with $\theta^+ = 15$, $\theta^- = 0^o$, and $\phi_o = 120^o$.

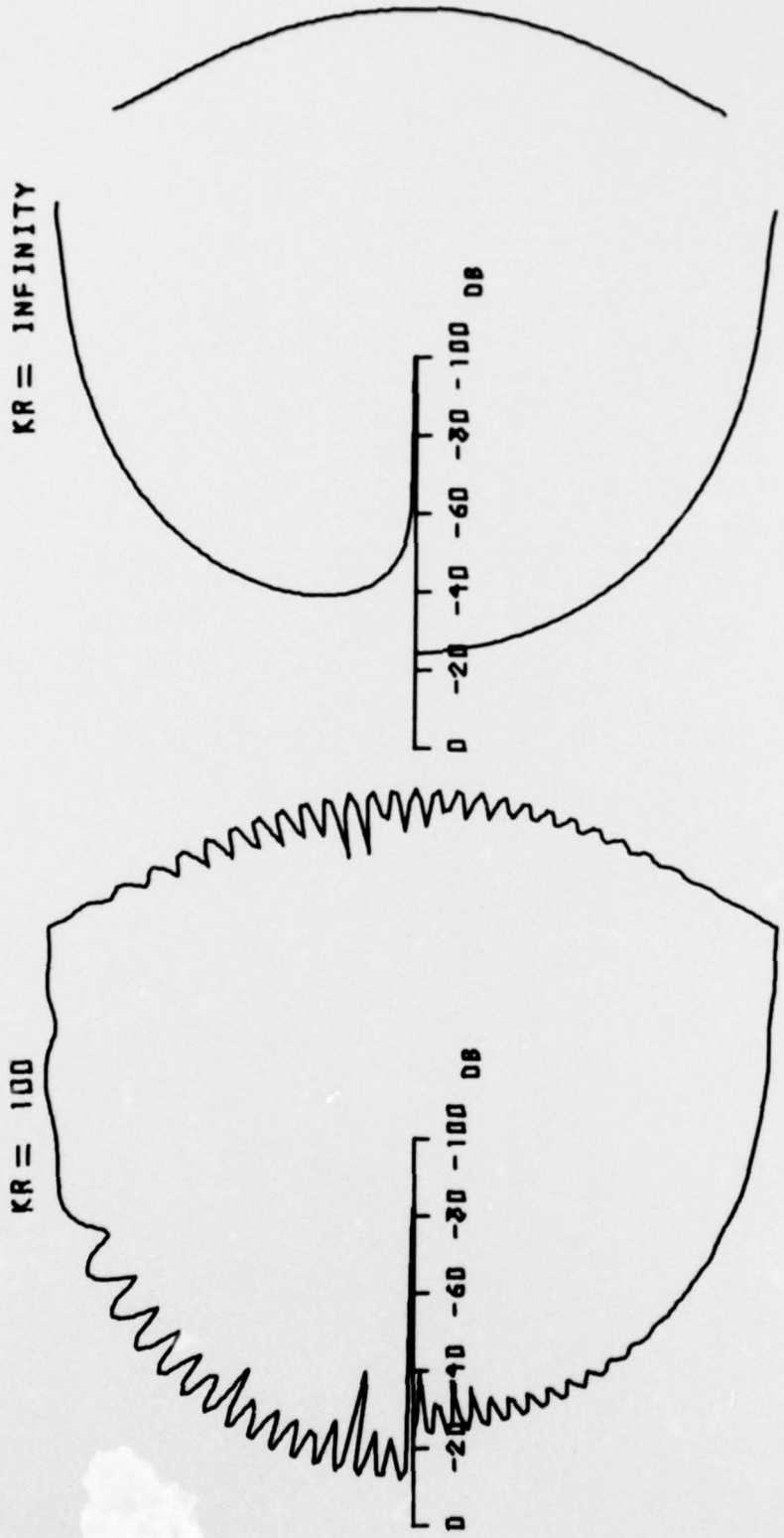

Figure 3.8. Diffraction of a plane wave with $\theta^+ = 15$, $\theta^- = 0^o$, and $\phi_o = 120^o$.

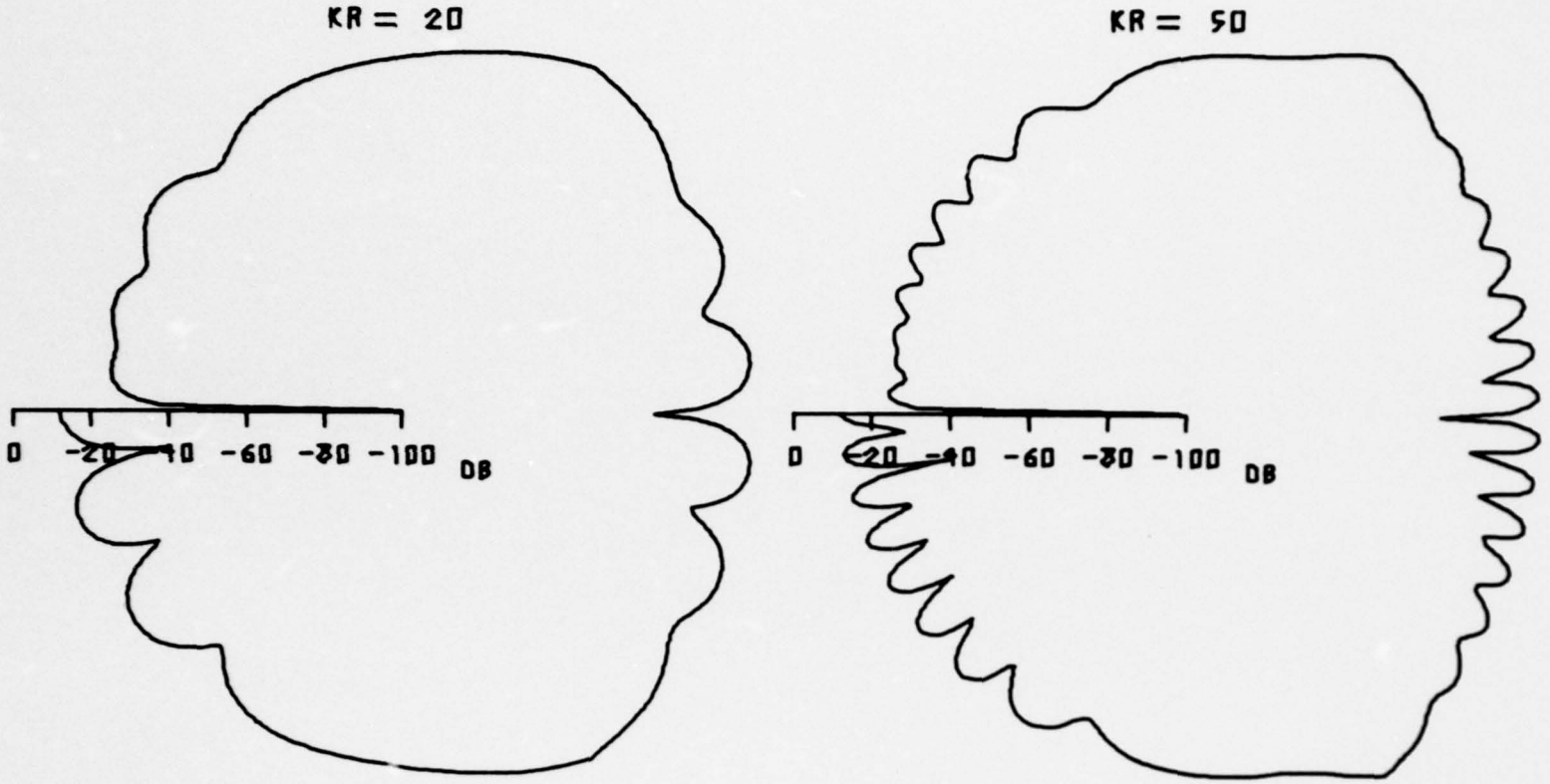

Figure 3.9. Diffraction of a plane wave with $\theta^+ = 15$, $\theta^- = 0^\circ$, and $\phi_o = -120^\circ$.

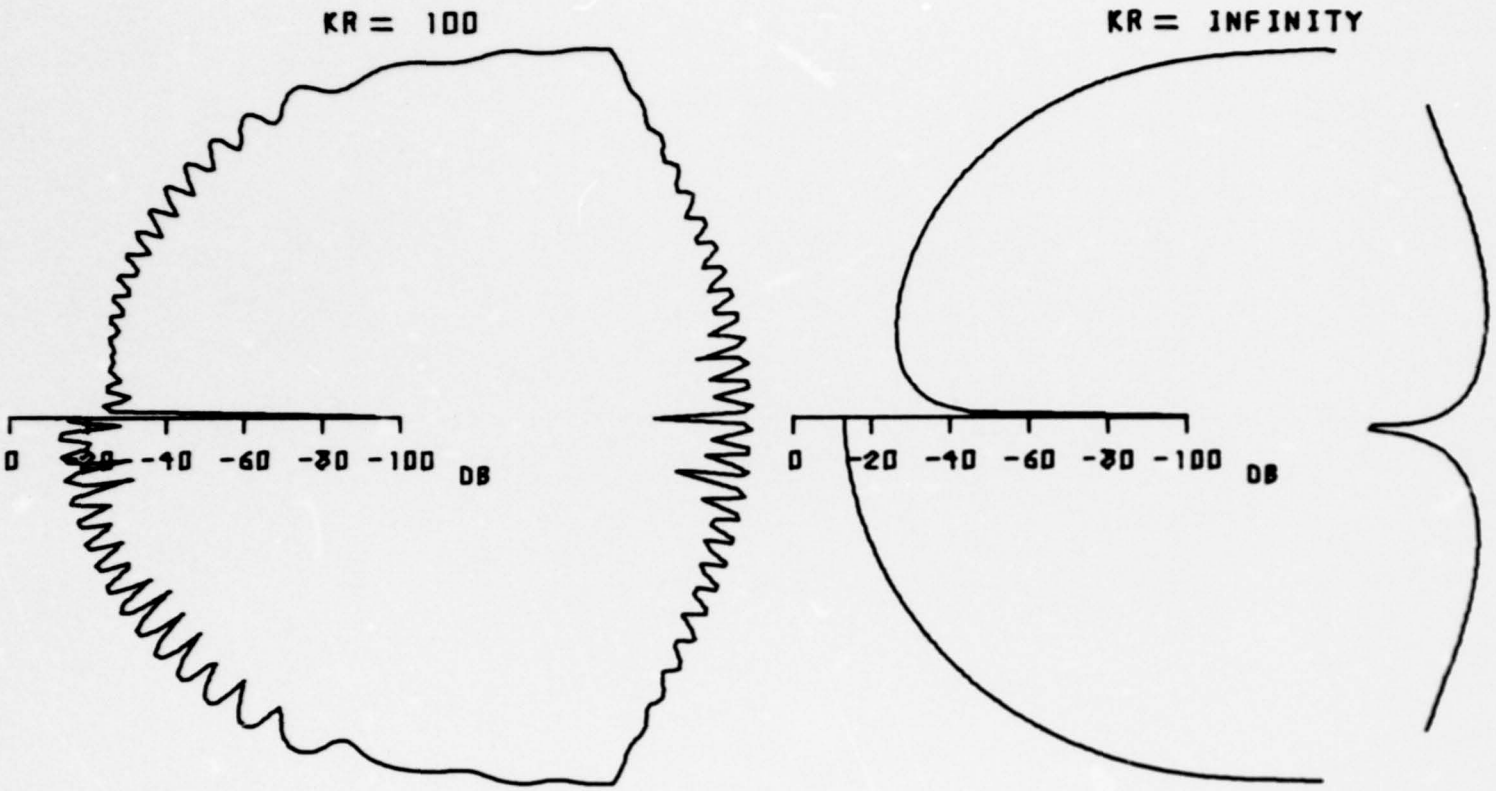

Figure 3.10. Diffraction of a plane wave with $\theta^+ = i5$, $\theta^- = 0^o$, and $\phi_o = -120^o$.

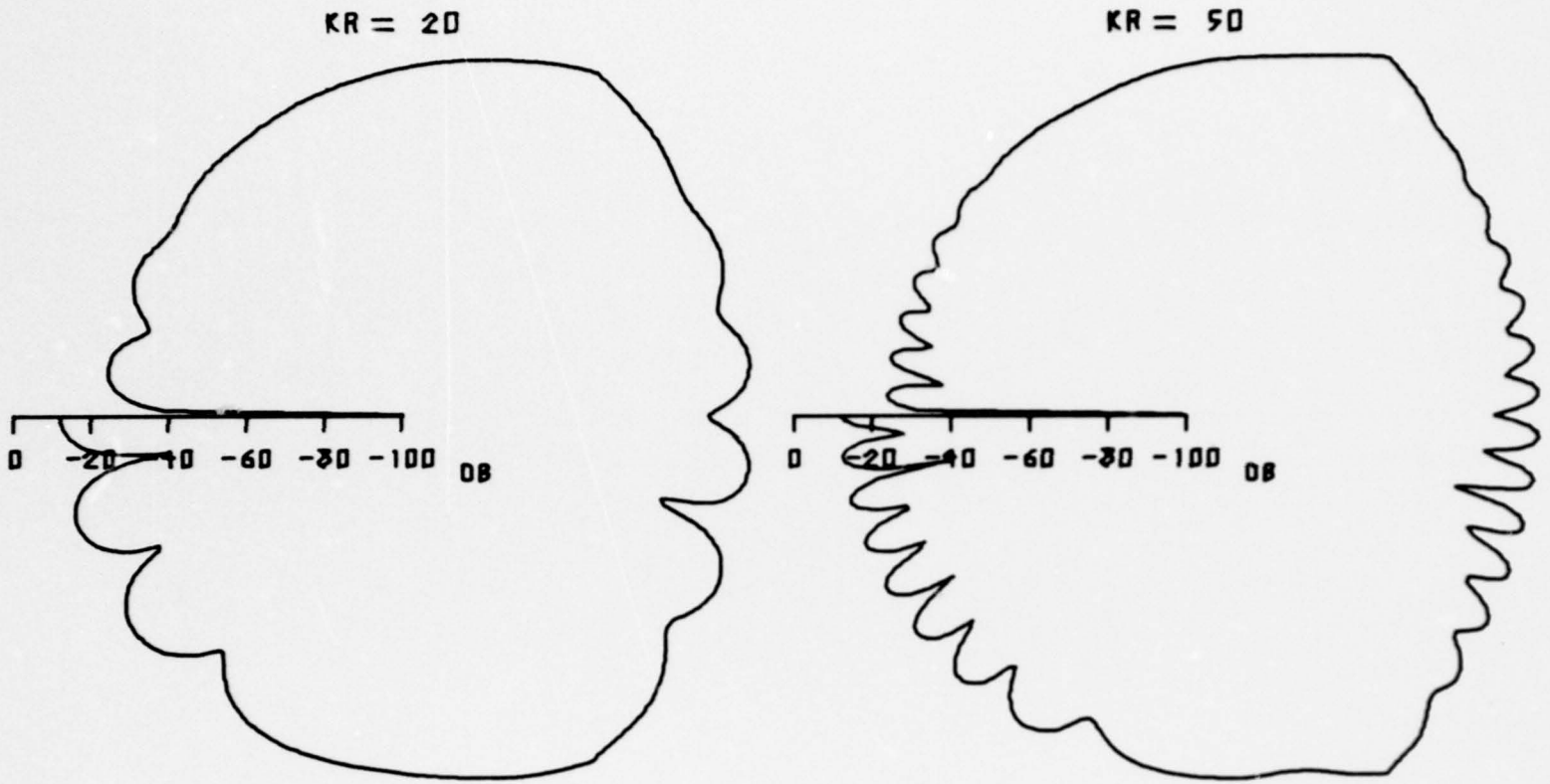

Figure 3.11. Diffraction of a plane wave with $\theta^+ = 90^\circ$, $\theta^- = 0^\circ$, and $\phi_o = -120^\circ$.

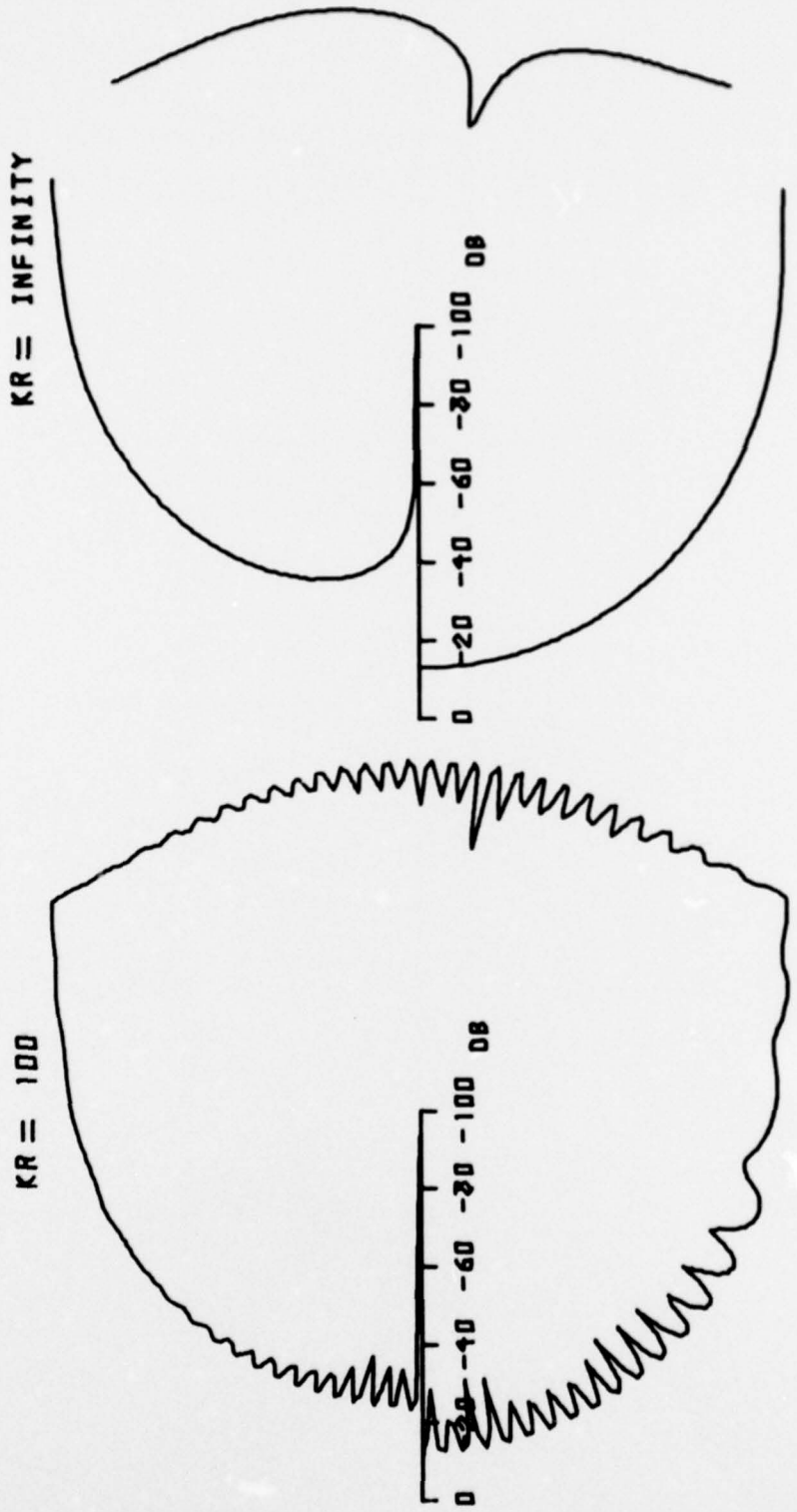

Figure 3.12. Diffraction of a plane wave with $\theta^+ = 90^\circ$, $\theta^- = 0^\circ$, and $\phi_o = -120^\circ$.

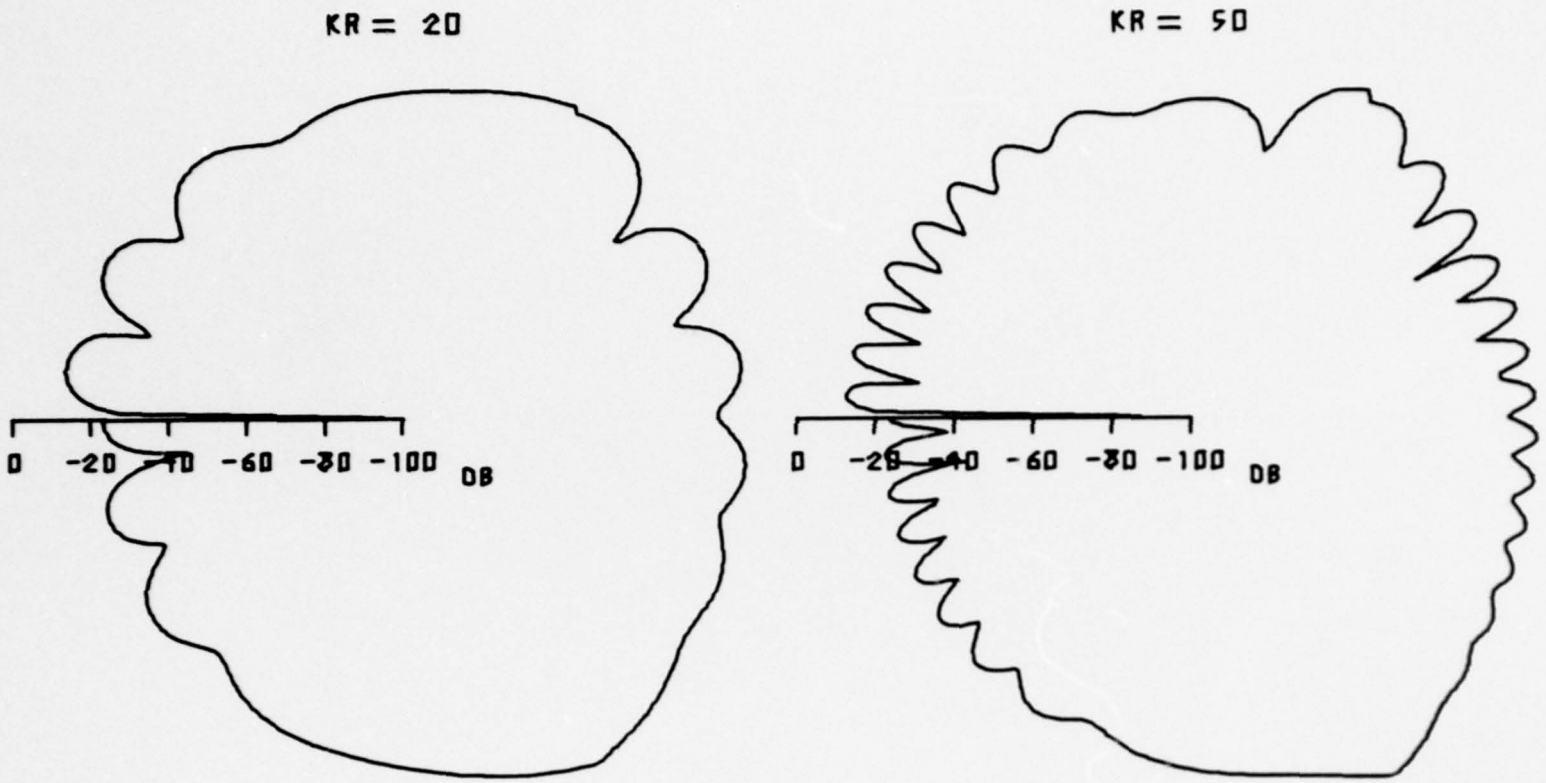

Figure 3.13. Diffraction of a plane wave with $\theta^+ = 30^\circ + i.1$, $\theta^- = 0^\circ$, and $\phi_o = 120^\circ$.

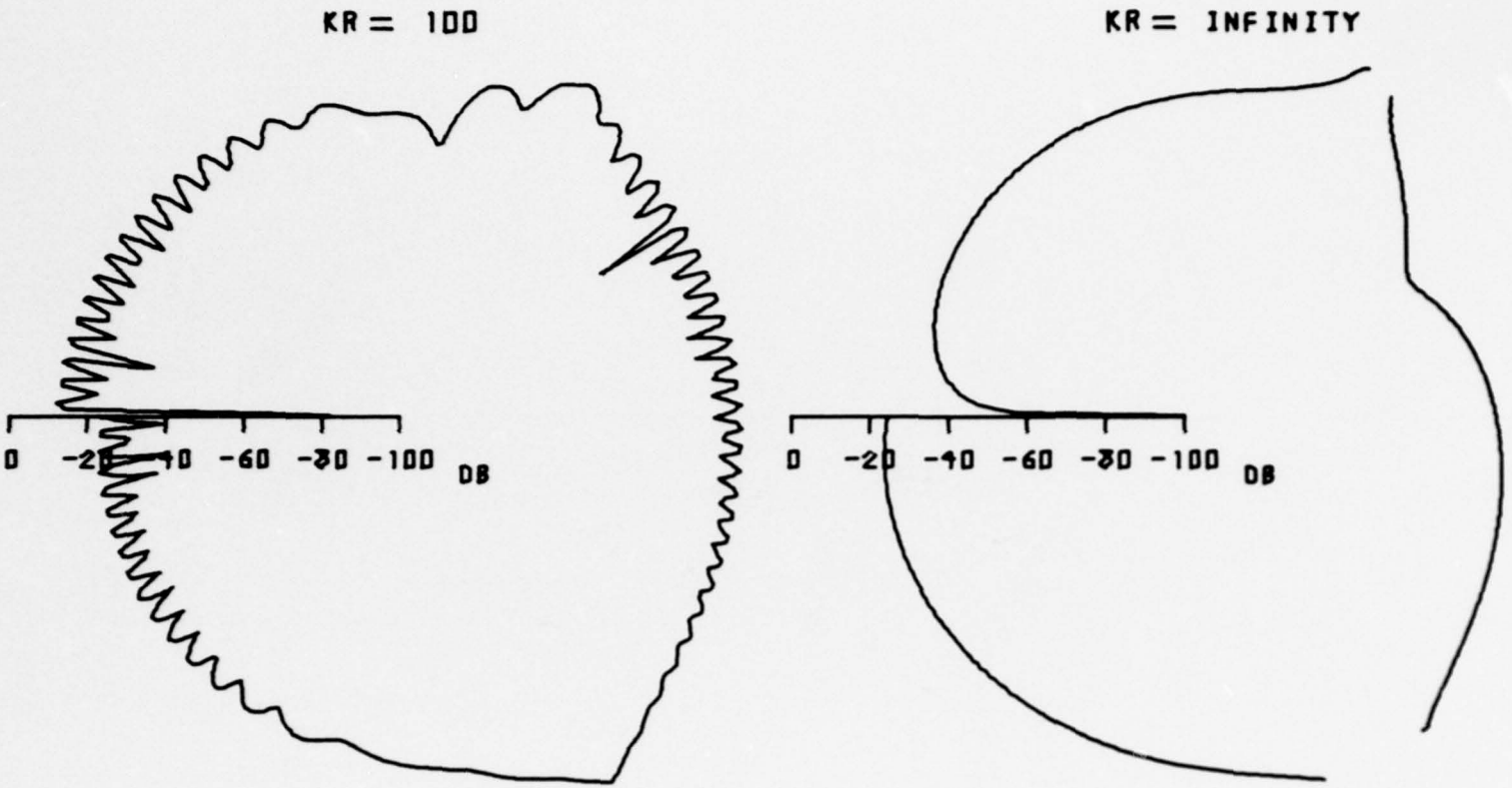

Figure 3.14. Diffraction of a plane wave with $\theta^+ = 30^\circ + i.1$, $\theta^- = 0^\circ$, and $\phi_o = 120^\circ$.

The next ten plots are concerned with the backscattered pressure. For this situation, the source and observer are at the same position, i.e. $\phi = \phi_o$ in Equations (2.42) and (2.52). The dependence of the backscattered pressure on the impedance cover can be studied by comparing the following plots:

1. The impedance conditions for Figures 3.15 and 3.16 are $\theta^+ = 30^o$ and $\theta^- = 0$. The variable kr is 20 and 50 in Figure 3.15, and kr is 100 and infinity in Figure 3.16.
2. In Figures 3.17 and 3.18, $\theta^+ = 60^o$ and $\theta^- = 90^o$ while kr = 20 and 50 in Figure 3.17, and kr = 100 and infinity in Figure 3.18.
3. Figures 3.19 and 3.20 have a totally absorbing upper surface with $\theta^+ = 90^o$ while $\theta^- = 0^o$. In Figure 3.19, kr is 20 and 50, while kr is 100 and infinity in Figure 3.20.
4. The impedance conditions in Figures 3.21 and 3.22 represent a pressure release upper surface $\theta^+ = i5$ and a rigid lower surface $\theta^- = 0^o$. Again, kr is 20 and 50 in Figure 3.21, and kr is 100 and infinity in Figure 3.22.
5. In Figures 3.23 and 3.24, the impedance cover is the same on both sides with $\theta^+ = \theta^- = 30^o$. The values of kr in Figure 3.23 are 20 and 50, while in Figure 3.24 they are 100 and infinity.

3.5 Diffraction and Backscattering of Line Source Radiation by an Impedance Covered Half-Plane

Computations for the line source are made primarily to study the effect of the source type and location on the diffracted and backscattered pressure. In order to compare these graphs with the

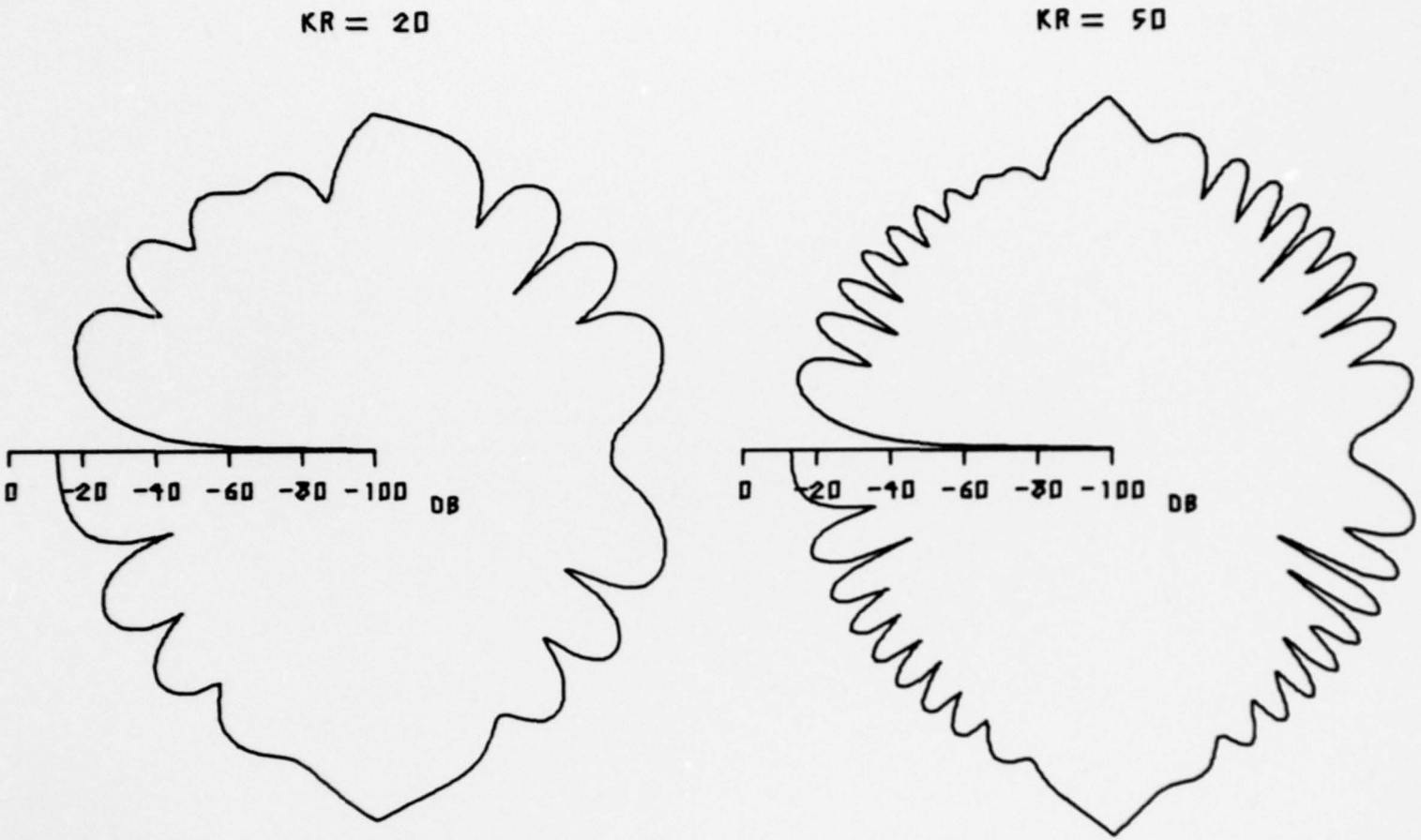

Figure 3.15. Backscattering of a plane wave with $\theta^+ = 30^\circ$ and $\theta^- = 0^\circ$.

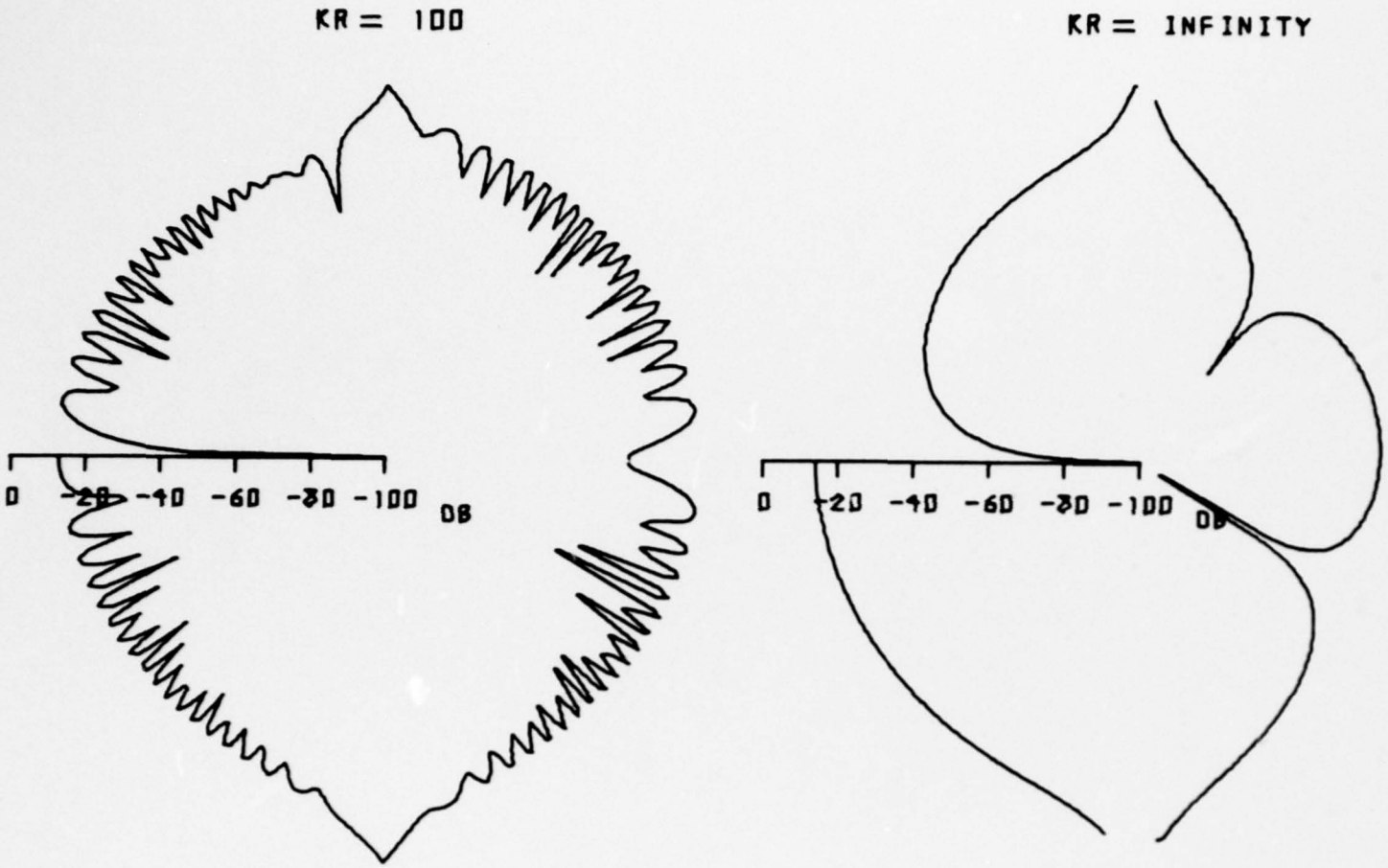

Figure 3.16. Backscattering of a plane wave with $\theta^+ = 30^o$ and $\theta^- = 0^o$.

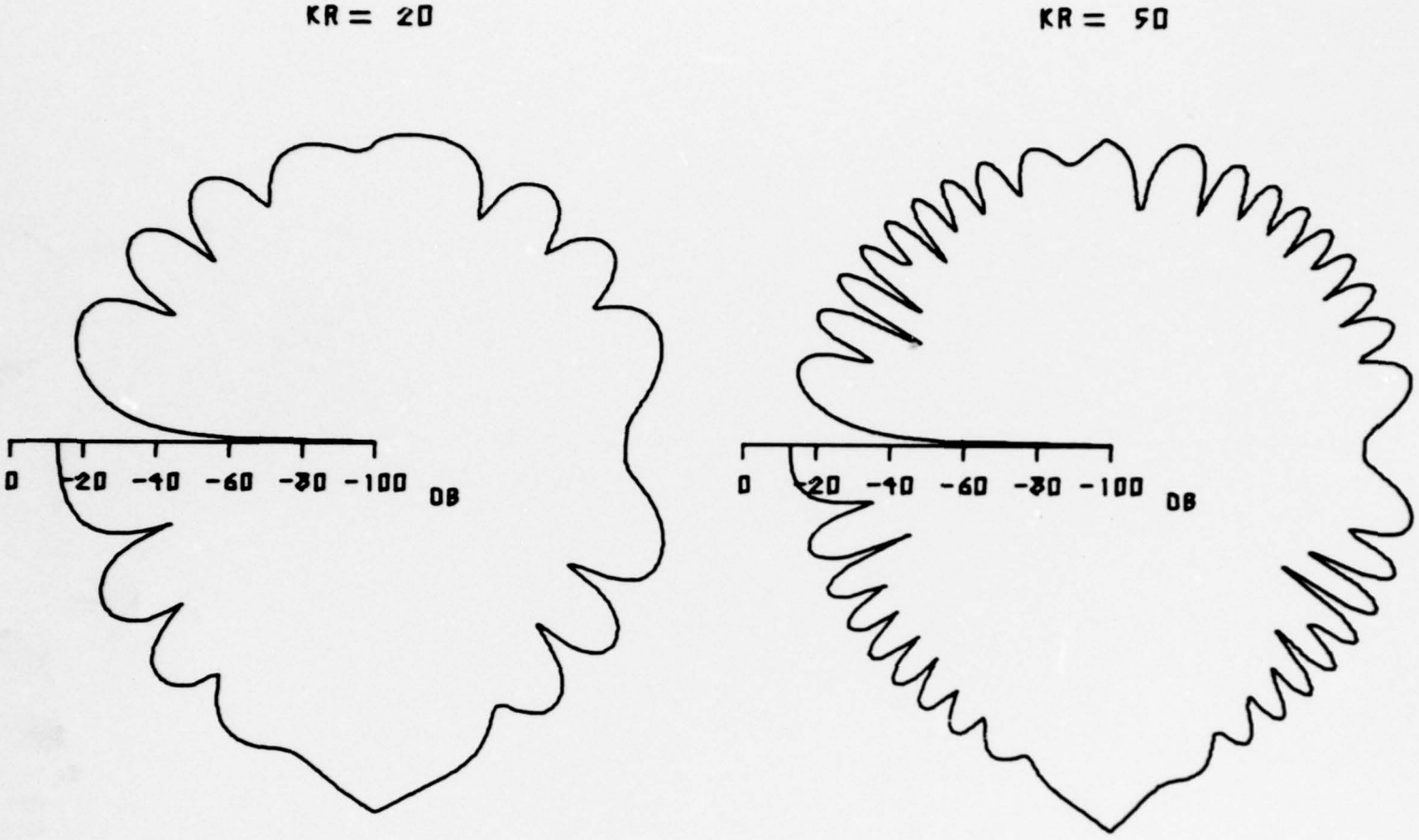

Figure 3.17. Backscattering of a plane wave with $\theta^+ = 60^\circ$ and $\theta^- = 0^\circ$.

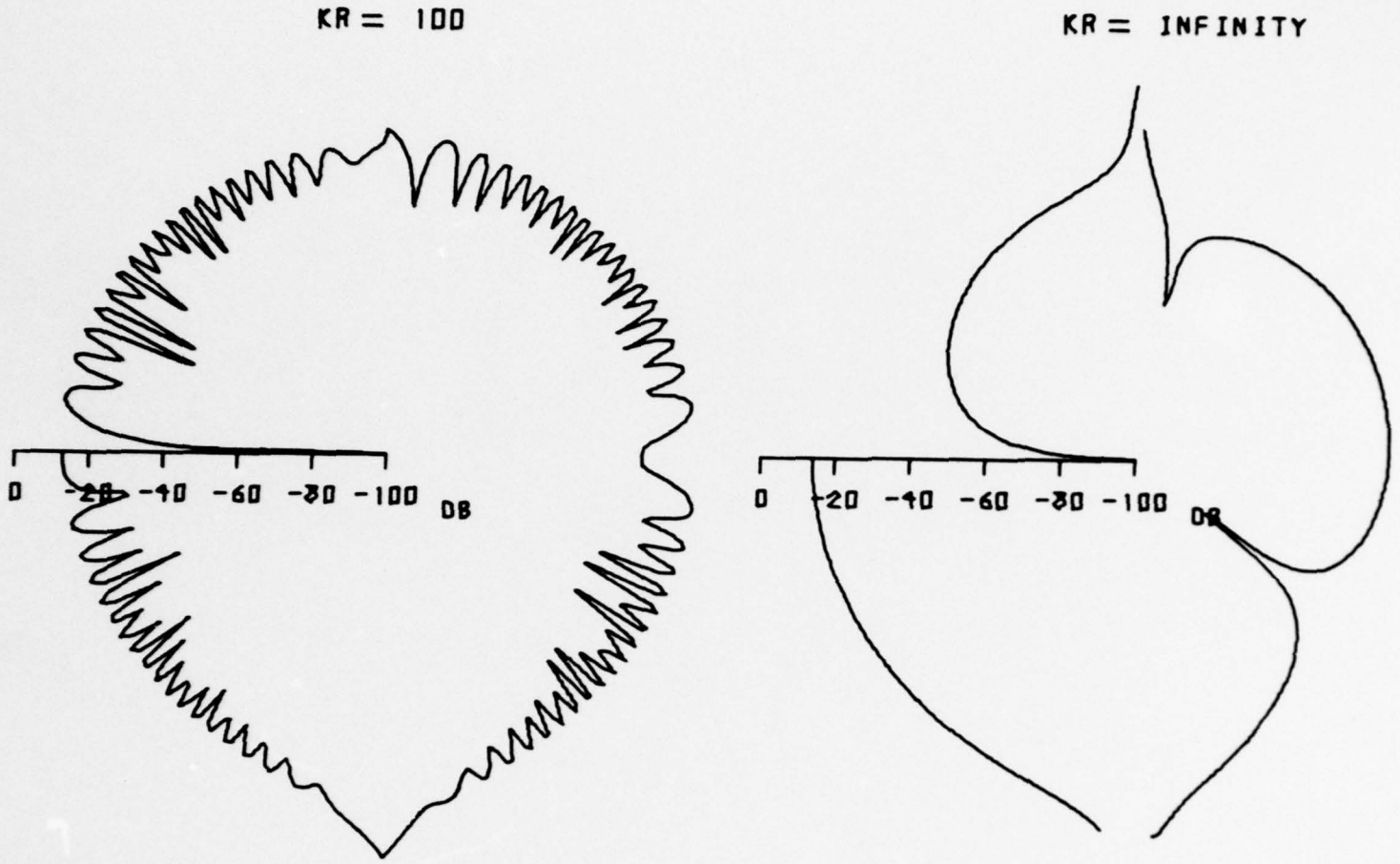

Figure 3.18. Backscattering of a plane wave with $\theta^+ = 60^o$ and $\theta^- = 0^o$.

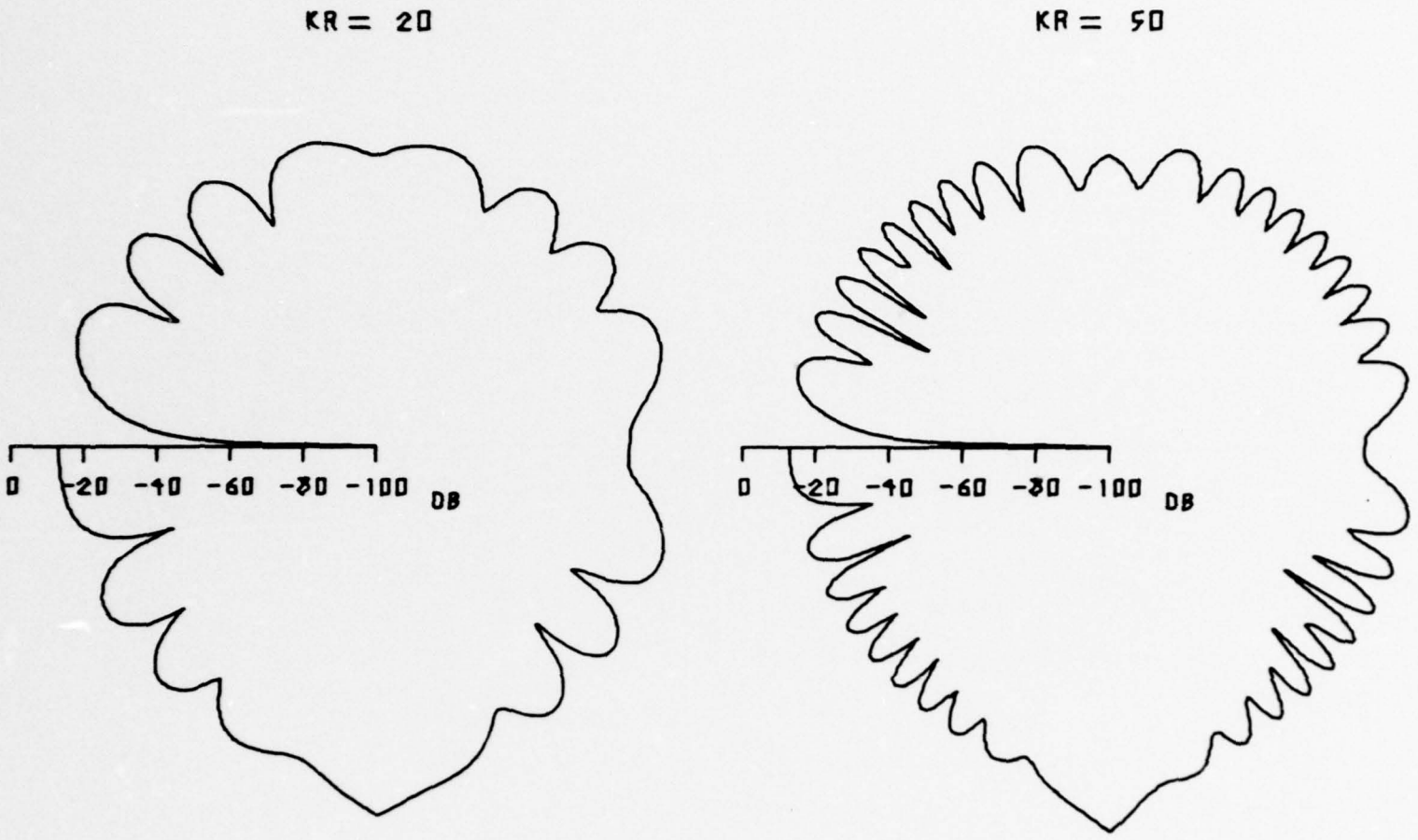

Figure 3.19. Backscattering of a plane wave with $\theta^+ = 90^\circ$ and $\theta^- = 0^\circ$.

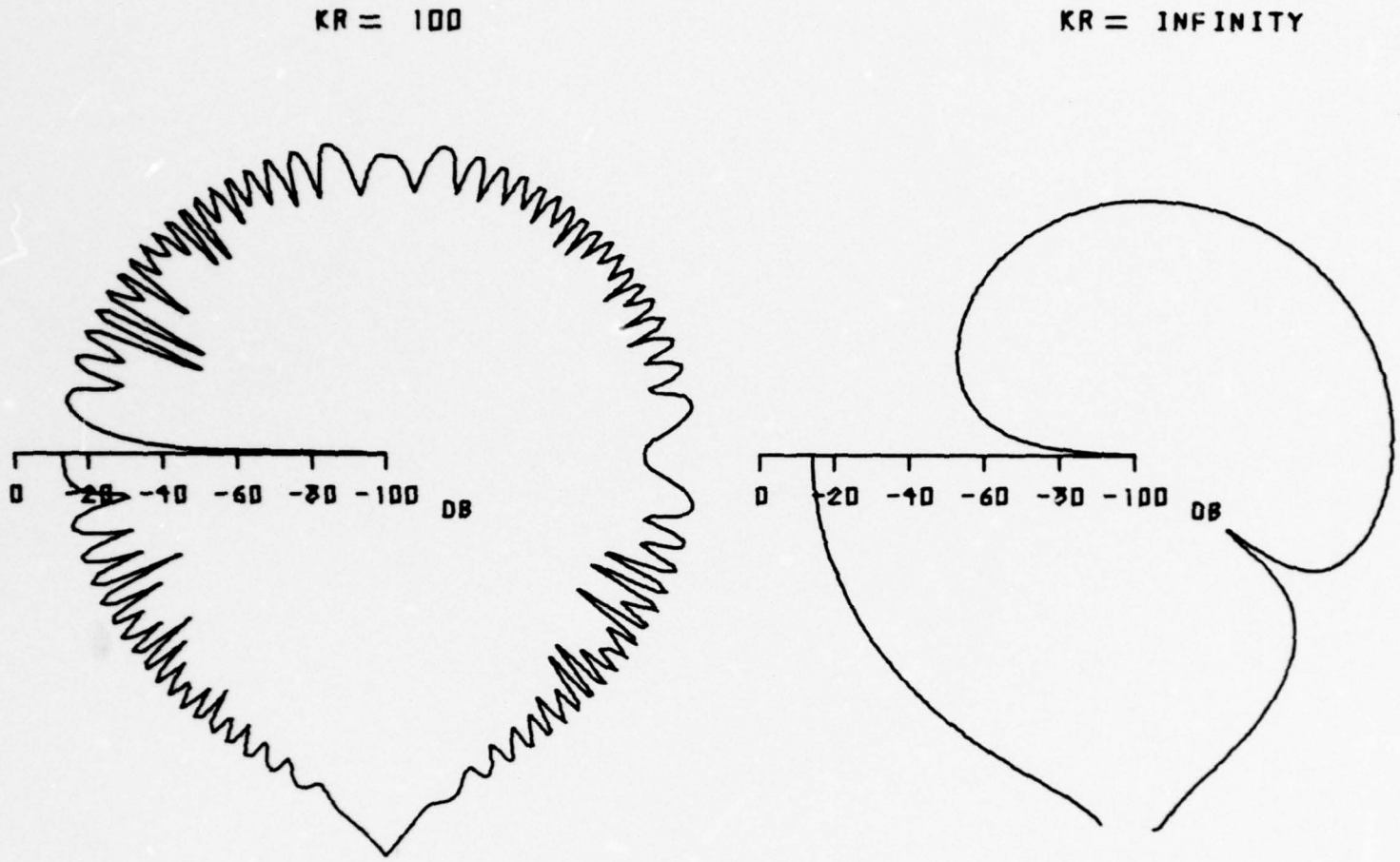

Figure 3.20. Backscattering of a plane wave with $\theta^+ = 90^o$ and $\theta^- = 0^o$.

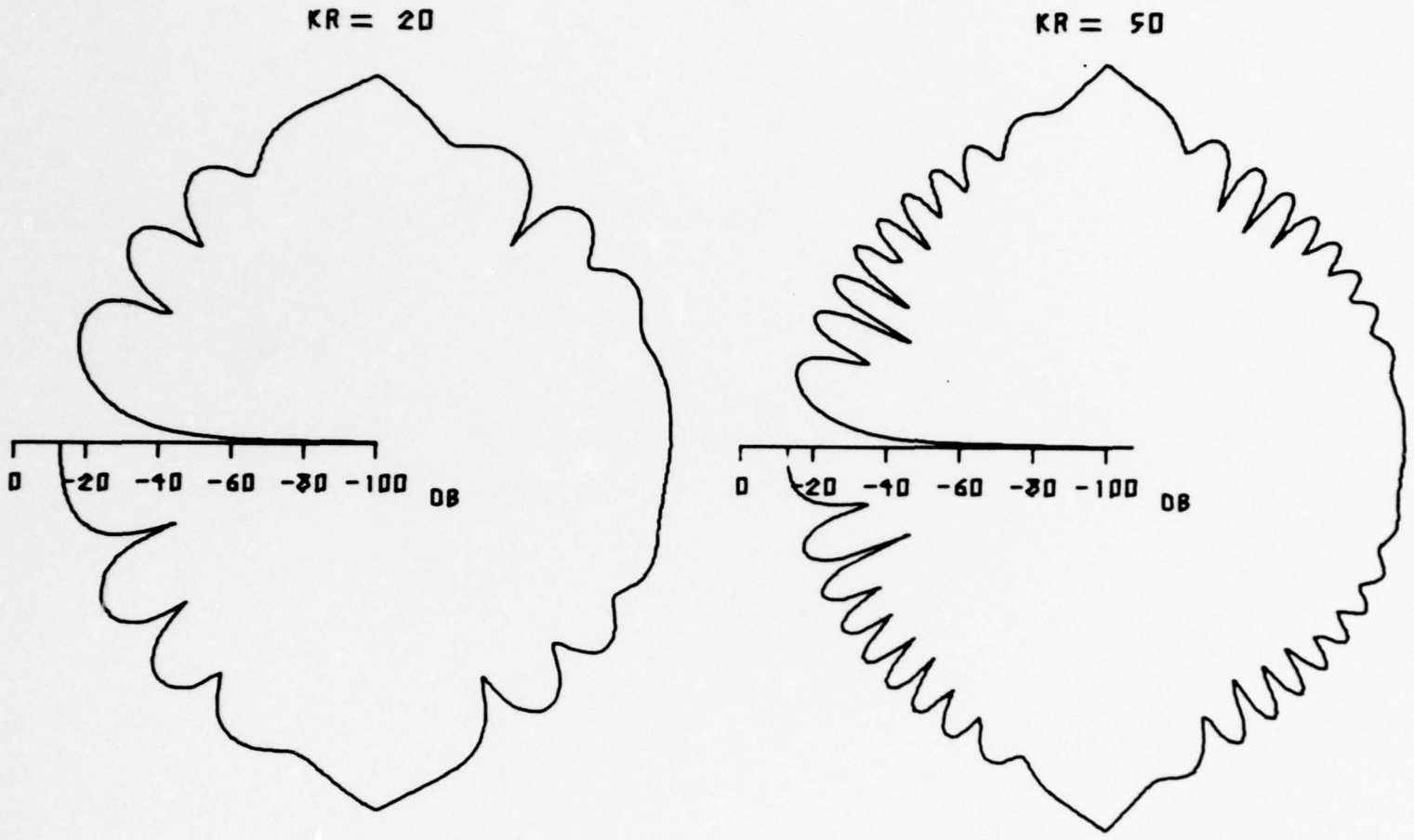

Figure 3.21. Backscattering of a plane wave with $\theta^+ = i5$ and $\theta^- = 0^o$.

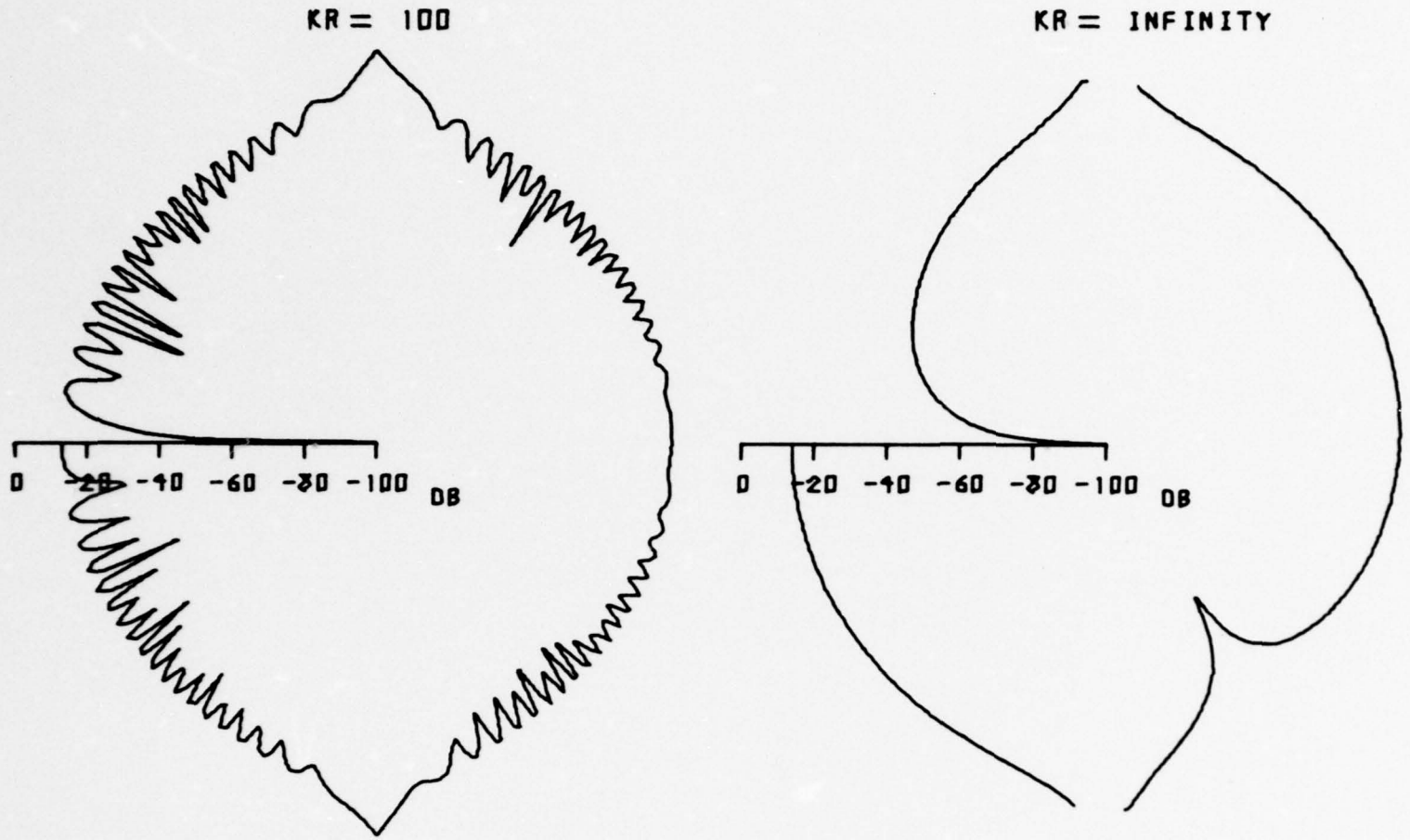

Figure 3.22. Backscattering of a plane wave with $\theta^+ = i5$ and $\theta^- = 0^o$.

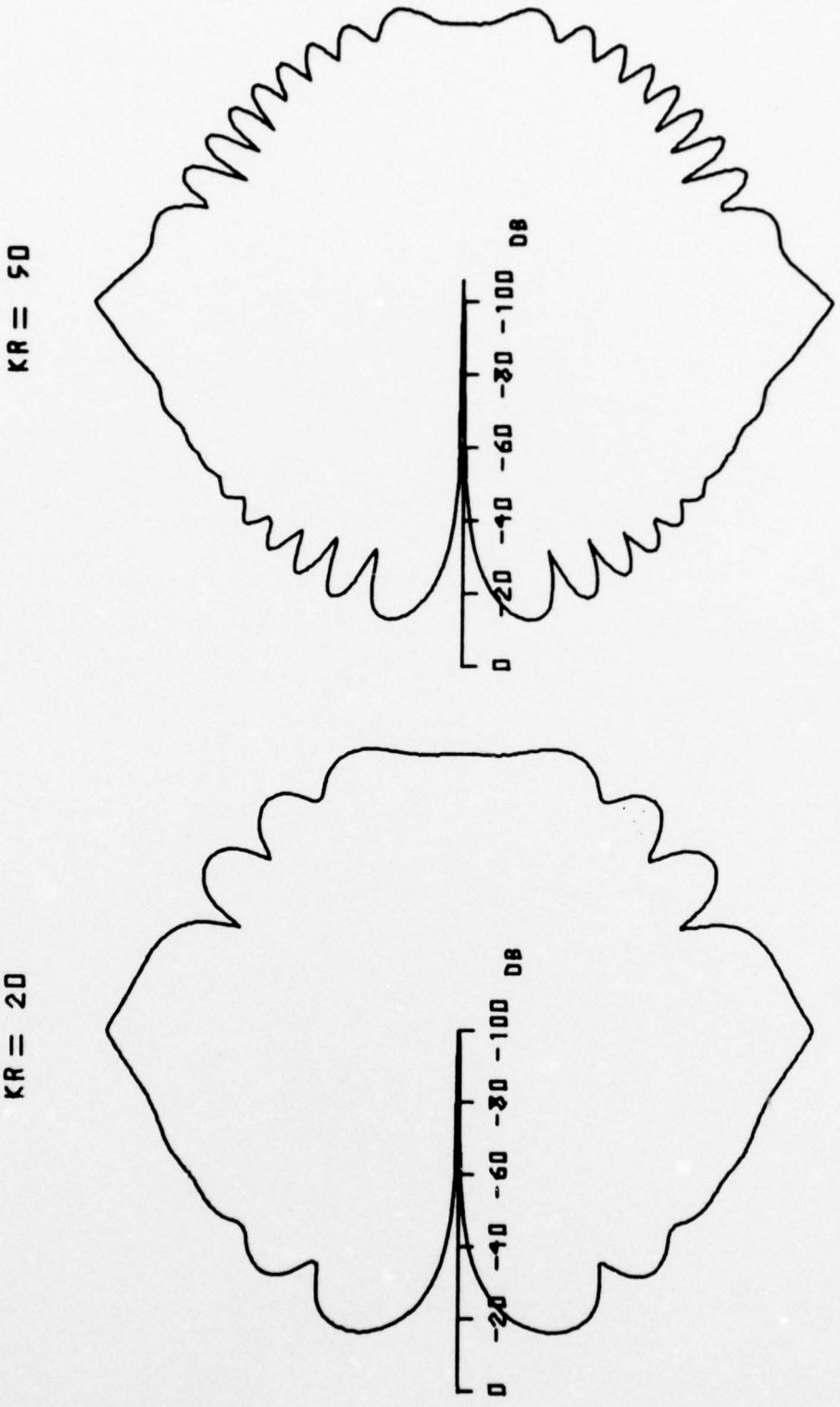

Figure 3.23. Backscattering of a plane wave with $\theta^+ = \theta^- = 30^\circ$.

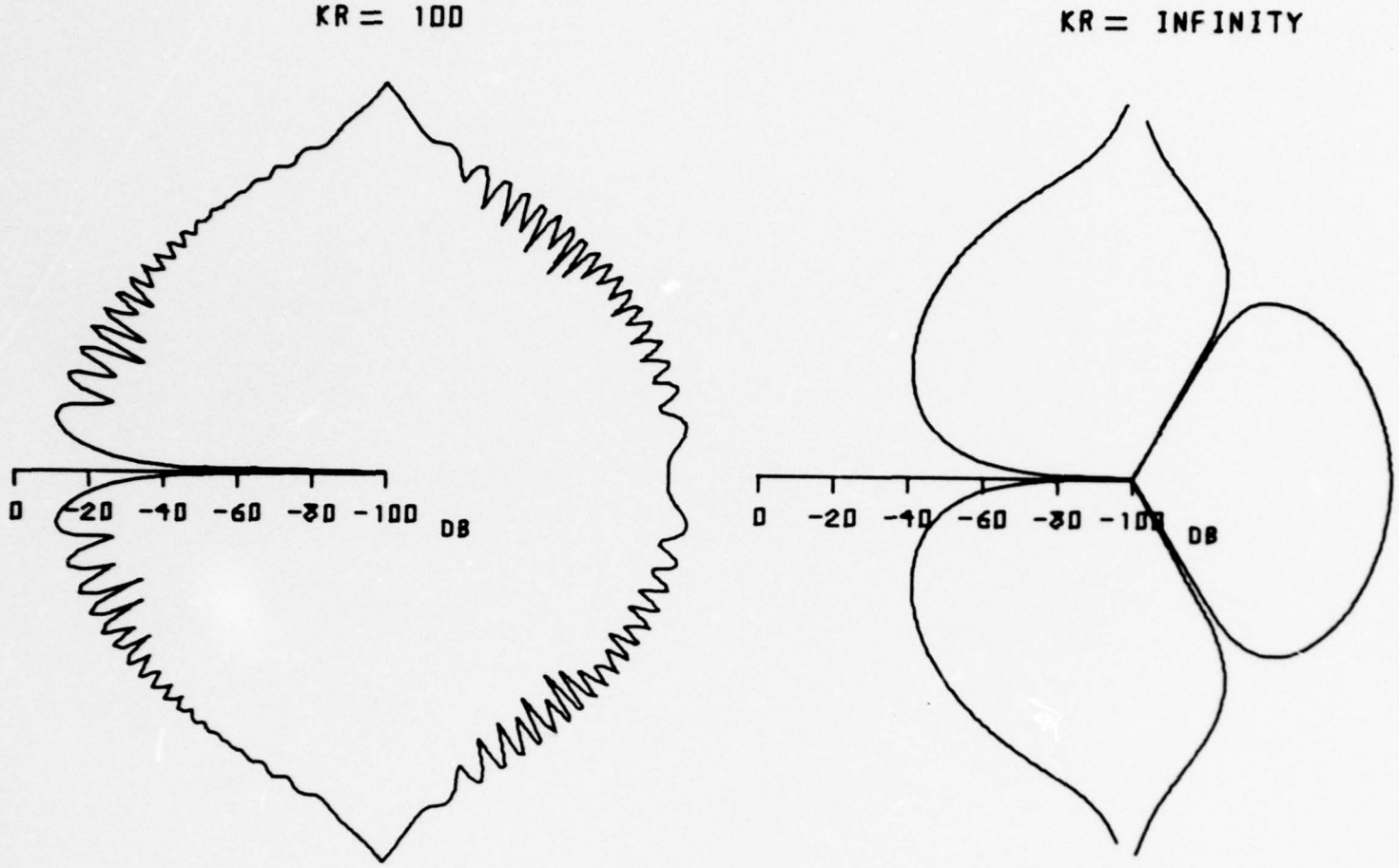

Figure 3.24. Backscattering of a plane wave with $\theta^+ = \theta^- = 30^\circ$.

diffraction of a plane wave, the angle of incidence is kept at $\phi_o = 120^o$. For the line source the magnitude of the pressure diminishes at a rate proportional to $1/\sqrt{kr} \cdot 1/\sqrt{kr_o}$ as implied by the argument of Fresnel Integrals in Equation (2.113) and the demoninator of Equation (2.114). Consequently, the calculations for the line source are normalized by the factor $\sqrt{kr} \cdot \sqrt{kr_o}$ in order to permit a better comparison of results.

The next four figures are concerned with the diffraction of line source radiation. They are shown in an attempt to illustrate the influence of kr_o on the behavior of the diffracted pressure. The values of kr_o are chosen to be $kr_o = 20, 50, 100$ in order to provide a range of values.

In Figures 3.25 and 3.26, the impedance on the two surfaces are $\theta^+ = 60^o$ and $\theta^- = 0$. The value of kr is fixed at 50, while $kr_o = 20$ and 50 in Figure 3.25 and $kr_o = 100$ in Figure 3.26.

The impedances in Figures 3.27 and 3.28 are $\theta^+ = 90^o$ (totally absorbing) and $\theta^- = 0$. Again, in each of these figures, kr = 50. In Figure 3.27, $kr_o = 20$ and 50, while in Figure 3.28 $kr_o = 100$.

The next three figures represent the backscattered pressure of a line source. For this situation, the source and observer are at the same location; i.e., $kr = kr_o$ and $\phi = \phi_o$ in Equation (2.113). In each of the following figures, the impedances on the two surfaces are equal. In Figure 3.29, the impedance conditions are $\theta^+ = \theta^- = 30^o$, while $kr = kr_o = 20$, and $kr = kr_o = 100$. The impedances in Figure 3.30 are $\theta^+ = \theta^- = 60^o$. Again, the radial parameters are $kr = kr_o = 20$, and $kr = kr_0 = 100$. In Figure 3.31, the impedance conditions are $\theta^+ = \theta^- = 90^o$, while $kr = kr_o = 20$ and $kr = kr_o = 100$.

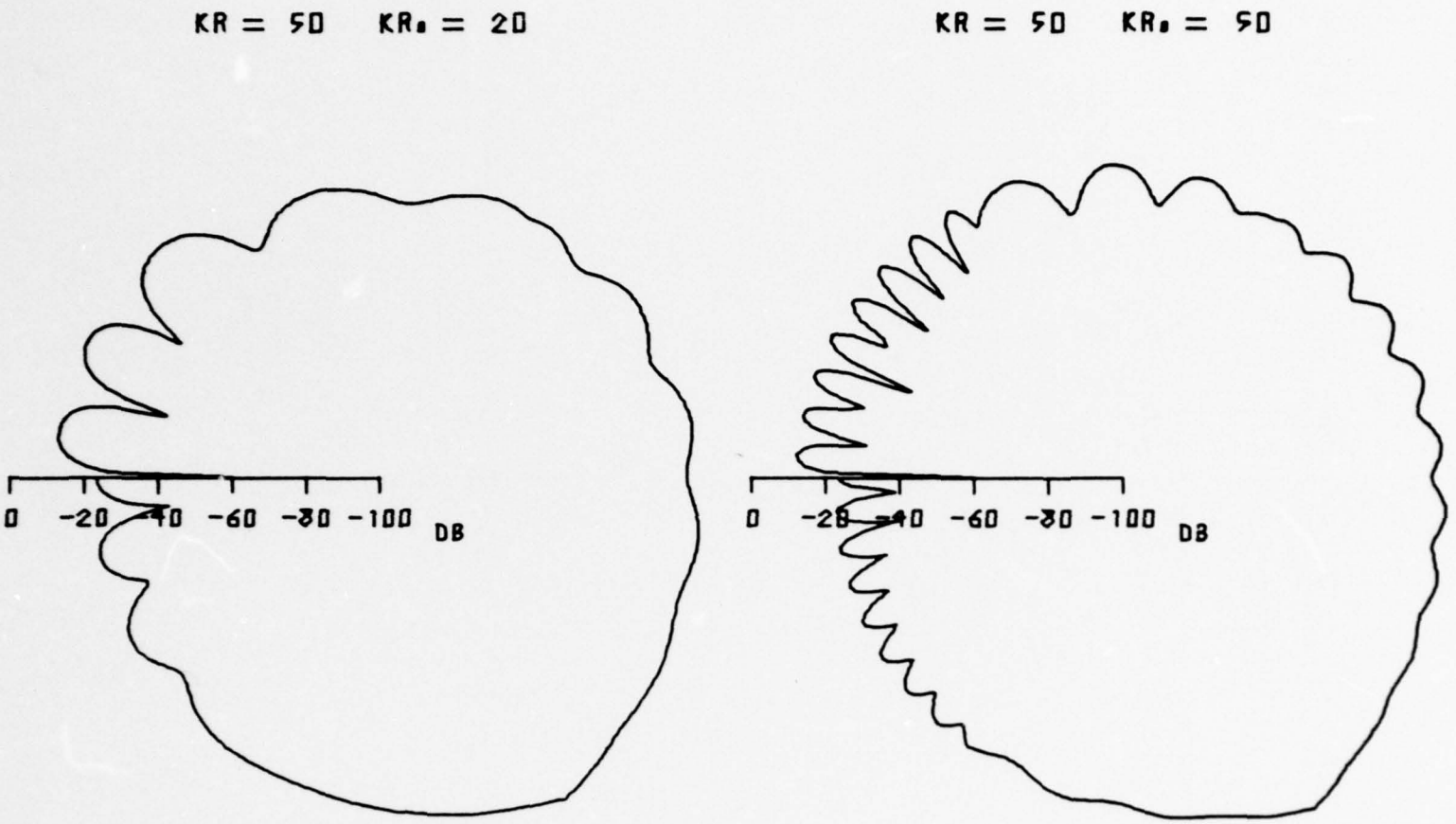

Figure 3.25. Diffraction of line source radiation with $\theta^+ = 60^\circ$, $\theta^- = 0^\circ$, and $\phi_o = 120^\circ$.

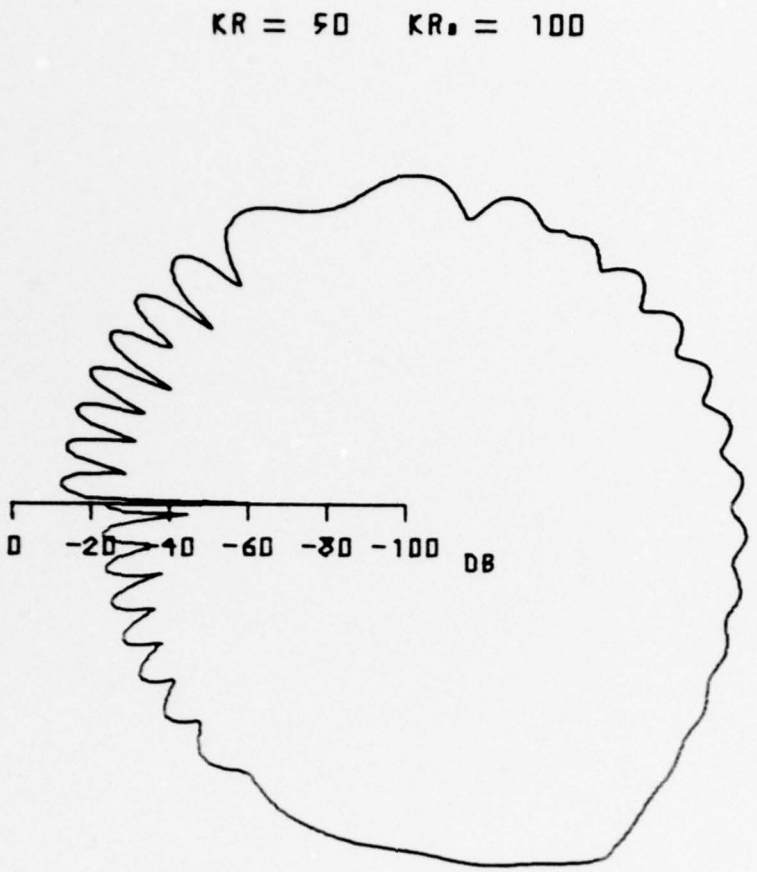

Figure 3.26. Diffraction of line source radiation with $\theta^+ = 60^\circ$, $\theta^- = 0^\circ$, and $\phi_o = 120^\circ$.

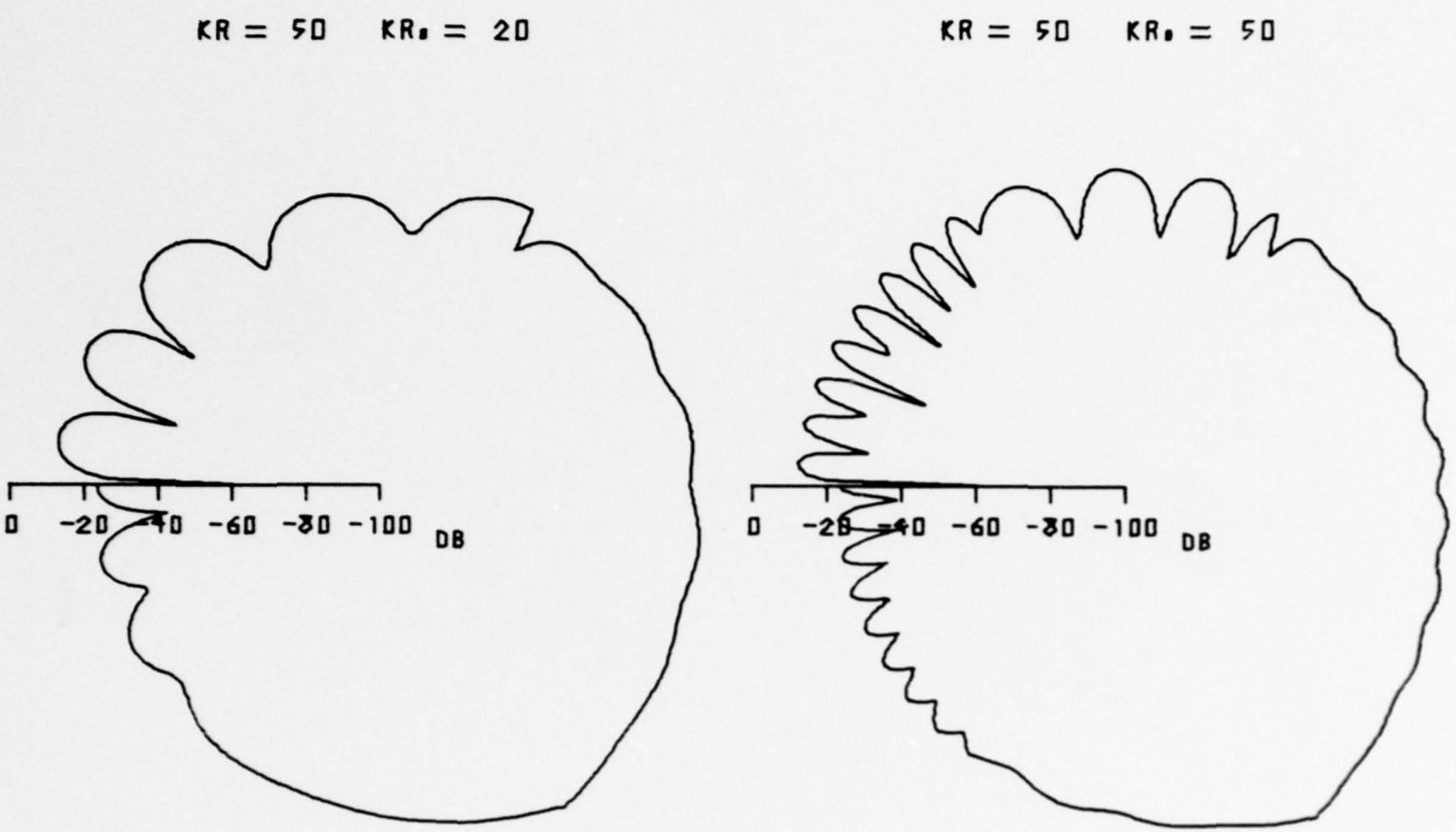

Figure 3.27. Diffraction of line source radiation with $\theta^+ = 90^\circ$, $\theta^- = 0^\circ$, and $\phi_o = 120^\circ$.

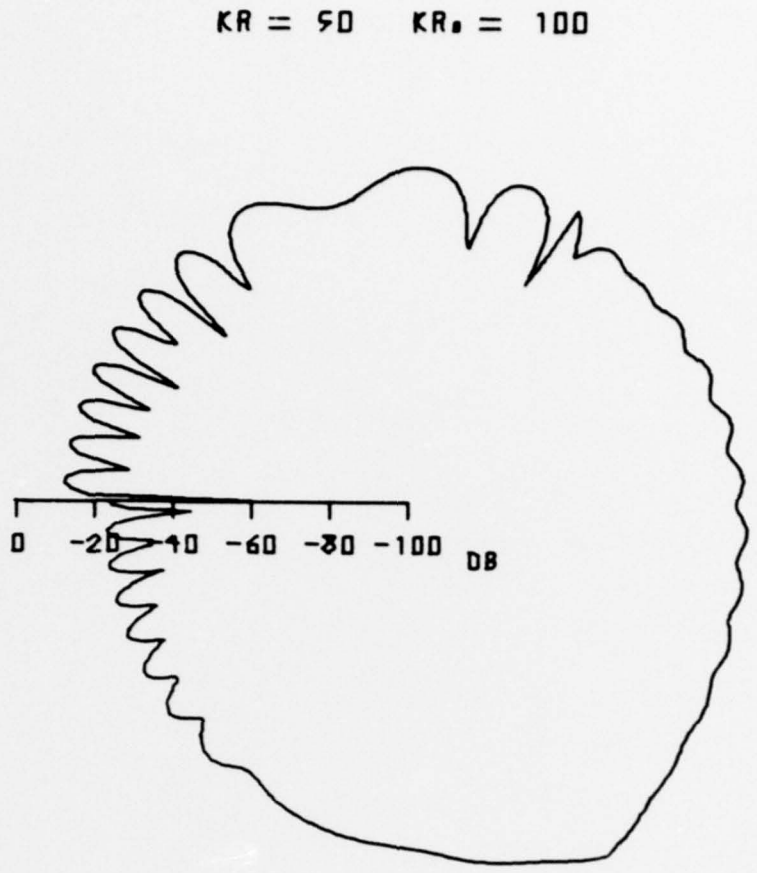

Figure 3.28. Diffraction of line source radiation with $\theta^+ = 90^o$, $\theta^- = 0^o$, and $\phi_o = 120^o$.

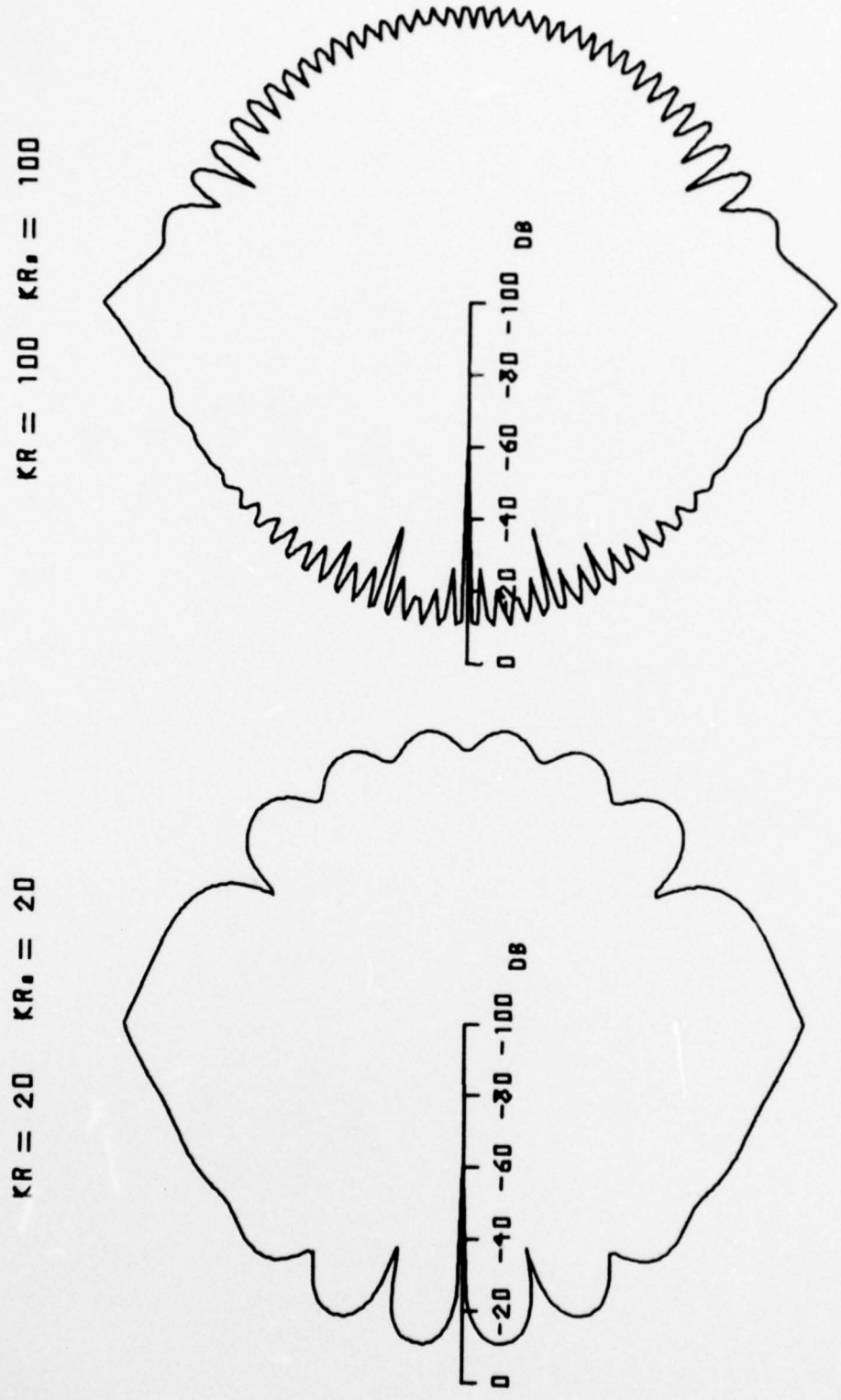

Figure 3.29. Backscattering of line source radiation with $\theta^+ = \theta^- = 30^\circ$.

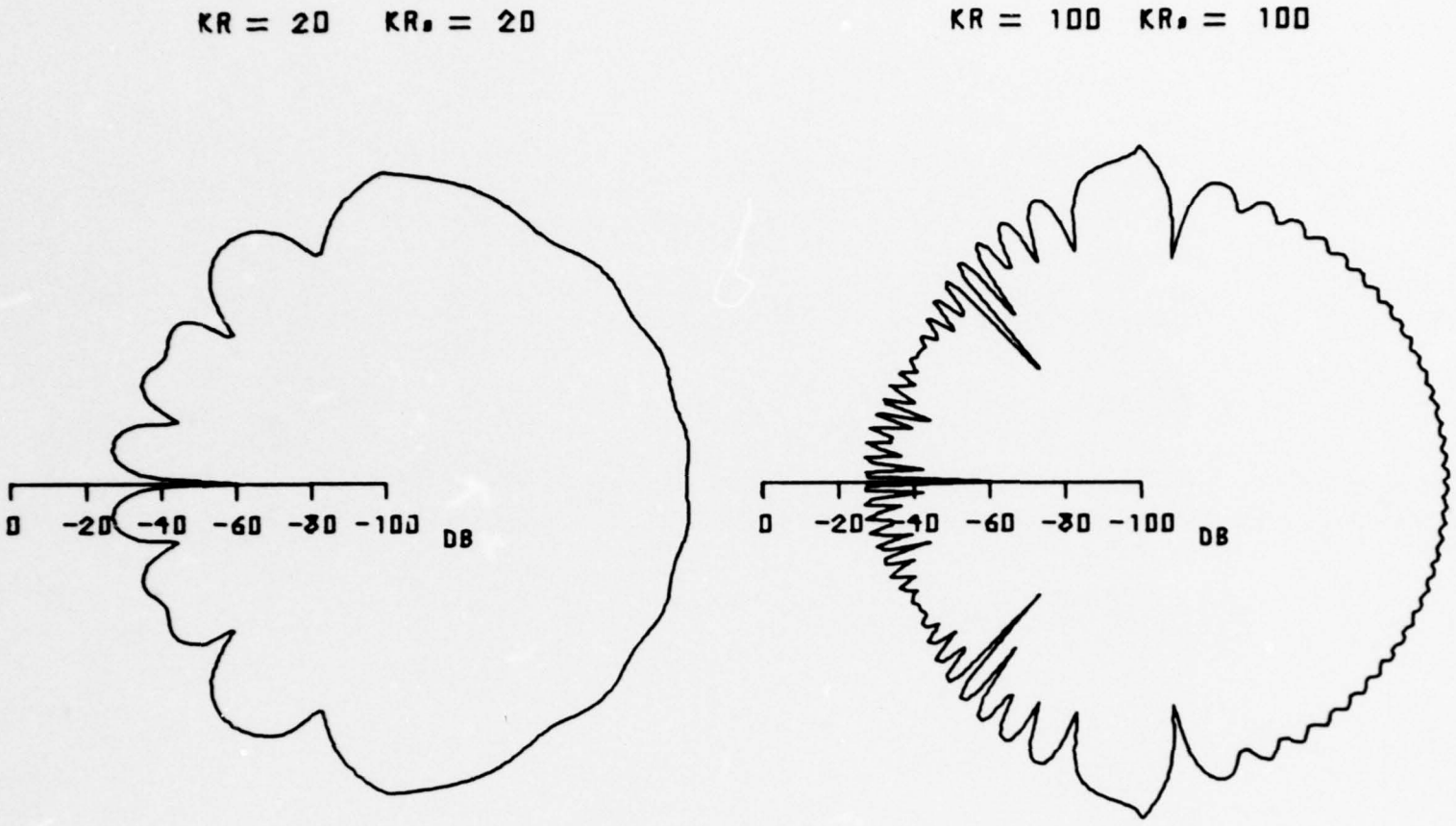

Figure 3.30. Backscattering of line source radiation with $\theta^+ = \theta^- = 60^o$.

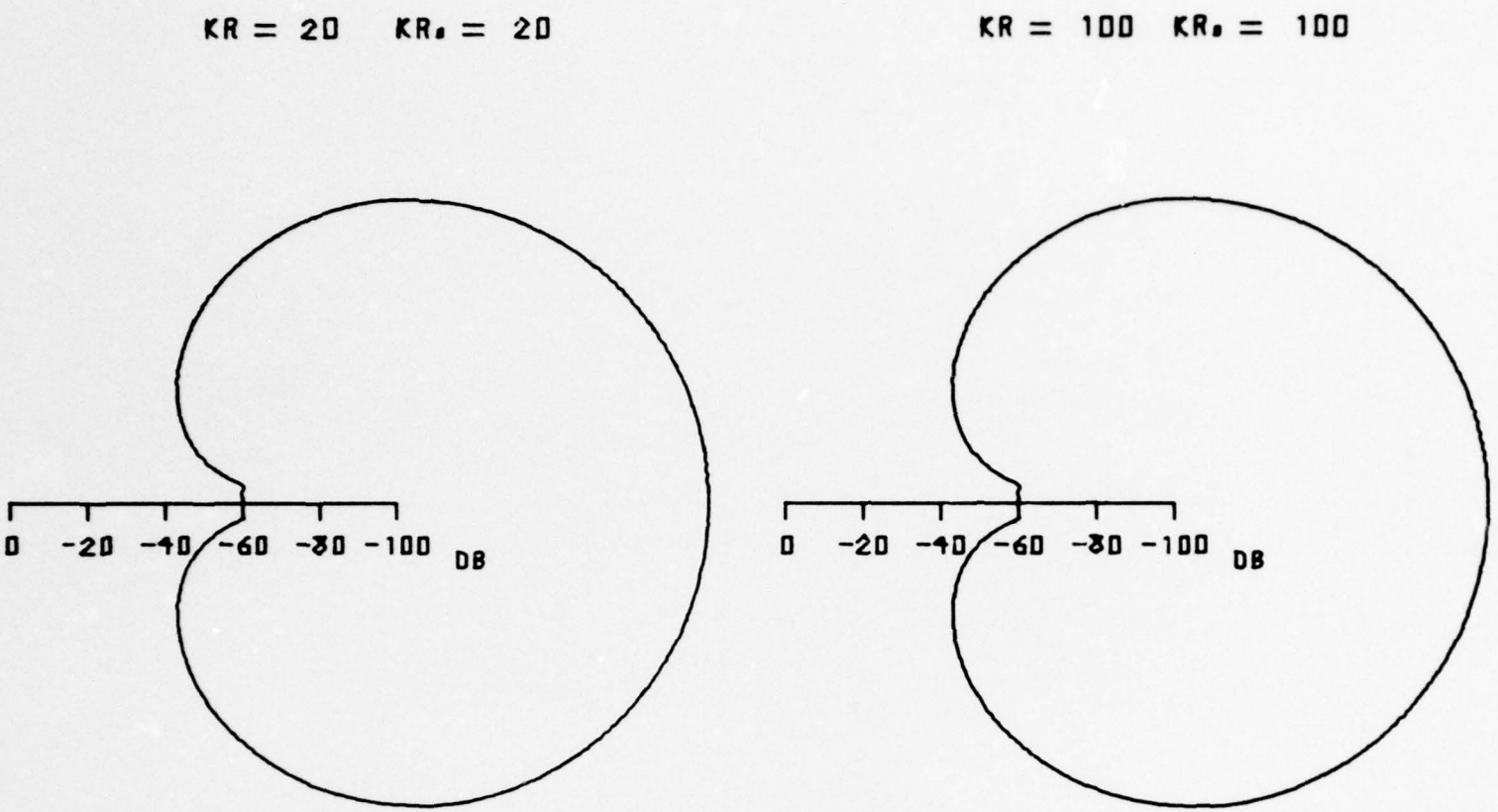

Figure 3.31. Backscattering of line source radiation with $\theta^+ = \theta^- = 90^o$.

3.6 Diffraction and Backscattering of Point Source by an Impedance Covered Half-Plane

The last type of source to be considered is the point source. For this case, it is necessary to specify the relative distance in the z-direction, $k(z-z_o)$, between the source and the observer, as well as the parameters kr and kr_o. The dependence of the diffracted pressure and backscattered pressure on $k(z-z_o)$ is explored in this last section. The magnitude of the pressure for a point source decays at a rate proportional to $1/\sqrt{kr}_1 \cdot 1/\sqrt{kr}_o \cdot 1/\sqrt{kr}$ as demonstrated in Equations (2.133) and (2.135). Consequently, the calculations are normalized by this factor in order to facilitate comparisons between the different plots.

The diffracted pressure is considered in the next group of figures. The parameter $k(z-z_o)$ takes on the values 0 and 100. The purpose of using these values is to investigate its influence. There are two combinations for the variables kr and kr_o that are used. these combinations are $kr - kr_o = 20$, and $kr = kr_o = 100$. Again this choice is made to provide a range of cases suitable to explore their influence on the behavior of the diffracted pressure. The graphs are displayed in such a manner that one may examine the trends as $k(z-z_o)$ varies and as kr and kr_o vary. These calculations are then made for two representative impedance conditions. In both cases, the impedance on the lower surface is fixed at $\theta^- = 0^o$, while the impedance on the illuminated side has the values $\theta^+ = 60^o$ and 90^o. The location of the source is fixed at $\phi_o = 120^o$.

The diffracted pressure of point source radiation is illustrated in the next six plots.

Figure 3.32 shows the diffraction by a surface with impedance conditions $\theta^+ = 60^o$ and $\theta^- = 0^o$ for $kr = kr_o = 20$. In this figure $k(z-z_o) = 0$ and 100.

Figure 3.33 has the same surface condition with $\theta^+ = 60^o$ and $\theta^- = 0^o$ but $kr = kr_o = 100$. Again, one may judge the influence of $k(z-z_o)$ since it has the values of 0 and 100.

The impedance conditions in Figure 3.34 are once again $\theta^+ = 60^o$ and $\theta^- = 0^o$ but $k(z-z_o) = 0$. One may consider the effect of kr and kr_o since they take the values of $kr = kr_o = 20$ and $kr = kr_o = 100$.

In Figure 3.35, $\theta^+ = 90^o$ (totalling absorbing) $\theta^- = 0^o$ and $kr = kr_o = 20$. The two plots in this figure are for $k(z=z_o) = 0$, and $k(z-z_o) = 100.0$.

Figure 3.36 shows a half-plane with $\theta^+ = 90^o$ and $\theta^- = 0^o$ with $kr = kr_o = 100$.

In the last figure for diffraction, $\theta^+ = 90^o$ and $\theta^- = 0^o$ while $k(z-z_o) = 0$. The plots in Figure 3.37 are for $kr = kr_o = 20$ and $kr = kr_o = 100$. They illustrate the effect of kr and kr_o.

The final series of figures investigates the backscattered pressure of an impedance covered half-plane for a point source excitation. For backscatter, the source and receiver are at the same location, so $k(z-z_o)$ is always zero. Computations are made for $kr = kr_o = 20$, and $kr = kr_o = 100$. These values for kr and kr_o represent the cases when the source is close to the edge and also when it is far from the edge. The two representative impedance conditions used for this group of figures are $\theta^+ = \theta^- = 30^o$, and $\theta^+ = \theta^- = 60^o$.

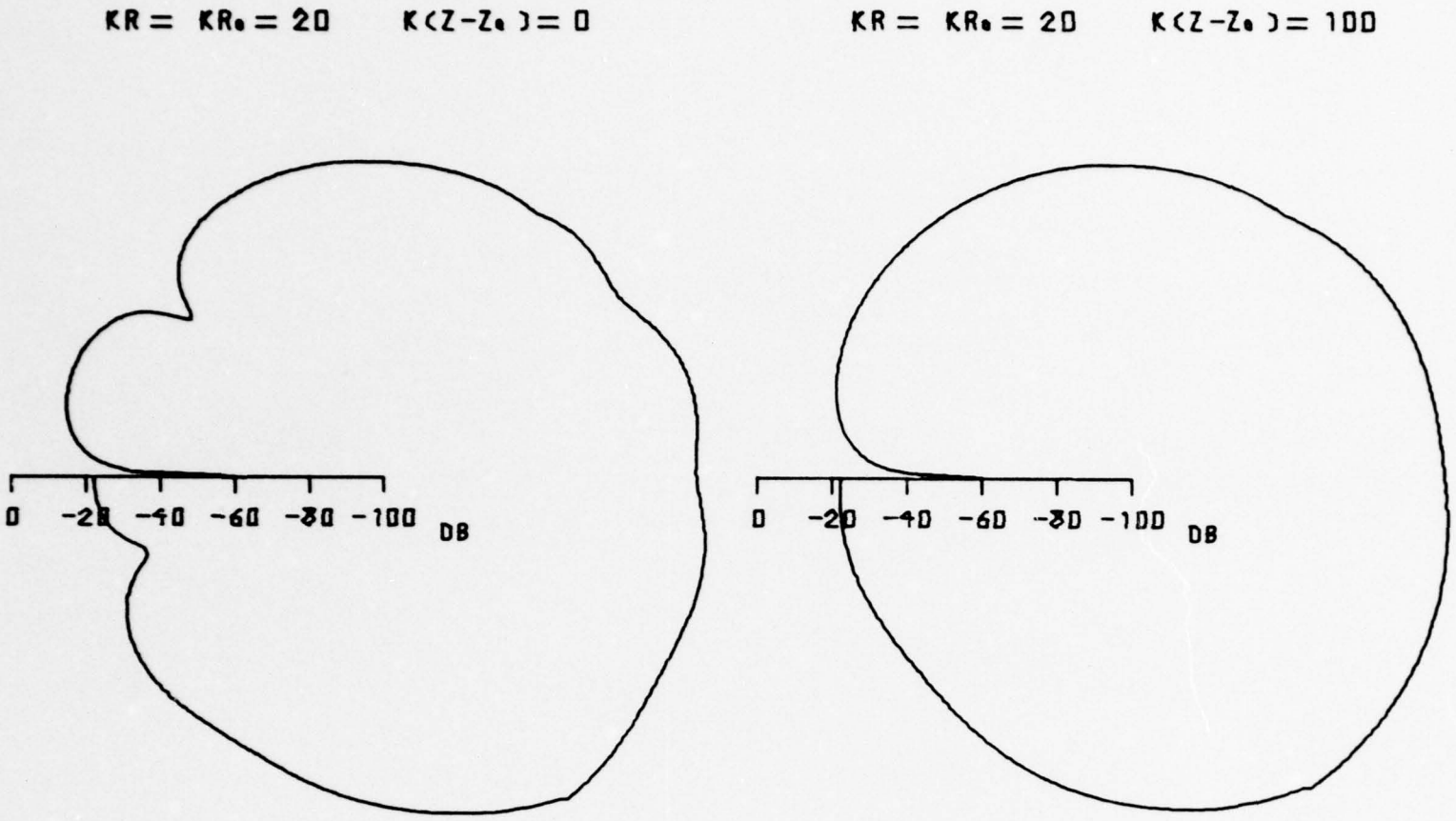

Figure 3.32. Diffraction of point source radiation with $\theta^+ = 60^o$, $\theta^- = 0^o$ and $\phi_o = 120^o$.

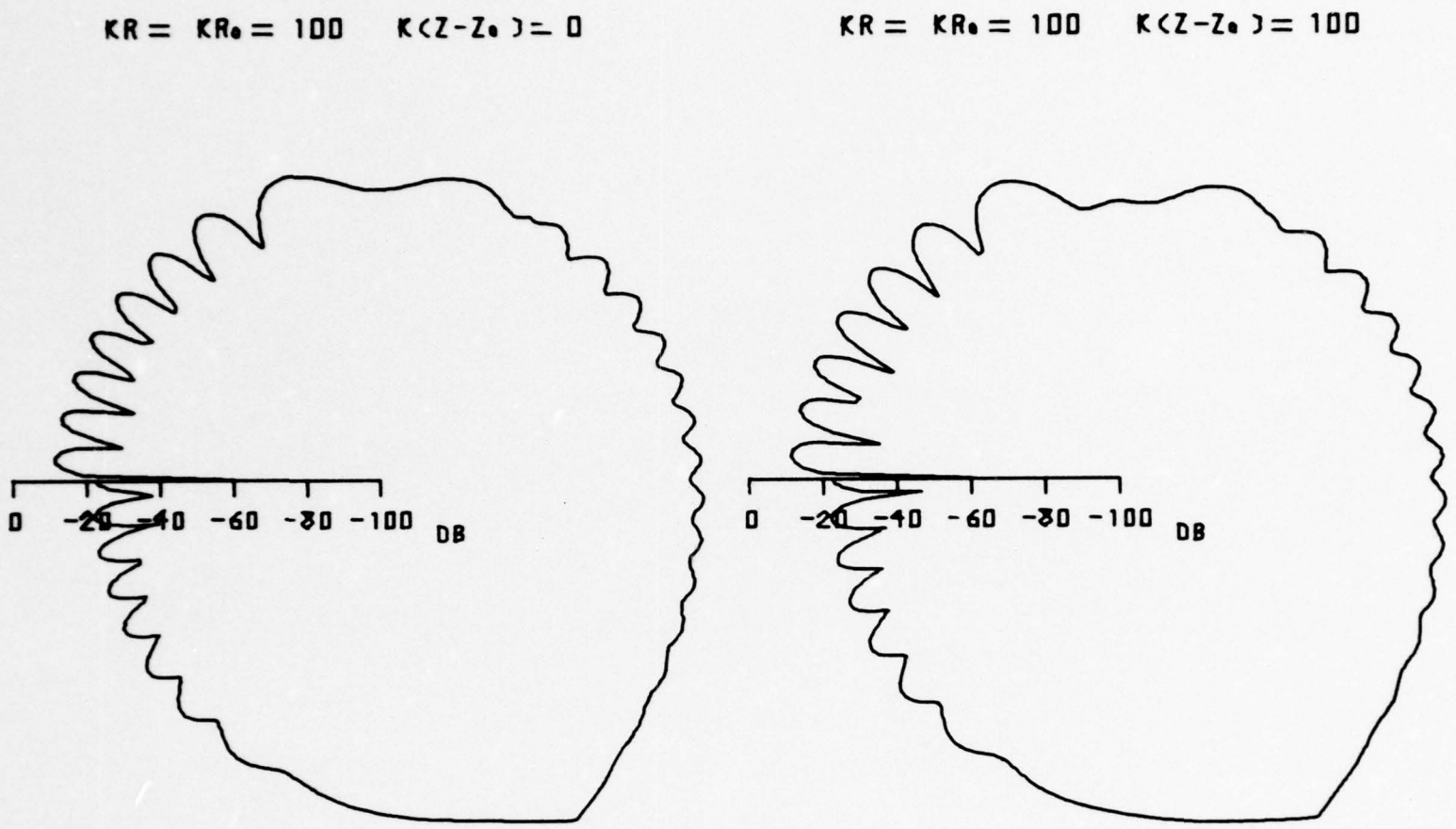

Figure 3.33. Diffraction of point source radiation with $\theta^+ = 60^\circ$, $\theta^- = 0^\circ$, and $\phi_o = 120^\circ$.

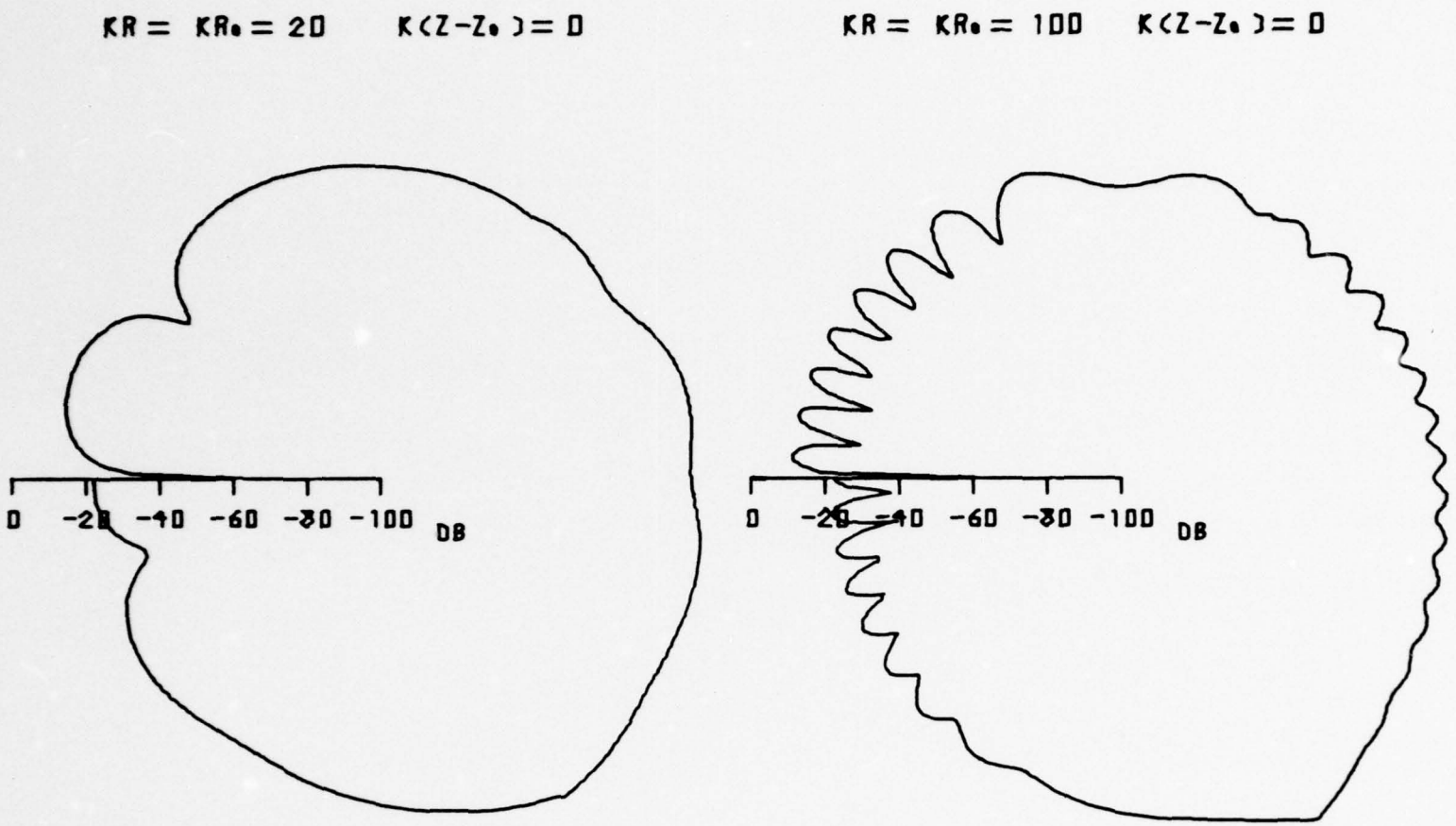

Figure 3.34. Diffraction of point source radiation with $\theta^+ = 60^\circ$, $\theta^- = 0^\circ$, and $\phi_o = 120^\circ$.

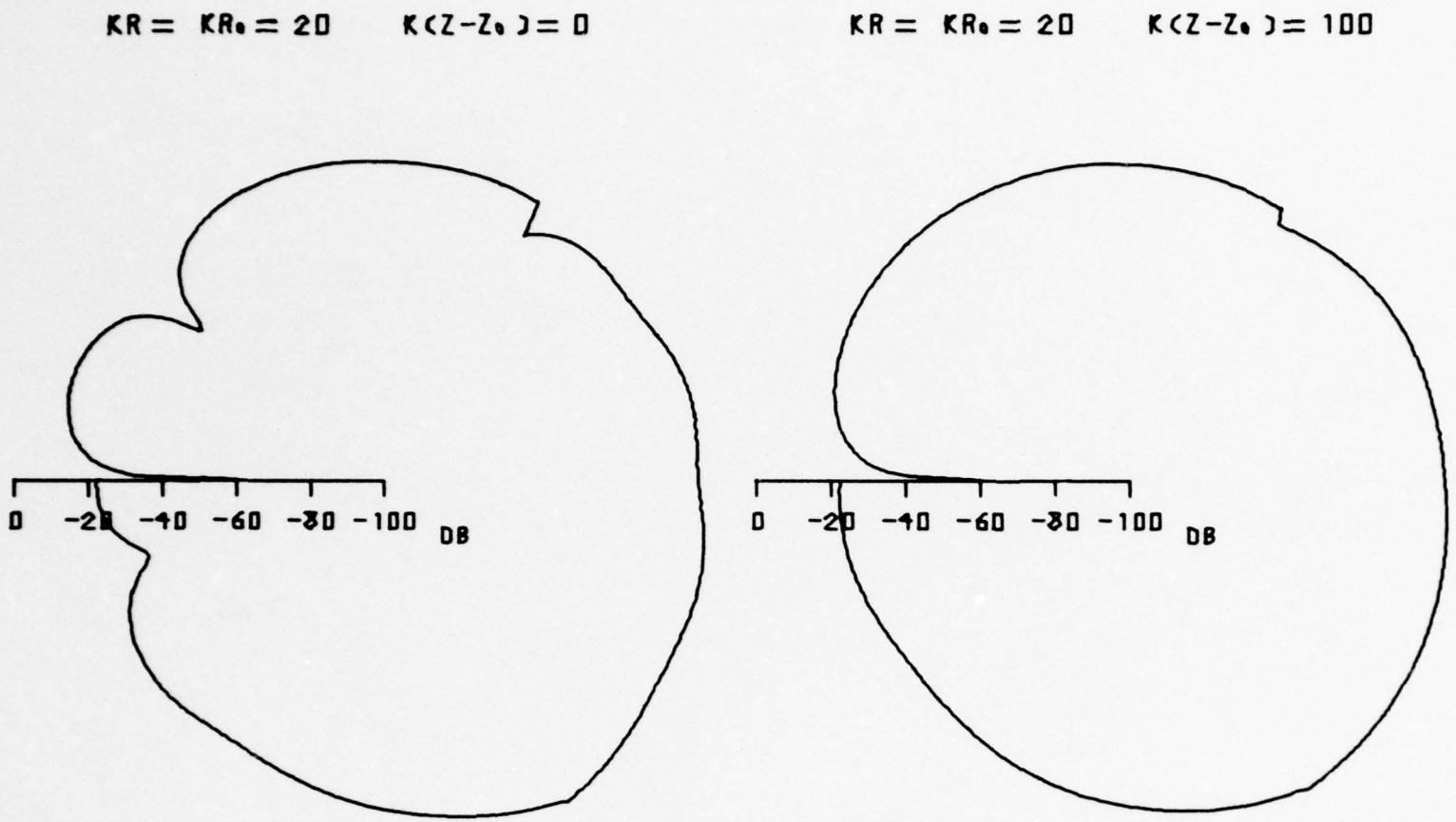

Figure 3.35. Diffraction of point source radiation with $\theta^+ = 90^o$, $\theta^- = 0^o$, and $\phi_o = 120^o$.

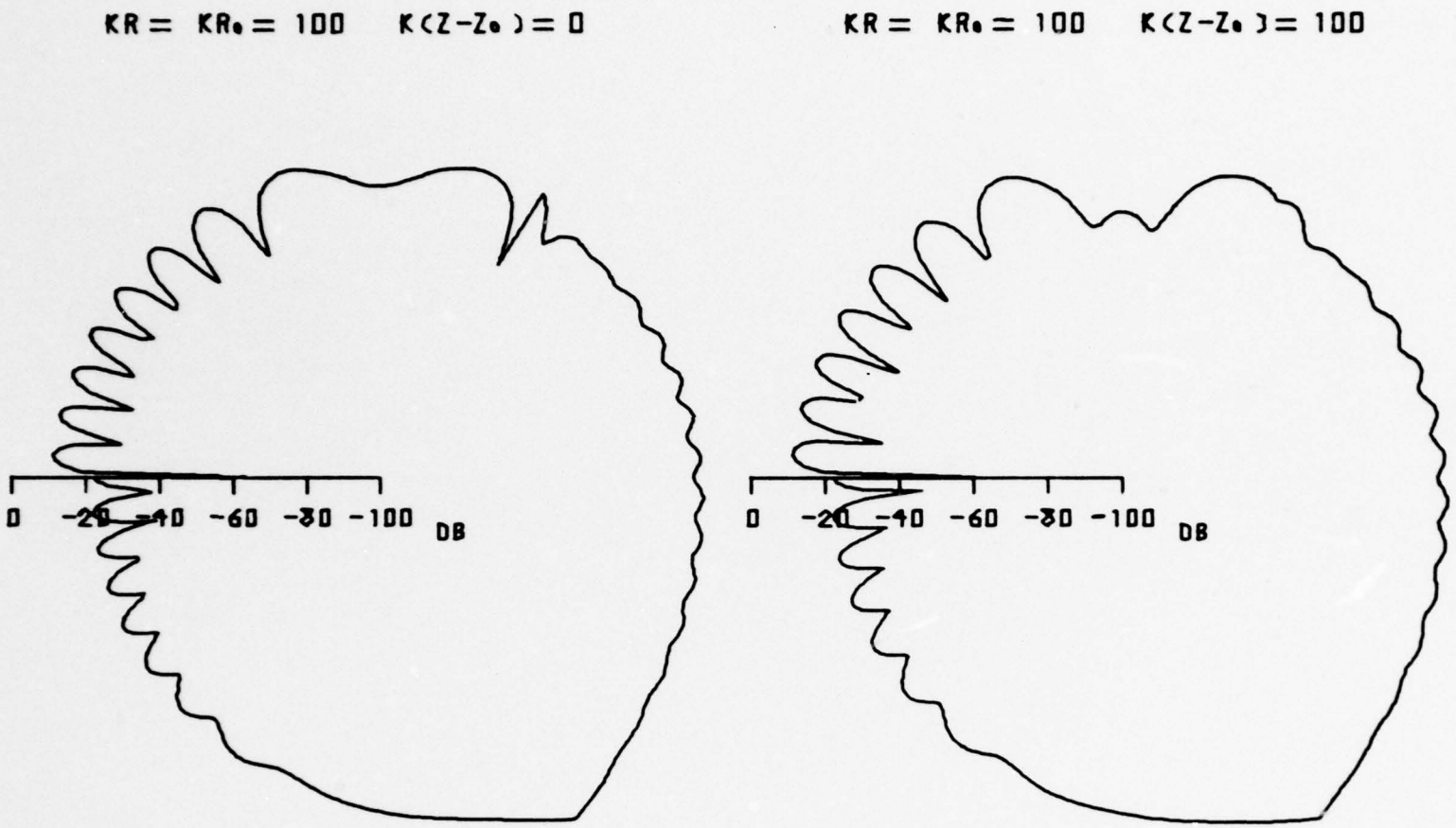

Figure 3.36. Diffraction of point source radiation with $\theta^+ = 90^o$, $\theta^- = 0^o$, and $\phi_o = 120^o$.

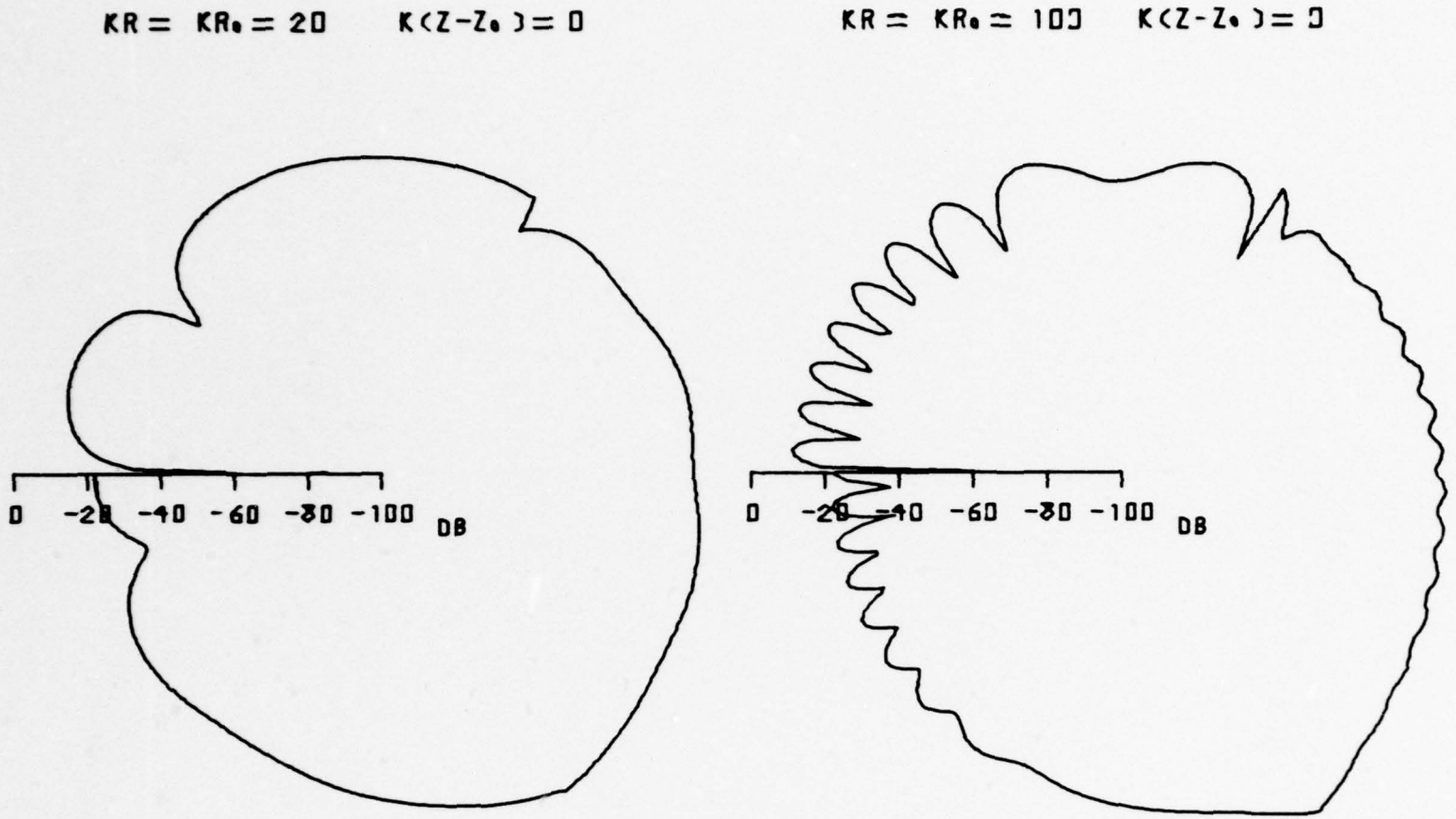

Figure 3.37. Diffraction of point source radiation with $\theta^+ = 90^\circ$, $\theta^- = 0^\circ$, and $\phi_o = 120^\circ$.

Figure 3.38 shows the backscattered pressure for $kr = kr_o = 20$ and $kr = kr_o = 100$ when $\theta^+ = \theta^- = 30^o$.

Figure 3.39 whows the backscattered pressure for $kr = kr_o = 20$ and $kr = kr_o = 100$ when $\theta^+ = \theta^- = 60$.

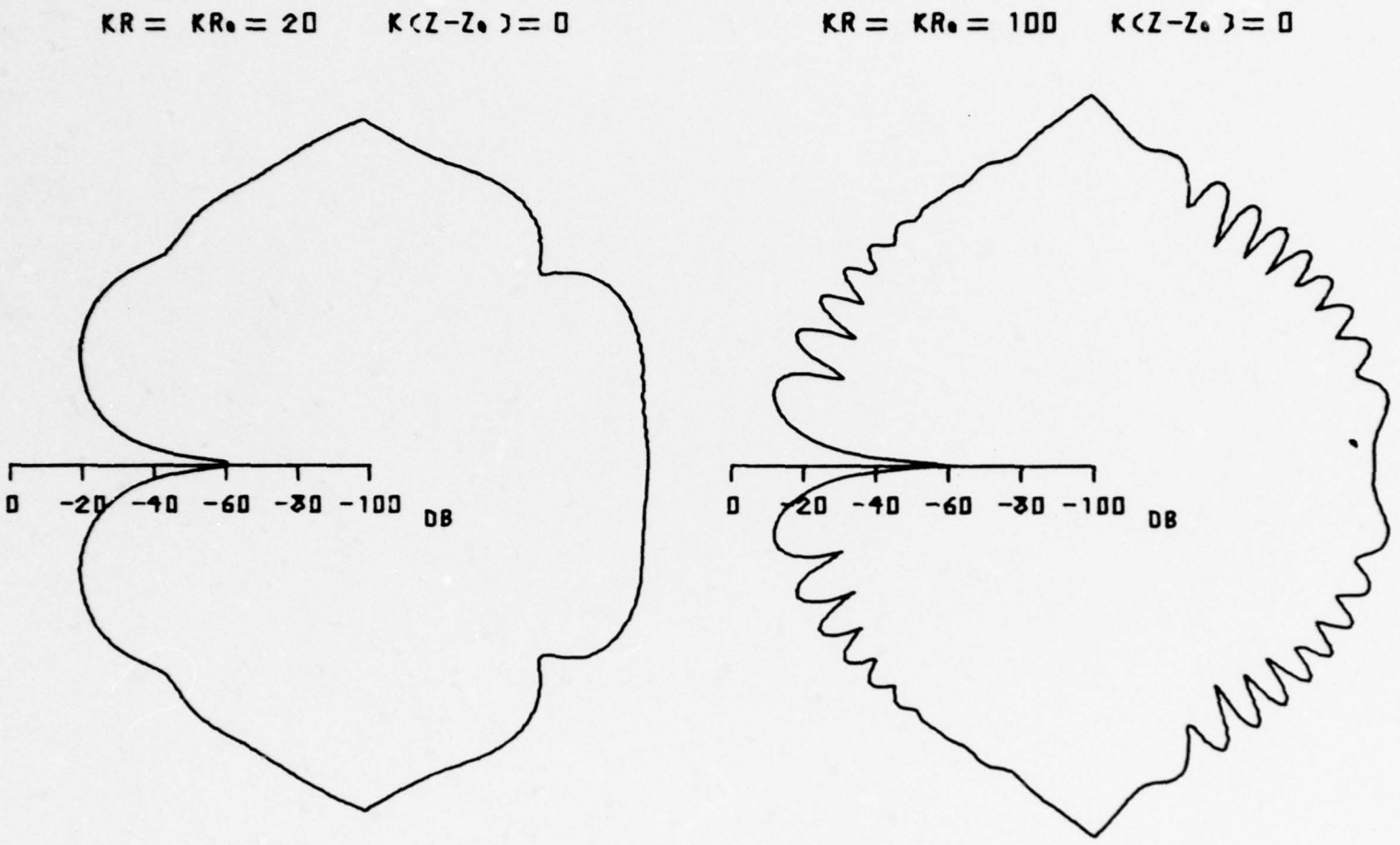

Figure 3.38. Backscattering of point source radiation with $\theta^+ = \theta^- = 30^\circ$.

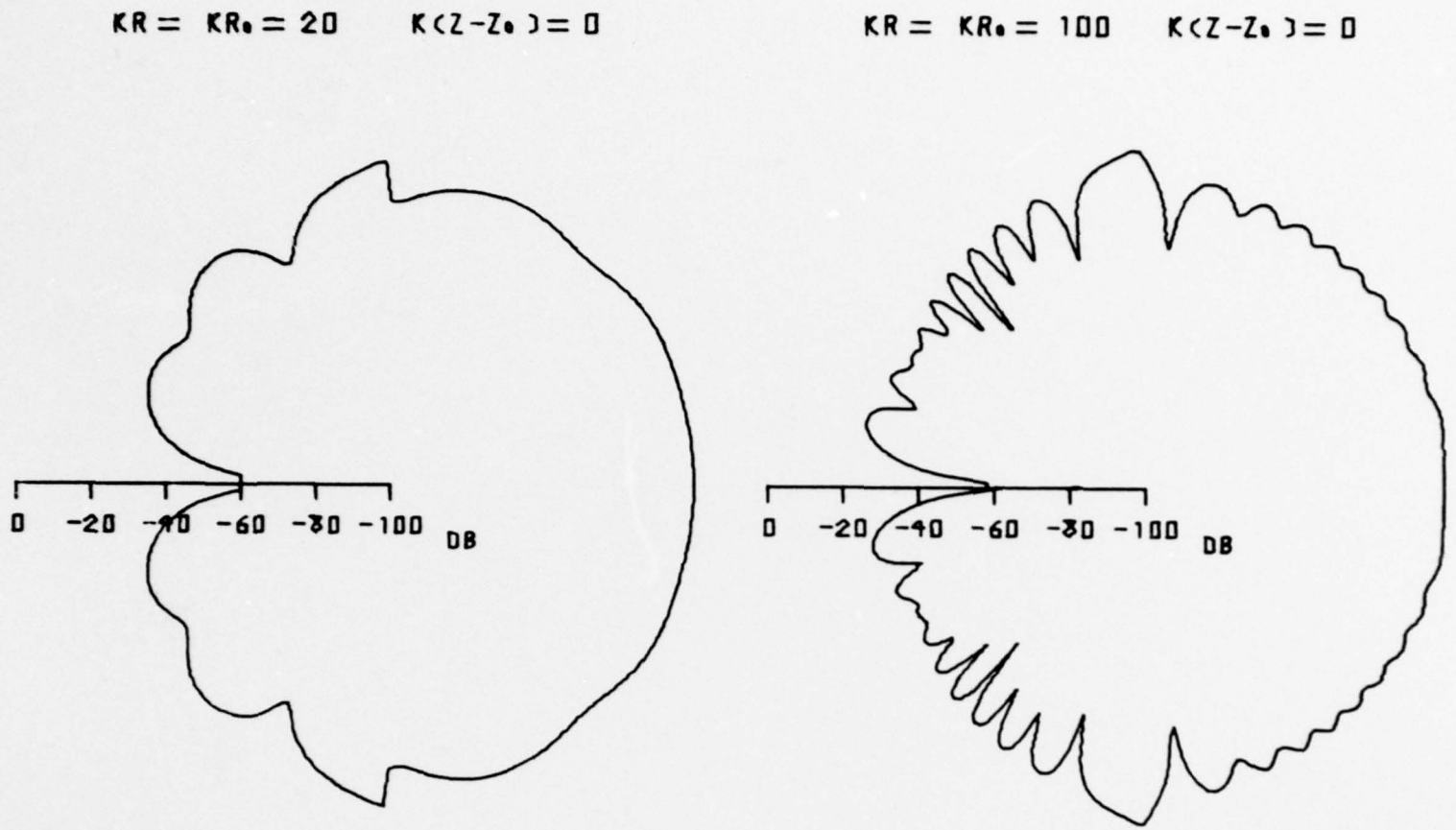

Figure 3.39. Backscattering of point source radiation with $\theta^{+} = \theta^{-} = 60^{o}$.

CHAPTER IV

DISCUSSION OF RESULTS AND CONCLUSIONS

4.1 Introduction

The major task of this investigation is to model mathematically a certain physical situation and derive a solution based upon that sodel. Specifically, the problem of the diffraction of acoustic waves by a locally reacting impedance covered half-plane is solved. The solution resulting from this analysis is significant in that it is a closed form solution. Being a closed form solution facilitates the actual physical interpretation of the problem. A discussion of the physics of the diffraction problem solved in Chapter II follows in Section 4.2. Additionally, some specific cases are examined for the influence of the impedance cover on the diffracted and back-scattered pressure. These results are illustrated in Chapter III and are discussed in detail in Section 4.3.

4.2 Physical Interpretation of the Solution

The solution for the diffraction of sound radiated by various types of acoustic sources by a locally reacting impedance covered half-plane provides an opportunity to study the nature of the diffraction phenomenon as well as the effect of many parameters. Since there are three types of acoustic sources considered in this study, each is discussed in turn emphasizing the differences between them.

The solution for the diffraction of a plane wave consists of two terms. This is evident from the solution shown in Equation (2.88). The form of each term is really very similar, differing slightly in three places. The first two differences are the plus and minus signs in front of ϕ_o in both the exponents and in the arguments of the Fresnel Integrals. The third difference is in the functions Φ_1 and Φ_2. Each of the two terms have the exponential functions $e^{ikr\cos(\phi+\theta_o)}$ and $e^{-ikr\cos(\phi-\theta_o)}$, respectively. Taken by themselves, these two exponents represent plane waves propagating in the direction of the reflection and in the direction of incidence. The fact that these two factors are present in the solution hints at the existence of both a source and an image source in the solution. Incidently, Sommerfeld's formulation relies heavily on the concept of sources and image sources. These two terms in the diffraction solution are not sources and images, however, because each is multiplied by a term containing the Fresnel Integrals. The functions containing the Fresnel Integrals have certain interesting properties that characterize the diffraction solution.

When investigating the behavior of the Fresnel Integrals, it is most important to consider the arguments. The arguments of the two terms are, respectively:

$$\sqrt{2kr\,\cos^2\frac{\phi+\phi_o}{2}}\quad , \tag{4.1}$$

and

$$\sqrt{2kr}\cos\frac{\phi-\phi_o}{2} \quad . \tag{4.2}$$

It is immediately evident that each argument has the same $(kr)^{1/2}$ dependence. This dependence on $(kr)^{1/2}$ manifests itself in two aspects of the solution. First, as kr increases both Fresnel Integrals, C(X) and S(X) approach 1/2 at a rate proportional to $(kr)^{1/2}$. As a result, the entire quantity that contains the Fresnel Integrals decays to zero at a rate proportional to $(kr)^{-1/2}$. Subsequently, the diffracted pressure should also decay by the same rate which is the expected decay of line source radiation. Secondly, the quantity kr influences the oscillations in the diffracted pressure because of the varying phases of the two terms of the solution. Because of the nature of the Fresnel Integrals, the phase varies at a rate proportional to the square of the argument. This means that the phase is directly related to kr rather than $(kr)^{1/2}$. This can be demonstrated by comparing Figures 3.1 and 3.2. The number of oscillations occurring in the plots increases in direct proportion to kr. As kr is doubled from kr = 50 to kr = 100, the number of oscillations also doubles.

The arguments of the Fresnel Integrals in Equations (4.1) and (4.2) also show a dependence upon the angle. Note that at $\phi = \pi-\phi_o$, the argument in Equation (4.1) goes to zero while the other argument given in Equation (4.3) goes to zero at $\phi = -\pi+\phi_o$. It is no accident that these angles correspond to the reflection showdow boundary and

the incident shadow boundary, respectively. The Fresnel Integrals are zero when the arguments are zero. As a result, the two terms that contain the Fresnel Integrals are maxima at their respective shadow boundaries. This behavior of the arguments contributes to the ability of the diffraction solution to accommodate the dramatic transition that occurs across the shadow boundaries. Consider for the moment only the first term in Equation (2.86) evaluated at $\phi = \pi - \phi_o$. This term becomes

$$- \frac{P_o(\sin\theta^+ - \sin\phi_o)\, e^{-ikr}}{2(\sin\theta^+ + \sin\phi_o)} \quad . \tag{4.3}$$

Meanwhile, the argument of the Fresnel Integral in the second term is $\sqrt{2kr}\,\sin\phi_o$ and, if kr is sufficiently large, this second term as a whole will be negligible because of the $(kr)^{-1/2}$ decay. All that survives, then, at the reflection shadow boundary is what appears in Equation (4.3). Incidentally, this value has the specific physical interpretation of being $\frac{1}{2}C_r$, the reflected wave where

$$C_r = \frac{(\sin\phi_o - \sin\theta^+)}{(\sin\phi_o + \sin\theta^+)} \quad . \tag{4.4}$$

The quantity C_r is the coefficient of reflections of a plane wave incident at an angle ϕ_o on an impedance covered infinite plane whose Brewster angle if $\theta+$. At the incident shadow boundary, $-\pi+\phi_o$, the solution equals $-p_o/2$. This is one-half the incident wave. The

behavior at the two shadow boundaries demonstrates that the pressure is continuous across them. At the dramatic transition between the illuminated region and the shadow region, the pressure becomes the average of the pressure between the two regions.

It has been previously mentioned that the figures in Chapter III illustrate dramatic oscillations. This behavior results from the interference of waves as they propagate away from the edge. The exact mechanism that causes this phenomena is not immediately clear from the solution. To explain this interference phenomenon, it is helpful to consider a plot for the diffraction of an incident plane wave at $\phi_o = 120^o$ by a perfectly rigid half-plane. This plot is now shown in Figure 4.1 for two different values of kr. Note that there exists the same kind of oscillations that occur for an impedance covered half-plane. This suggests that the oscillations do not result from the influence of an arbitrary impedance cover. If, however, the absolute values of the two terms in the solution for the diffracted pressure are plotted separately they appear as smooth functions as illustrated in Figure 4.2.

Note that these two smooth, pear-shaped plots have their respective maxima at the location of the two shadow boundaries and then each diminishes away from that angle in both directions. It seems then that the oscillations results from the interference between these two terms. Since they are both complex functions, the phase differences gives rise to the interference behavior as they add in and out of phase. In addition, the plots in Figure 4.2 suggest that the oscillations result from the wave interference

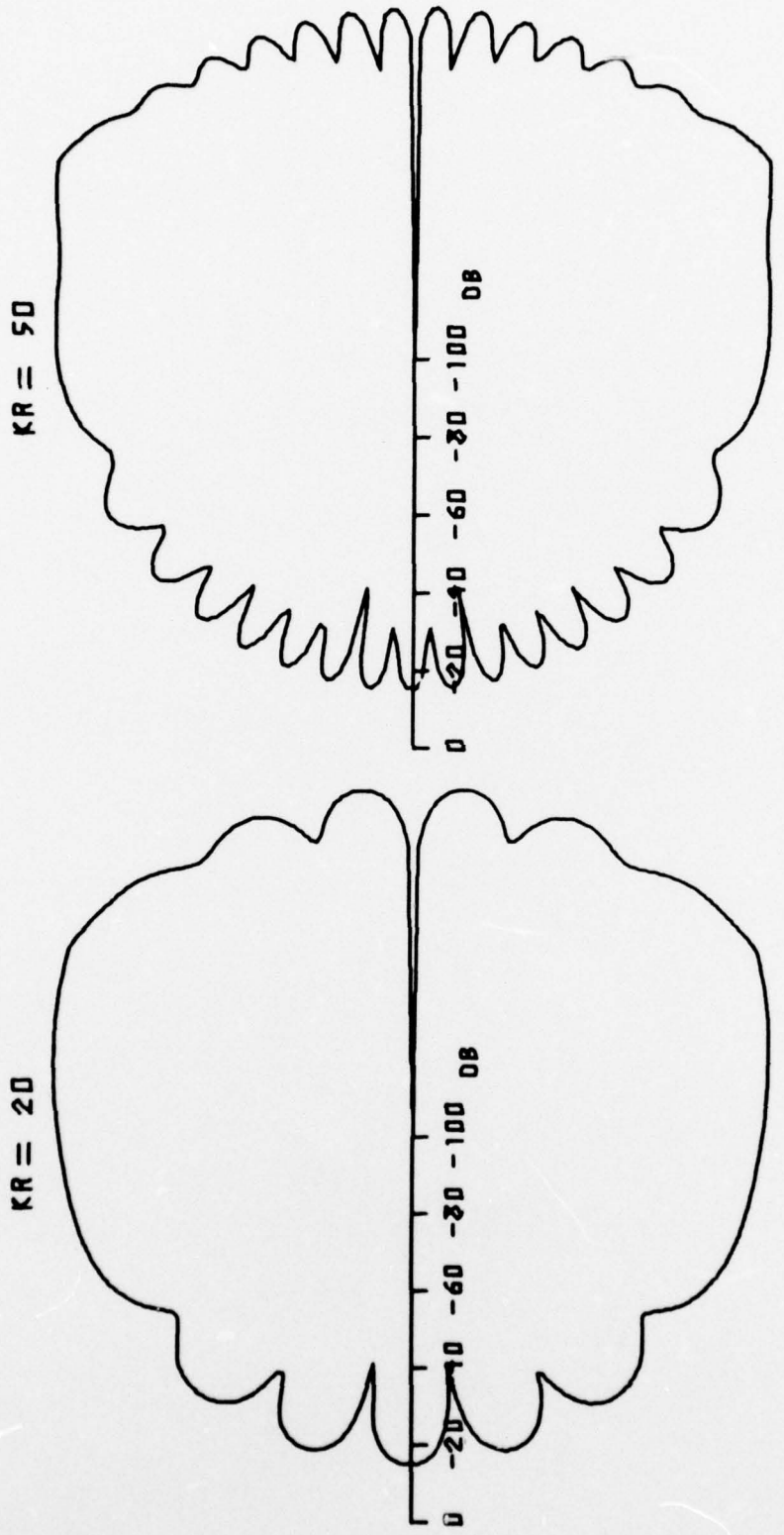

Figure 4.1. Diffraction of a plane wave by a rigid half-plane.

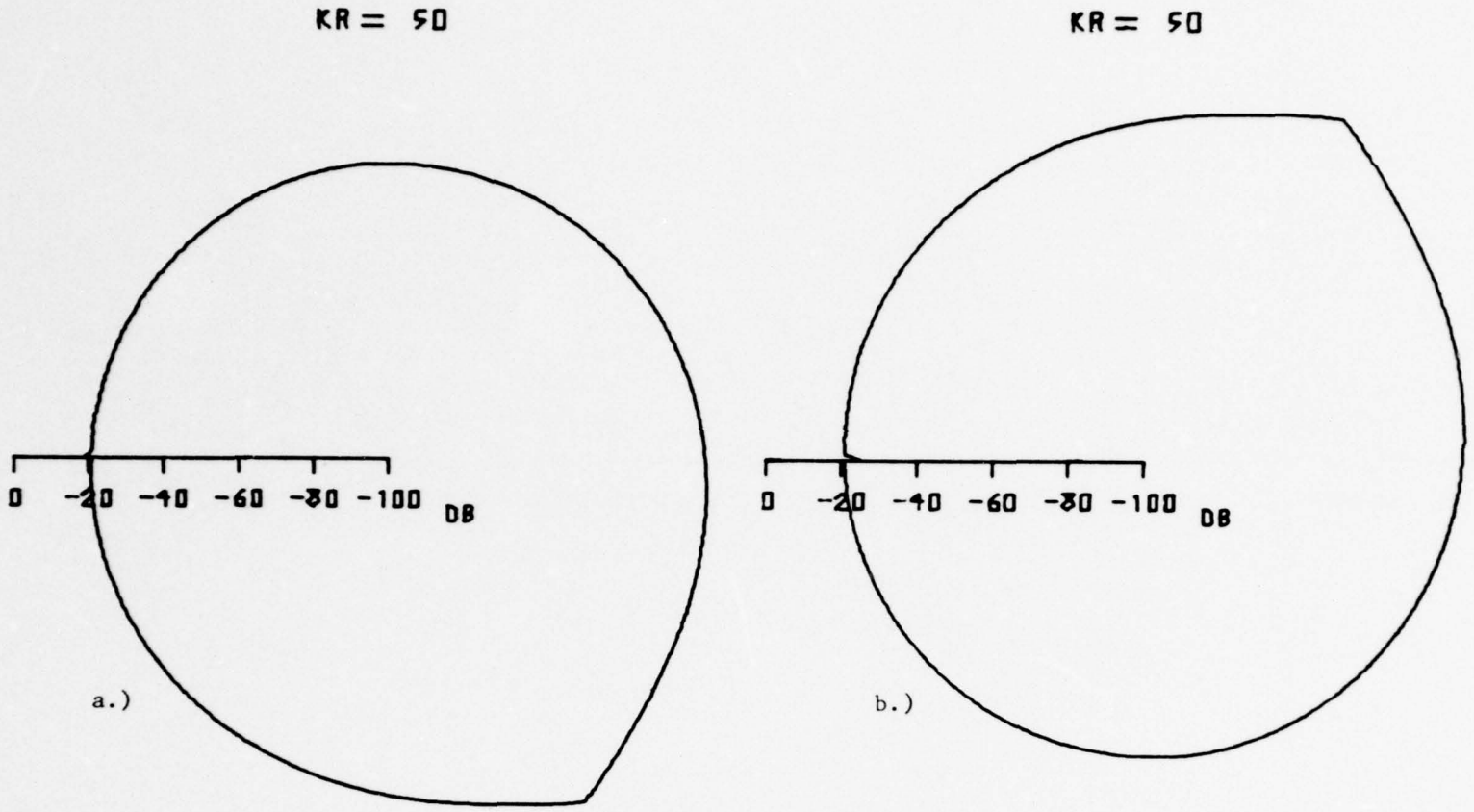

Figure 4.2. The two terms of the diffraction solution plotted separately with kr = 50, $\phi_o = 120^o$, $\theta^+ = \theta^- = 0^o$.
a.) Diffraction from the shadow boundary.
b.) Diffraction from the reflection shadow boundary.

developed between the four boundaries: the two shadow boundaries at $\pi-\phi_o$ and at $-\pi+\phi_o$ and the physical boundaries $\pm\pi$. In light of this interpretation, it is interesting to look at a plot for each of the two terms when the angle of incidence matches the Brewster angle. For this case, there should be no reflection. Figure 4.3 represents the two terms for a 120^o incident plane wave where $\theta^+ = 60^o$ and $\theta^- = 0^o$. Note that, in the plot for the first term, there is a zero at the exact reflection shadow boundary. However, even though there is no reflection, there is still a contribution away from the reflected shadow boundary. The plot is almost omnidirectional except for the null at $\pi-\phi_o$. On the other hand, the plot for the second term clearly indicates the shadow boundary at $-\pi+\phi_o$. Again the interference phenomenon occurs when these two complex terms are summed and plotted in Figure 4.3. In short, the implication is that the oscillations in the diffracted pressure are a result of the interference between the waves interacting with the four boundaries, the two shadow boundaries, and the two physical boundaries at $\pm\pi$.

The fact that at the exact shadow boundary the diffracted pressure converges to the mean value between the two regions is particularly interesting when viewed in comparison with the result given by the far-field solution at the exact shadow boundary. The far-field solution is given in Equation (2.49). In the far-field solution there are singularities at $\phi = \pi-\phi_o$ and at $\phi = -\pi+\phi_o$ because of the denominator. Consequently, the solution blows up

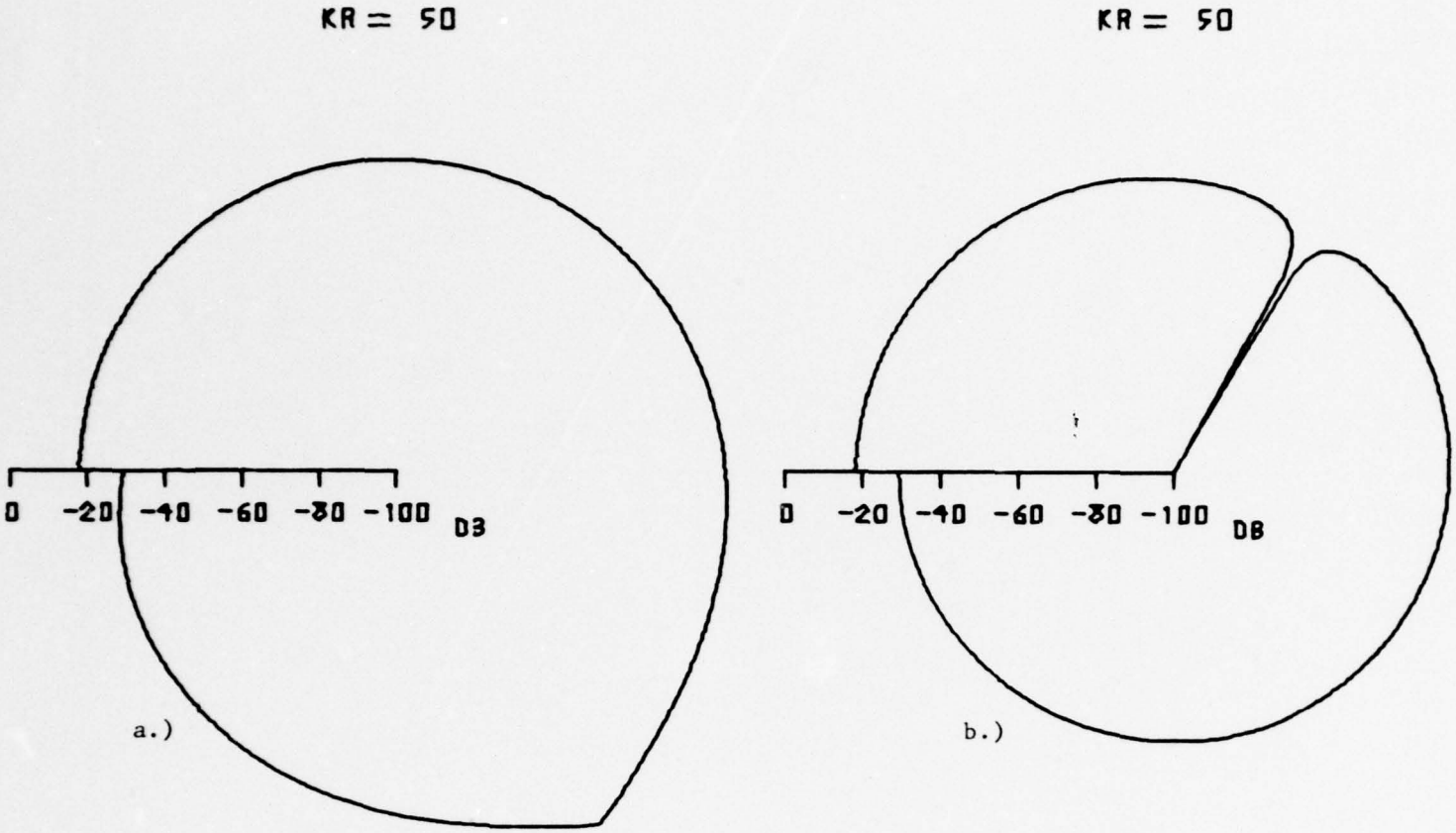

Figure 4.3. The two terms of the diffraction solution for a plane wave plotted separately with $\theta^+ = 60^o$, $\theta^- = 0^o$, $\phi_o = 120^o$, and kr = 50.

a.) Diffraction from the shadow boundary.

b.) Diffraction from the reflection shadow boundary.

at the shadow boundaries. This, of course, is not realistic. One does not actually have an infinite pressure. To explain the apparent fallacy, recall that the far-field solution results from the steepest descent approximation. If the saddle point, however, lies near a singularity, the method fails. This is, indeed, the case when $\phi = \pi-\phi_o$ or $\phi = -\pi+\phi_o$. Consequently, the far-field solution is not really valid when it predicts infinite pressure at the shadow boundaries. It is in these regions, close to the shadow boundaries, where the behavior of the Fresnel Integrals is necessary to account for the dramatic transition across the shadow boundaries.

It is appropriate, though, in cases where kr is very large to accept the far-field solution because it does illustrate that the greatest diffraction effect does occur at the shadow boundaries. It is good enough to satisfy one's physical intuition so long as one recalls that the pressure has diminished at a rate of $(kr)^{-1/2}$ and that, at the exact boundary, what appears to be an infinity should really be one-half the mean between the two regions.

The far-field plots are helpful in searching for the nulls in the diffracted and backscattered fields. If the solution is considered in the form given in Equation (2.49), an expression for the zeroes of the diffracted pressure and backscattered pressure may be found. These expressions may be found in Equations (2.51) and (2.52).

Much of what occurs in the plane wave solution also occurs in the solutions for the line source and the point source. All three

are essentially examples of constructive and destructive wave interference between the two shadow boundaries and the two physical boundaries. There are, however, a number of minor differences in each solution that require some amplification.

The diffraction solution for a line source is given in Equation (2.113). One can apply a limited geometric interpretation to this solution by once again thinking in terms of a line source and a corresponding image. In order to appreciate this, consider Figure 4.4.

The parameters that appear in the solution are R_1, R, and S. From Figure 4.4, the values R and S are the distances from the source and image to the observer point, while the value $R_1 = r + r_o$ is the path distance a wave must travel from the source to the edge and from there to the observer.

The famous reciprocity theorem is also verified by this solution. If the values for kr and kr_o are reversed in Equation (2.113), which is essentially reversing the position of the source and observer, there is no change in the solution.

The solution for the point source is given in Equation (2.132). Like the solution for the line source, there is a similar geometric interpretation. Also note that for this solution, the reciprocity theorem is once again validated. By reversing the values of kr and kr_o and also the values for kz and kz_o, the result remains unaltered.

In the point source solution, the variable kR_1 has an interesting physical interpretation. The length R_1 is the shortest

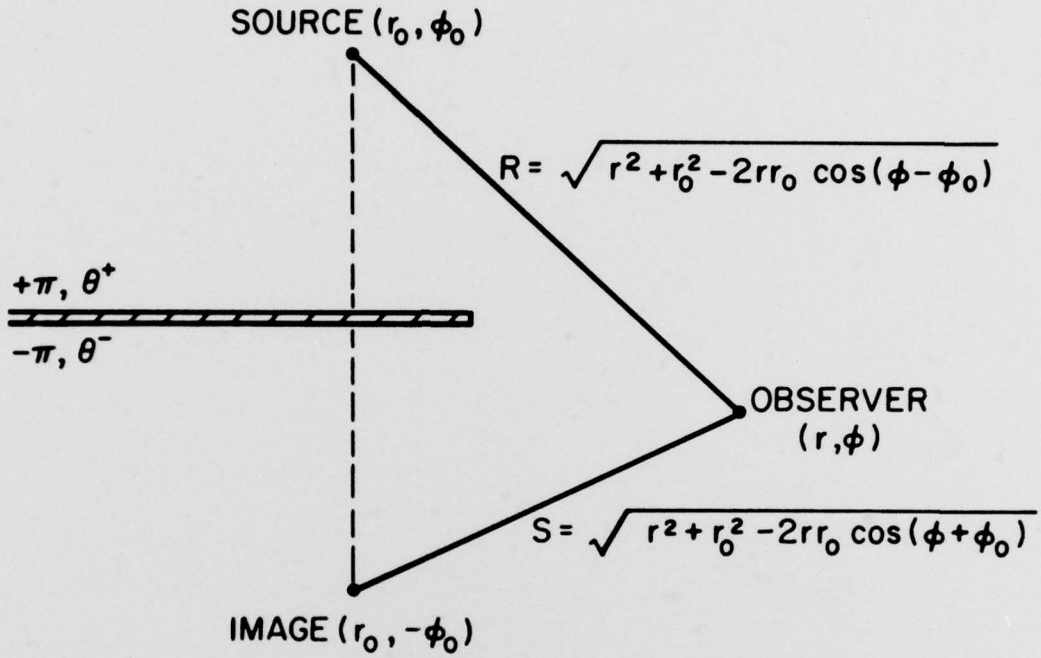

Figure 4.4. The geometry for the source, image source, and observer for an incident line source.

distance a ray may travel from the source to the edge of the half-plane and finally to the observer. The appearance of the shortest path distance in the formula is a manifestation of Fermat's principle on the diffraction of a bundle of rays. The fact that R_1 appears in the solution verifies the principle. Figure 4.5 illustrates the geometry for the point source, image point source and observer. The dashed line indicates the shortest distance a ray would travel when going from the source to the edge and finally to the observer. The geometry for the path of the ray is detailed in Figure 4.6. From this figure, one realizes that the triangles OAB and SAC are similar, the length from B to C is $(z-z_o)$, the length OB is r and the length SC is r_o. It follows that

$$\frac{\overline{AB}}{r} = \frac{\overline{AC}}{r_o} \tag{4.5}$$

and

$$\begin{aligned}(z-z_o) &= \overline{AB} + \overline{AC} \\ &= \overline{AB} + AB\,\frac{r_o}{r} \\ &= \overline{AB}\;\frac{r+r_o}{r} \quad .\end{aligned} \tag{4.6}$$

Consequently

$$\overline{AB} = \frac{r(z-z_o)}{(r+r_o)} \tag{4.7}$$

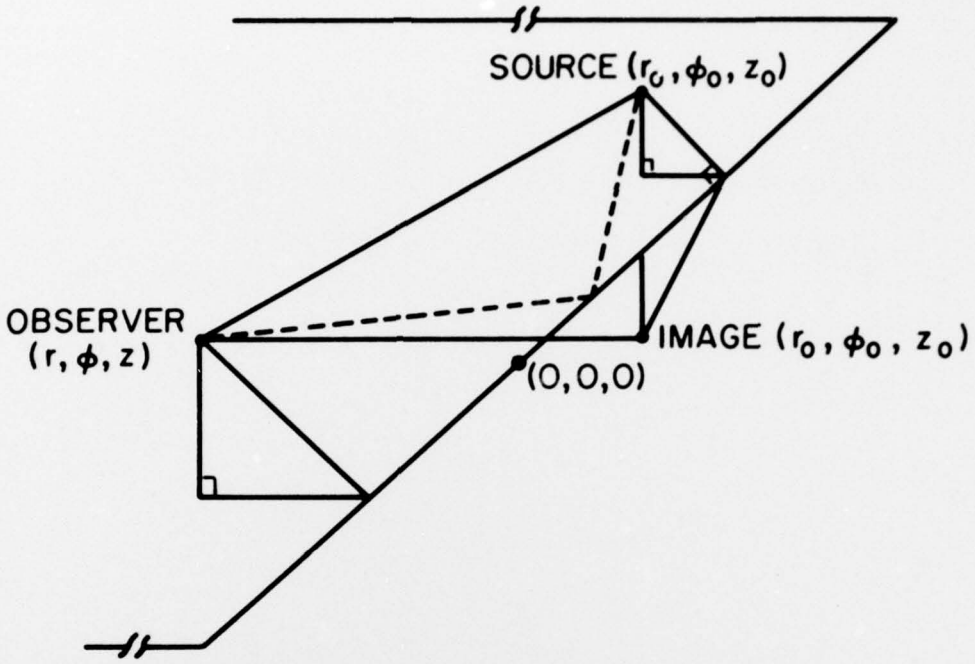

Figure 4.5. The geometry for the source, image source, and observer for an incident line source.

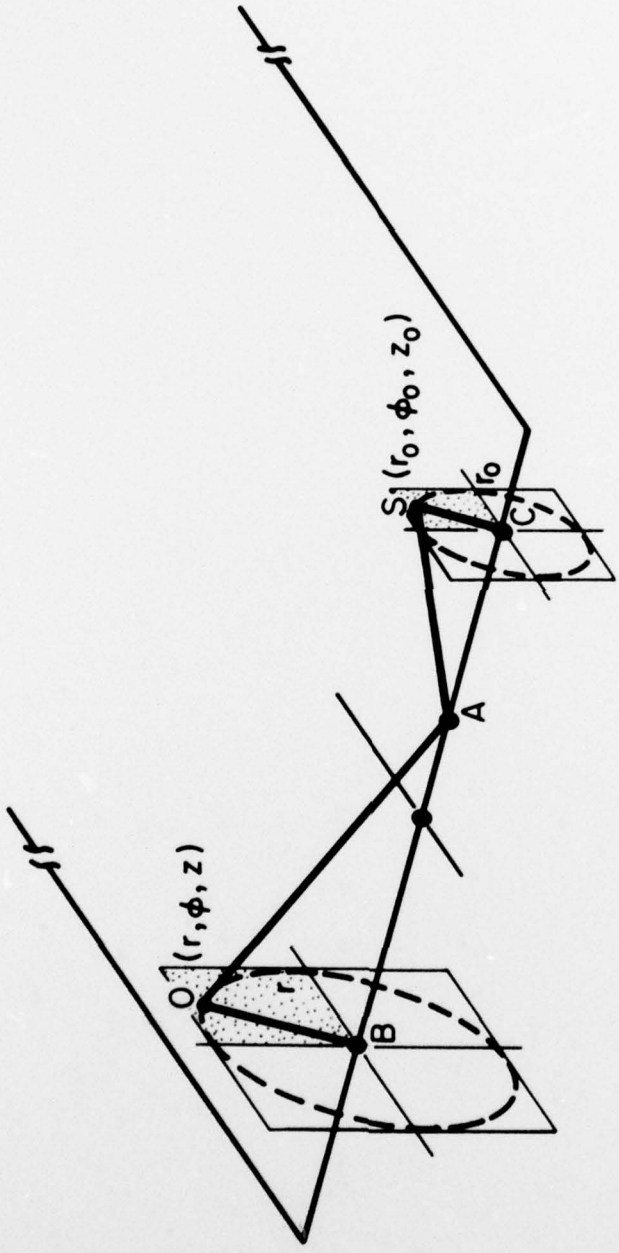

Figure 4.6. The path of the shortest ray from the source to the edge and back to the observer.

and

$$\overline{AC} = \frac{r_o(z-z_o)}{(r+r_o)} \quad . \tag{4.8}$$

The distance

$$\overline{OA} = r^2+r^2 \left(\frac{z-z_o}{r+r_o}\right)^2 \tag{4.9}$$

and the distance

$$\overline{AS} = r_o^2+r_o^2 \left(\frac{z-z_o}{r+r_o}\right)^2 \quad . \tag{4.10}$$

Finally, one can calculate the distance R_1 from Equations (4.9) and (4.10) as follows:

$$R_1 = \overline{OA} + \overline{AS}$$

$$= \frac{r^2[(r+r_o)^2 + (z-z_o)^2]}{(r+r_o)^2} + \frac{r_o^2[(r+r_o)^2 + (z-z_o)^2}{(r+r_o)^2}$$

$$= \sqrt{(r+r_o)^2 + (z-z_o)^2} \quad . \tag{4.11}$$

In summary, the solution for the diffraction of the radiation of each type of acoustic source illustrates the occurrence of constructive and destructive interference and demonstrates the validity of the Reciprocity Theorem and Fermat's Principle.

4.3 Discussion of Results

The numerical results that were compiled in Chapter III are discussed in this section.

For the plane wave one may compare the transition from the near-field solution to the far-field solution from any of the Figures 3.1 to 3.14. For example, in Figures 3.1 and 3.2, it is evident that increasing kr results in a more complicated phase interaction as indicated by the increase in the number of oscillations in the plots. It is also curious that even at kr = 100, which represents approximately 15 wavelengths from the edge, the solution does not yet produce the clearly defined null that appears in the plot of the far-field. This is a consequence of the fact that the exact phase cancellation required to form this null only occurs at kr equal to infinity, which does not exist in reality.

The first eight figures show how the diffracted pressure varies as a function of the impedance cover on the illuminated surface. Specifically, compare the Figures 3.2, 3.4, 3.6, and 3.8 where the Brewster angles for the illuminated surface are $\theta+ = 30^{\circ}$, 60°, 90°, and $i\infty$ (pressure release), respectively. It appears that as this impedance cover on the illuminated surface varies, there is a significant change in the diffracted pressure.

In contrast, compare these same four figures with Figures 3.10 and 3.12, where the Brewster angle on the unilluminated surface is varied from the extremes of $\theta^{+} = 90^{\circ}$, for a totally absorbing surface to $\theta+ = 5i$, for a pressure release surface. What becomes

evident from this comparison is that the impedance of the surface lying in the shadow region has little effect on the diffracted pressure while the impedance cover on the illuminated surface has a significant effect, being most apparent in the illuminated region. One concludes that the impedance cover of the illuminated surface dominates the diffracted pressure in the illuminated region. Although the surface condition on the opposite side may influence the diffracted pressure, it is to a much smaller degree.

Figures 3.13 and 3.14 are interesting in contrast to Figures 3.1 and 3.2. The impedance cover of the half-plane in Figures 3.13 and 3.14 is almost equivalent to that in Figures 3.1 and 3.2 except for a small imaginary (reactive) component added to the impedance on the upper surface. This small imaginary part seems to have little effect on the near-field solution. However, in the far-field, where a true null is shown in Figure 3.2, only a minimum is shown at approximately the same angle in Figure 3.14. It is evident, then, that nulls exist in the far-field solution only when the impedance is real, i.e., absorptive. In addition, if the impedance is complex, with a small imaginary part, the null becomes a minimum at approximately the same location. Also, increasing the imaginary part further may remove the minimum altogether.

The plots of the backscattered pressure further establish the conclusion that the effect of the impedance on the illuminated surface dominates the backscattered pressure in the half-space that faces the illuminated surface. Compare Figures 3.16, 3.18, 3.20,

and 3.22. In each, the lower surface is rigid while the Brewster angles for the upper surface are $\theta^+ = 30^o$, 60^o, 90^o and i5, respectively. Recall that for backscattered pressure, the source and observer are at the same location. Then, the backscattered pressure in the lower half-plane appears to be the same for all of the Brewster angles θ^+ since the illuminated lower surface is always rigid. The backscattered pressure remains the same in the lower half-plane regardless of what happens on the upper surface. In contrast, however, when the source and the receiver are in the upper half-plane the backscattered pressure from the different plots changes corresponding to each different impedance conditions. The implication is that the impedance condition on the illuminated surface has the dominant influence on the behavior of the backscattered pressure.

A comparison of the plots for both the line source and the point source to those for the plane wave incidence demonstrates a similar dependence on the impedance cover.

4.4 Summary and Conclusions

The problem of diffraction and backscattering of various types of sources was attempted by means of a so-called dual integral formulation. The dual integral formulation resulted in a new and closed form solution for the diffraction of various acoustic sources by an impedance covered half-plane. The closed form solution illustrates that the diffraction is a phenomenon manifested by wave interference.

Of an exhaustive number of numerical results compiled for many parameter combinations, only a portion are presented in this thesis. They demonstrate that the effect of the surface impedance dominates in the illuminated half-space into which it faces, even though the influence of each surface extends with diminishing effect into the opposite half-space behind the barrier.

At the geometric shadow boundary, the diffracted pressure becomes one-half the incident pressure, while at the reflection shadow boundary, the diffracted pressure is equal to one-half the reflected pressure from an impedance covered infinite surface.

The results also indicate that, although the near-field solution approaches the far-field solution as kr becomes large, it never equals the far-field solution. Both the source and observer must be at an infinite distance from the edge to allow the precise phase cancellations necessary to yield the far-field solution.

BIBLIOGRAPHY

1. A. Sommerfeld, Optics, Academic Press, New York and London, (1964).

2. A. Sommerfeld, "Mathematische Theorie der Diffraction," Math. Ann. 47, 317-374, (1896)

3. D.S. Jones, "A Simplifying Technique in the Solution of a Class of Diffraction Problems," Quart. J. Math., (2) 3, 189-196, (1952).

4. P.C. Clemmow, The Plane Wave Spectrum Representation of Electromagnetic Waves, Pergammon Press, London, (1966).

5. T.B.A. Senior, "Diffraction by a semi-infinite metallic sheet," Proc. Roy. Soc. Lond. A 213, 436-458, (1952).

6. W.E. Williams, "Diffraction of and E-polarized Plane Wave by an Imperfectly Conducting Wedge," Proc. Roy. Soc. Lond. A 252, 376-393, (1959).

7. E.W. Barnes, "The Linear Difference Equation of the First Order," Proc. Cond. Math. Soc., (2), 2, 428-269, (1904).

8. A.D. Rawlins, "The Solution of a Mixed Boundary Value Problem in the Theory of Diffraction by a Semi-Infinite Plane," Proc. Roy. Soc. Lond. A 346, 469-484, (1975).

9. G.D. Malyuzhinets, "The Radiation of Sound by Vibrating Boundaries of an Arbitrary Wedge Parts 1 & 2," Soviet Physics Acoustics, 152-174, 240-248, (1955).

10. G.D. Malyuzhinets, "Das Sommerfeldeche Integral und die Losung Von Beugungsaufgaben in Winkelgebieten," Ann. der Physik, 6, 107-112, (1962).

11. G.D. Malyuzhinets, and A.A. Tuzhlin, "Plane Acoustic Wave Diffraction at a Semi-Infinite Thin Elastic Plate," Zh. vychrist, Mat. Mat. Fiz., 10, 5, 1210-1227, (1970).

12. S.W. Redfearn, "Some Acoustical Source-Observer Problems," Phil. Mag., 30, 223-236, (1940).

13. A.D. Pierce, "Diffraction of Sound Waves Around Corners and Over Wide Barriers," Jour. Acous. Soc. Am., 55, 941-955, (1974).

14. A. Erdilyi, Asymptotic Expansions, Dover Publications Inc., New York, (1968).

15. E. Skudrzyk, Simple and Complex Vibratory Systems, The Pennsylvania State University Press, University Park, (1968).

16. P.M. Morse, and K. UnoIngard, Theoretical Acoustics, McGraw Hill Book Co., New York, (1968).

17. B. Nobel, Methods Based on the Weiner-Hopf Technique, Pergammon Press, New York, (1968).

18. J.S. Gradshteyn and I.M. Ryzhik, Table of Integral Series and Products, Academic Press, New York, (1965).

19. G.R. Van Lennep, "The Kernel of Sommerfeld's Transform as Solution to Difference Equations for a Class of Diffraction Problems," J. App. Phys., 45, 4401-4405, (1974).

20. H.M. MacDonald, "A Class of Diffraction Problems," Proc. Lond. Math. Soc., 14, 410-427, (1915).

21. E. Janke and F. Emde, Tables of Functions, Dover Publications, New York, (1945).

22. J.J. Bowman and T.B.A. Senior, "The Half Plane," Chapter 8 in Electromagnetic and Acoustic Scattering by Simple Shapes, edited by J.J. Bowman, T.B.A. Senior, and P.L.E. Uslenghi (North-Holland, Amsterdam, 1969).

VITA

Robert Paul Kendig was born in Danville, Pennsylvania on February 17, 1949. His primary and secondary education was received in the State College Area School District in State College, Pa. Later he attended Lehigh University in Bethlehem, Pa. where he graduated with honors, receiving a BA degree in Mathematics in 1971. Beg-inning in 1971 he became a graduate student in the Department of Engineering Mechanics at The Pennsylvania State University. From 1973 to the present he served as an instructor in the Department of Engineering Science and Mechanics at The Pennsylvania State University.

DISTRIBUTION

Commander (NSEA 09G32)
Naval Sea Systems Command
Department of the Navy
Washington, D. C. 20362 — Copies 1 and 2

Commander (NSEA 0342)
Naval Sea Systems Command
Department of the Navy
Washington, D. C. 20362 — Copies 3 and 4

Defense Documentation Center
5010 Duke Street
Cameron Station
Alexandria, VA 22314 — Copies 5 through 16